ผลของภาวะแอโนไดซ์และการฉายรังสีอัลตราไวโอเลตต่อความชอบน้ำ
ของฟิล์มแอโนไดซ์บน Ti-6Al-4V

นางสาวพนาวรรณ หวังดี

วิทยานิพนธ์นี้เป็นส่วนหนึ่งของการศึกษาตามหลักสูตรปริญญาวิทยาศาสตรดุษฎีบัณฑิต
สาขาวิชาวัสดุศาสตร์ ภาควิชาวัสดุศาสตร์
คณะวิทยาศาสตร์ จุฬาลงกรณ์มหาวิทยาลัย
ปีการศึกษา 2557

EFFECT OF ANODIZING CONDITIONS AND ULTRAVIOLET IRRADIATION ON HYDROPHILICITY OF ANODIZED FILMS ON Ti-6Al-4V

Miss Phanawan Whangdee

A Dissertation Submitted in Partial Fulfillment of the Requirements
for the Degree of Doctor of Philosophy Program in Materials Science
Department of Materials Science
Faculty of Science
Chulalongkorn University
Academic Year 2014

Thesis Title	EFFECT OF ANODIZING CONDITIONS AND ULTRAVIOLET IRRADIATION ON HYDROPHILICITY OF ANODIZED FILMS ON Ti-6Al-4V
By	Miss Phanawan Whangdee
Field of Study	Materials Science
Thesis Advisor	Assistant Professor Dujreutai Pongkao Kashima, D.Eng.
Thesis Co-Advisor	Assistant Professor Viritpon Srimaneepong, Ph.D.

Accepted by the Faculty of Science, Chulalongkorn University in Partial Fulfillment of the Requirements for the Doctoral Degree

.....Dean of the Faculty of Science
(Professor Supot Hannongbua, Dr. rer. nat.)

THESIS COMMITTEE

.....Chairman
(Assistant Professor Sirithan Jiemsirilers, Ph.D.)

.....Thesis Advisor
(Assistant Professor Dujreutai Pongkao Kashima, D.Eng.)

.....Thesis Co-Advisor
(Assistant Professor Viritpon Srimaneepong, Ph.D.)

.....Examiner
(Associate Professor Supatra Jinawath, Ph.D.)

.....Examiner
(Professor Pasutha Thunyakitpisal, Ph.D.)

.....Examiner
(Associate Professor Paiparn Santisuk)

.....External Examiner
(Professor Tomoaki Watanabe, Ph.D.)

พนาวรรณ หวังดี : ผลของภาวะแอโนไดซ์และการฉายรังสีอัลตราไวโอเลตต่อความชอบน้ำของฟิล์มแอโนไดซ์บน Ti-6Al-4V (EFFECT OF ANODIZING CONDITIONS AND ULTRAVIOLET IRRADIATION ON HYDROPHILICITY OF ANODIZED FILMS ON Ti-6Al-4V) อ.ที่ปรึกษาวิทยานิพนธ์หลัก: ผศ. ดร. ดุจฤทัย พงษ์เก่า คะชิมา, อ.ที่ปรึกษาวิทยานิพนธ์ร่วม: ผศ. ทพ. ดร. วิริทธิ์พล ศรีมณีพงศ์, 139 หน้า.

โดยทั่วไปฟิล์มแอโนไดซ์บนโลหะผสม Ti-6Al-4V เกิดจากกระบวนการแอโนไดเซชั่นโดยการใช้ค่าความหนาแน่นกระแสไฟฟ้าหรือความต่างศักย์ไฟฟ้าสูง เทคนิคนี้ถูกใช้กันอย่างแพร่หลายในการเพิ่มความชอบน้ำให้แก่ฟิล์มแอโนไดซ์เพื่อการประยุกต์ใช้งานทางด้านทันตกรรม งานวิจัยนี้จึงมุ่งพัฒนาฟิล์มแอโนไดซ์ที่เตรียมขึ้นที่ค่าความหนาแน่นกระแสไฟฟ้าหรือความต่างศักย์ไฟฟ้าต่ำเพื่อให้มีสมบัติด้านความชอบน้ำใกล้เคียงกับฟิล์มที่เตรียมขึ้นจากความหนาแน่นกระแสไฟฟ้าหรือความต่างศักย์ไฟฟ้าสูง โดยเตรียมฟิล์มแอโนไดซ์บนโลหะผสม Ti-6Al-4V ด้วยวิธีกัลวาโนสแตติกและโพเทนชิโอสแตติก โดยใช้อิเล็กโตรไลต์สองชนิดคือ กรดฟอสฟอริกและโมโนแคลเซียมฟอสเฟตโมโนไฮเดรต ในช่วงความหนาแน่นกระแสไฟฟ้าต่ำ 0.25-2 มิลลิแอมแปร์ต่อตารางเซนติเมตร หรือความต่างศักย์ไฟฟ้าต่ำในช่วง 2-10 โวลต์ เป็นเวลา 30 นาที ฟิล์มแอโนไดซ์ที่ได้จากการป้อนความหนาแน่นกระแสไฟฟ้า 2 มิลลิแอมแปร์ต่อตารางเซนติเมตร ในกรดฟอสฟอริก และ 1 มิลลิแอมแปร์ต่อตารางเซนติเมตรในสารละลายโมโนแคลเซียมฟอสเฟตโมโนไฮเดรต และฟิล์มแอโนไดซ์ที่เตรียมได้จากการป้อนค่าความต่างศักย์ 6 โวลต์ในอิเล็กโทรไลต์ทั้งสองชนิดแสดงค่าความชอบน้ำเพิ่มขึ้นภายหลังการฉายยูวีนาน 24 ชั่วโมง โดยพบว่ามุมสัมผัสน้ำมีค่าลดลงอย่างมีนัยสำคัญ ลักษณะพื้นผิวของฟิล์มไม่เปลี่ยนแปลง ผลจากสเปคตรัม FTIR ไม่พบหมู่ไฮดรอกซิลที่เลขคลื่น 3,000 – 3,600 ต่อเซนติเมตร ภายหลังการฉายยูวีพบว่า หมู่ไฮดรอกซิลไม่เสถียร ผลจากสเปคตรัม XPS พบความเข้มพีคของ Ti 2p และ O 1s เพิ่มขึ้นและความเข้มพีคของ C 1s ลดลง อย่างไรก็ตามตำแหน่งของพลังงานยึดเหนี่ยวไม่เปลี่ยนแปลง ชี้ให้เห็นว่าฟิล์มแอโนไดซ์เหล่านี้ไม่ใช่ไทเทเนียมไดออกไซด์ แต่อาจจะเป็นไฮดรอกซิเลตไทเทเนียมออกไซด์

ภาควิชา วัสดุศาสตร์ ลายมือชื่อนิสิต .....

สาขาวิชา วัสดุศาสตร์ ลายมือชื่อ อ.ที่ปรึกษาหลัก .....

ปีการศึกษา 2557 ลายมือชื่อ อ.ที่ปรึกษาร่วม .....

5472838223 : MAJOR MATERIALS SCIENCE
KEYWORDS: TI-6 AL-4 V / HYDROPHILICITY / LOW CURRENT DENSITY / LOW VOLTAGE / UV IRRADIATION

PHANAWAN WHANGDEE: EFFECT OF ANODIZING CONDITIONS AND ULTRAVIOLET IRRADIATION ON HYDROPHILICITY OF ANODIZED FILMS ON Ti-6Al-4V. ADVISOR: ASST. PROF. DUJREUTAI PONGKAO KASHIMA, D.Eng., CO-ADVISOR: ASST. PROF. VIRITPON SRIMANEEPONG, Ph.D., 139 pp.

The anodized films on Ti-6Al-4V alloy are normally formed by anodization process at high current densities or voltages. This film formation technique has been widely used to improve the hydrophilicity of the film for dental implant applications. Our attempt is exploring whether anodized films with proper hydrophilicity can be performed by anodization at low current densities or voltages. The anodized films on Ti-6Al-4V were prepared by both of galvanostatic and potentiostatic method in either 1M H_3PO_4 or 1M MCPM ($Ca(H_2PO_4)_2•H_2O$) with current densities 0.25-2 mA/cm^2 or applied voltage 2-10 V for 30 min. The hydrophilicity was improved on the anodized films formed at low current density of 2 mA/cm^2 in 1M H_3PO_4 and 1 mA/cm^2 in 1M MCPM and low voltage of 6 V in both electrolytes, consequently subjected to UV irradiation for various times up to 24 h. After UV irradiation the contact angles of films significantly decreased however the surface morphology did not change. FTIR spectra confirmed that -OH groups around 3,000-3,600 cm^{-1} disappeared. It is indicated that –OH group was not stable under UV irradiation. XPS spectra investigated that the peak intensities of Ti 2p and O 1s increased, while C 1s peak decreased. However, the binding energy shown in XPS spectra did not change. It is indicated that these anodized films were not TiO_2 but it might be hydroxylated TiO_x.

Department:	Materials Science	Student's Signature	.....
Field of Study:	Materials Science	Advisor's Signature	.....
Academic Year:	2014	Co-Advisor's Signature	.....

ACKNOWLEDGEMENTS

Firstly, I would like to express my sincere appreciation to my advisor, Asst. Prof. Dr. Dujreutai Pongkao Kashima and my co-advisor, Asst. Prof. Dr. Viritpon Srimaneepong, for invaluable support, including their kindness and guidance. Their comments and suggestions not only provide valuable knowledge but also broaden perspective in practical applications.

I would like to thank the chairman, Asst. Prof. Dr. Sirithan Jiemsirilers and other committee members, Assoc. Prof. Dr. Supatra Jinawath, Prof. Dr. Pasutha Thunyakitpisal, Assoc. Prof. Paiparn Santisuk and Prof. Dr. Tomoaki Watanabe for many valuable comments and their perceptive suggestions.

I would like to gratefully acknowledge the Development and Promotion of Science and Technology Talents Project (DPST) for financially supporting this work.

I would like to thank Prof. Dr. Tomoaki Watanabe and my colleagues at Watanabe Lab, Department of Applied Chemistry, School of Science and Technology, Meiji University, Japan for their kindness and hospitality. I also thank Prof. Dr. Mamoru Aizawa for contact angle measurement, Prof. Dr. Suzuki Yoshitake for XPS measurement and Dr. Chihiro Izawa for helping me in this work during my stay in Japan.

I would like to thank all my colleagues and staff members in the Department of Materials Science, Faculty of Science, Chulalongkorn University for their friendship and encouragement.

Finally, I am eternally grateful to my beloved family for their constant support, love and encouragement throughout my life.

CONTENTS

Page

Page

Page

Page

LIST OF TABLES

Page

LIST OF FIGURES

Page

CHAPTER 1

INTRODUCTION

Ti-6Al-4V has been used as dental implant because of its good mechanical properties, high corrosion resistance and excellent biocompatibility. A small amount of Al and V is added into Ti in order to improve the mechanical properties [1,2,3,4,5,6]. Ti-6Al-4V can osseointegrate to bone because of its oxide. Surface modification of Ti surface is essentially important for promoting osseointegration on Ti-6Al-4V [7]. The term of osseointegration has been used to describe the adherence of bone and implant surface without the formation of fibrous layer. Therefore, there will be no movement between implant and bone which directly bond at the interface [8,9].

The surface roughness, surface species, surface functional groups, surface energies and hydrophilicity are important factors to enhance the osseointegration [10,11]. The surface roughness can interlock between implant and bone and also improve the adsorption of biological fluid on the implant [11,12]. The surface species and surface functional groups are essentially important for good bonding interface between implant and living bone which will promote the osseointegration [7]. The surface energy and hydrophilicity are important factors to understand the biological performance of biomaterial surfaces [13]. The hydrophilicity can also improve the cellular response [14]. For example, the osteoblast cell growth and protrusion often show better performance on hydrophilic surface [15].

Several surface modification techniques [7,16] have been developed for increasing the bioactivity and promoting the osseointegration on titanium surface such as sandblasting, acid etching, heat treatment, sol-gel process and anodization. Anodization has become an interesting surface modification technique because it rapidly promote surface roughness, perform at room temperature, coat on complex shapes and it is also inexpensive [12,17]. Therefore, anodization is one of the surface modification techniques proposed to improve the surface roughness, surface chemical species and hydrophilicity [15,18], in order to promote the osseointegration process.

Several works reported that the anodized films were produced at high current

density or high voltage. However, there were disadvantages such as high energy consumed, expensive and dangerous. Therefore, the low current density and low voltage were considered to produce the anodized films in order to solve these problems. The anodized films could be formed at a low voltage [19]. These anodized films consisted of the mixed oxide of TiO_2 and Ti_2O_3. Thus, it is possible to prepare the anodized films at low voltage or low current density. Oshida, Y. [20] reported the phase change of titanium oxide from lower to higher oxides; $TiO \longrightarrow Ti(O) \longrightarrow Ti_6O \longrightarrow Ti_3O \longrightarrow Ti_2O \longrightarrow TiO \longrightarrow Ti_2O_3 \longrightarrow Ti_3O_5 \longrightarrow TiO_2$. It is indicated that applied low voltage or current density is not enough to form TiO_2 but it can form a mix oxide of TiO_2 and Ti_2O_3 or TiO. Consequently, the anodization at a low current density or low voltage has become an alternative for the anodized films preparation with lower energy consumption, lower cost and safer in the production process.

UV irradiation is considered to improve the hydrophilicity to the anodized films formed at low current density or low voltage. There are two mechanisms of UV induced hydrophilicity of TiO_2, the first is the formation of oxygen vacancies and the second is the hydrocarbon removal on the TiO_2 surface. The pairs of the electrons (e^-) and the holes (h^+) were created after UV irradiation. The electrons tend to reduce the Ti^{4+} to Ti^{3+} and the holes react with the bridging site oxygen and oxygen atom is released, resulting in oxygen vacancies. Then water molecule can replace oxygen vacancy and absorb hydroxyl group and induce hydrophilicity on the TiO_2 films [21,22]. Another one is through the removal of hydrocarbon. It was decomposed by photocatalytic activity [23,24]. Then the water molecules were adsorbed on the surface films.

This study aims to investigate the surface morphologies, surface species, surface functional groups of the anodized films formed at low and high current densities (0.25-2 mA/cm^2 and 20-80 mA/cm^2) by galvanostatic method and low and high voltages (2-10 V and 20-150 V) by potentiostatic method in either H_3PO_4 or MCPM and explore their influences on the hydrophilicity of the films. Moreover, the influences of UV irradiation on the hydrophilicity of the anodized films formed at low current density and low voltage were also investigated.

Objectives

1. To investigate the surface morphologies, surface species, and surface functional groups of the anodized films formed at low current densities, high current densities, low voltages and high voltages in either H_3PO_4 or MCPM and to explore their influences on the hydrophilicity of the films.
2. To study on the influence of UV irradiation on hydrophilicity of anodized films on Ti-6Al-4V.

Expected Benefits

To attain an optimum current density and voltage for anodized film formation on Ti-6Al-4V and obtain improved hydrophilicity anodized film by UV irradiation.

CHAPTER 2
THEORIES AND LITERATURE REVIEWS

2.1. Titanium and its alloy properties for dental implant

Titanium is an allotropic element, which can exist in more than one crystallographic form such as the hexagonal close-packed crystal structure (hcp) called the alpha phase exist at room temperature and transform to the body centered cubic (bcc) or beta phase at T > 883 °C. The titanium alloys were classified in three groups; alpha, alpha-beta and beta. The elements used to stabilize the alpha phase such as aluminum, tin and oxygen. While those used to stabilize the beta phase such as niobium, molybdenum, tantalum, chromium, iron and vanadium [25].

2.1.1. Unalloyed titanium and alpha titanium alloys

These grades exhibit good elevated temperature creep properties which are weldable and hcp phase materials do not exhibit ductile-brittle transformation [25].

2.1.2. Beta titanium alloys

The bcc beta phase is ductile and the elements for beta alloys are more biocompatible than the alpha stabilizing elements [25].

2.1.3. Alpha-beta titanium alloys

Those alloys combine the metallurgically balanced amounts of both alpha and beta stabilizers. This balancing can be high tensile strength versus fracture toughness, good creep resistance versus low circle fatigue, high tensile strength versus high cycle fatigue [25].

Titanium and its alloys have been used for dental implants for several decades due to their low density, good biocompatibility, chemical stability and mechanical properties. However, there are reports about the metal ions released by corrosion of Ti-6Al-4V alloy. They may induce aseptic losing after implantation for long time, potential cytotoxic effects (ascribed to V) and Alzheimer disease (ascribed to Al). Therefore, surface modification of Ti-6Al-4V is used to resolve these problems [26].

2.2. Surface properties of biomaterials

A series of surface properties such as surface morphology, surface chemistry, surface charge and surface wettability is not a single property alone that is important factors affected to the cellular response and bone formation [27].

2.2.1. Surface morphology

The surface morphology is a key factor for interaction between implant and cell. The materials with more roughness or pores have greater surface area compared to smooth surface will interact with proteins more than smooth surface. The porous surface can be strongly bonded to bone. The bone ingrowth into porous surface can cause strong interlocking between porous surface and living tissue [27].

2.2.2. Surface chemistry

The surface chemistry is the most direct way to enhance protein adsorption and cell behavior. On titanium surface, the biological effects of surface chemistry depend on the titanium dioxide (TiO_2) layer. Anodization has been used to modify the surface chemistry of titanium. The osseointegration is related directly to implant thick TiO_2 layers resulting in a strong bone response on the implant surface [27].

2.2.3. Surface energy and wettability

The term of surface energy is closely linked with wettability (hydrophilicity and hydrophobicity). The surface energy describe the strenge of attraction between two surface, the higher the surface energy, the greater the molecular bond and the higher hydrophilicity [28] as shown in Fig. 2-1.

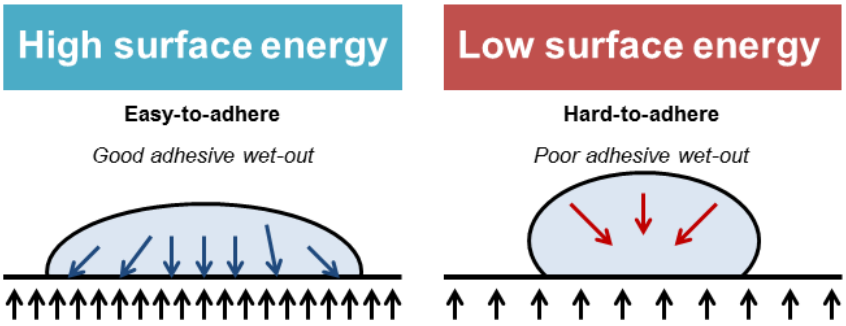

Fig. 2-1 Surface energy of materials [28]

The wettability of the materials surface is important for the proteins adsorption and cell adhesion. The important factors effect on the wettability of the materials surface such as its chemical composition, surface morphology and surface charge. Several studies have shown that the hydrophilicity surface with higher surface energy and more hydroxyl groups significantly increase in cell attachment, spreading proliferation and differentiation. Moreover, the refinement of coarse grains at the nanoscale have many atoms on the surface so there is a large surface energy [27].

2.3. Surface modification of titanium

The titanium surface was modified in order to induce biological responses at titanium surface, improving the amount and stability of biomolecules and finally, obtaining a desired tissue response. Many techniques were used to modify titanium surface such as grit blasting, chemical etching, ion beam-based process, electrochemical methods, etc. Grit blasting is technique that the microscopic particles were collided on the surface leading to the formation of porous layer on the titanium surface. Chemical etching is a technique that interacts with the native oxide layer of titanium in acidic or alkaline conditions. Ion beam-based process such as ion implantation, ion-beam-assisted deposition and plasma treatment is technique that the ion impacts on titanium surface. The advantages of technique are the possibility of accurate dose and depth control, low temperature processing and nonequilibrium process. However, the main drawback of this technique is high cost. Electrochemical methods consist of immersing the titanium in an electrolyte and connecting it to electrical circuit. This method can produce improved oxide layer and increased oxide

thickness, create porous surface leading to corrosion resistance and enhance attachment and proliferation of the cells. The advantages of this method are easy to control the process parameters, ecologically friendly and good adhesion. It can be accomplished at room temperature and coating on complex shapes is possible [12,17].

2.4. The titanium oxide films formation

2.4.1. Air formed oxide films

Titanium is a highly reactive metal so it easily produces oxide layer when it is exposed to the atmosphere such as cutting, milling or sawing. The thickness of this natural oxide film (TiO_2) on titanium is formed with 2-7 nm and high corrosion resistance to the titanium metal [20].

2.4.2. Passive oxide films

The biocompatibility of titanium and its alloys is required in surgical implant applications. When the passive oxide film is formed, the oxygen cannot react with the metal because this oxide is dense and semiconductive. Therefore, the passive film is the excellent corrosion resistant film due to the formation of a dense, protective and strongly adhere film [20].

Titanium has been improved to be a highly successful implant material. It will directly contact with the bone tissue in a process called osseointegration. The surface of titanium implant is important for a successful osseointegration and the bulk of titanium will serve in good mechanical properties which is equivalent to human bone [20].

The physiochemical property of titanium is an important factor for tissue response to the materials for example, surfaces chemistry, the oxide stoichiometry, crystal defect density and thickness [20].

The biocompatibility of implant materials depends on the chemical and electrochemical stability of surface oxide layer which interfaces with implant tissue. Phase change of titanium oxide layer formed in air from lower to higher oxides are in order: $TiO \longrightarrow Ti(O) \longrightarrow Ti_6O \longrightarrow Ti_3O \longrightarrow Ti_2O \longrightarrow TiO \longrightarrow Ti_2O_3 \longrightarrow Ti_3O_5 \longrightarrow TiO_2$. TiO_2 is very

resistant against chemical attack causing the most corrosion resistant metals. Moreover, TiO_2 is high dielectric constant resulting in stronger van der waal's bonds. TiO_2 is also catalytically active for decompose of inorganic and organic influencing attachment of biomolecule at the implant interface [20].

The passive films can be produced by either chemical or electrochemical process on titanium surface. The films show variation in oxygen stoichiometry, therefore they may contain various amounts of elements other than titanium and oxygen. Therefore, the anodic film is not necessarily stoichiometric TiO_2. These films display different compositions due to different conditions of oxidation [20].

The titanium passive oxide films are generally not only produces high corrosion resistance, but also allow physiological fluids, proteins, and hard and soft tissue to come very close and/or deposit on it directly. An increase of oxide thickness will develop the incorporation of elements such as Ca, P or S from fluid into the oxide films [20].

2.4.3. Crystal structures of Ti oxide

There are three type structure of TiO_2 such as anatase, rutile and brookite. Anatase is a tetragonal structure with a = 3.78 A^{o} and c = 9.50 A^{o}. Rutile is also a tetragonal structure with a = 4.58 A^{o} and c = 2.98 A^{o}. Brookite is an orthorhombic with a = 9.17 A^{o}, b = 5.43 A^{o} and c = 5.13 A^{o}. Rutile is the most stable phase [20].

2.4.4. The anodizing process

The anodic oxidation process can be discussed as shown in Fig. 2-2 [29]. The main reactions leading to oxidation at the anode can be written as:

At Ti/Ti oxide interface: $Ti \rightarrow Ti^{2+} + 2e^{-}$

At Ti oxide/electrolyte interface:

$2\ H_2O \rightarrow 2\ O^{2-} + 4\ H^{+}$ (Oxygen ions react with Ti to form oxide)

$2\ H_2O \rightarrow O_2$ (gas) + $4\ H^{+}\ 4e^{-}$ (O_2 gas evolves or sticks at electrode surface)

At both interfaces: $Ti^{2+} + 2\ O^{2-} \rightarrow TiO_2 + 2e^{-}$

The titanium and oxygen ions formed in these redox reactions are driven through the oxide by the externally applied electric field, leading to growth of the oxide [25].

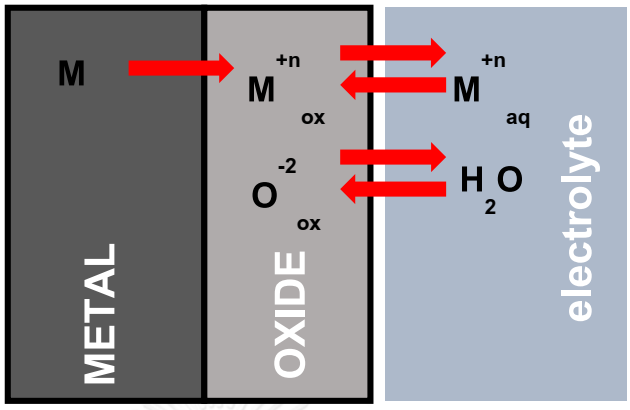

Fig. 2-2 Scheme of the passive film formation [29]

Atapour and colleagues [30] suggested that the potentials increase quickly during the initial time and then decrease slowly. This behavior shows the formation and growth of the oxide film on the substrate. Dalmau and colleagues [29] indicated that there are two different processes during passivation: growth of the oxide film and passive dissolution. An increasing of the potential causes an increasing of metallic cations, which could contribute to the growth of the oxide layer or could dissolve into the medium as shown in Fig. 2-2. Ibrahim and colleagues [19] also reported a similar phenomenon. The formation of the films contains two processes. Firstly, the corrosion increased with the reaction time and secondly the corrosion decreased because of the formation of passive oxide film on the surface.

Jiang et al. studied about plasma electrolytic oxidation treatment of titanium alloys. They found that the potential vs. time curve was used to explain the discharge phenomena during plasma electrolytic oxidation as shown in Fig. 2-3 [31]. Region I, the voltage linearly increases corresponding to a thin insulating film formation. Region II, the voltage slowly increases corresponding to decreasing in oxide film growth rate due to the competition of film growth and dissolution. Region III, the voltage increases rapidly to exceed the critical value resulting in a large number of discharge channels. At the same time, large amount of oxygen is released resulting in holes with volcano shapes. Region IV, the voltage remains stable until the end of process. The oxidation

process continues and repeats resulting in the uniform thickness. However, the strong arc discharges still appear.

Fig. 2-4 showed the detail of micro-discharge oxidation process and films structure changes during process [31]. Fig. 2-4 (a) shows a very thin natural insulating film on substrate because titanium surface always react with air and form native oxide layer on the surface [20]. After the applied voltage increases, a large number of gas bubbles are formed resulting in the formation of the porous insulating film with a columnar structure on the substrate as shown in Fig. 2-4 (b). When the voltage reaches to breakdown voltage as shown in Fig. 2-4 (c), the phenomenon of white spark discharge occurs in some regions across the insulating film resulting in the formation of a large number of small uniform micropores. After that the voltage increase and reach to a stable value. The color of sparks changes from white to yellow to orange-red, while the number of spark decrease. This stage, the films growth rate is faster which so call the microarc stage. The voltage increases resulting in increase thickness. Meanwhile the number of sparks reduces but their intensity increases inducing rougher surface morphologies as shown in Fig. 2-4 (d) and (e). During the voltage continued increasing, the strong large arc discharge appears as shown in Fig. 2-4 (f). However, in order to obtain high quality coating, this arc discharge stage should be avoided because this stage causes a splash of the coating resulting in forming porous and loose part of film coating [31].

It can be concluded that the films formation in plasma electrolytic oxidation process can be classified in three steps. The first step, a large number of discharges is produced when the breakdown voltage is reached. The electron move into the discharge channels rapidly due to high temperature and high pressure. The anionic components enter to these channels. At the same time, the alloying elements of the substrate melt and diffuse into the channels. The second step, the oxide is solidified (both on substrate surface and in electrolyte solution) due to the rapid cooling of electrolyte. Therefore, the thickness increases in the area near the discharge channels. The third step, the gases are driven from the discharge channels resulting in holes with volcano shapes. The oxidation process continues and repeats on the surface until the end of process inducing the uniform thickness [31].

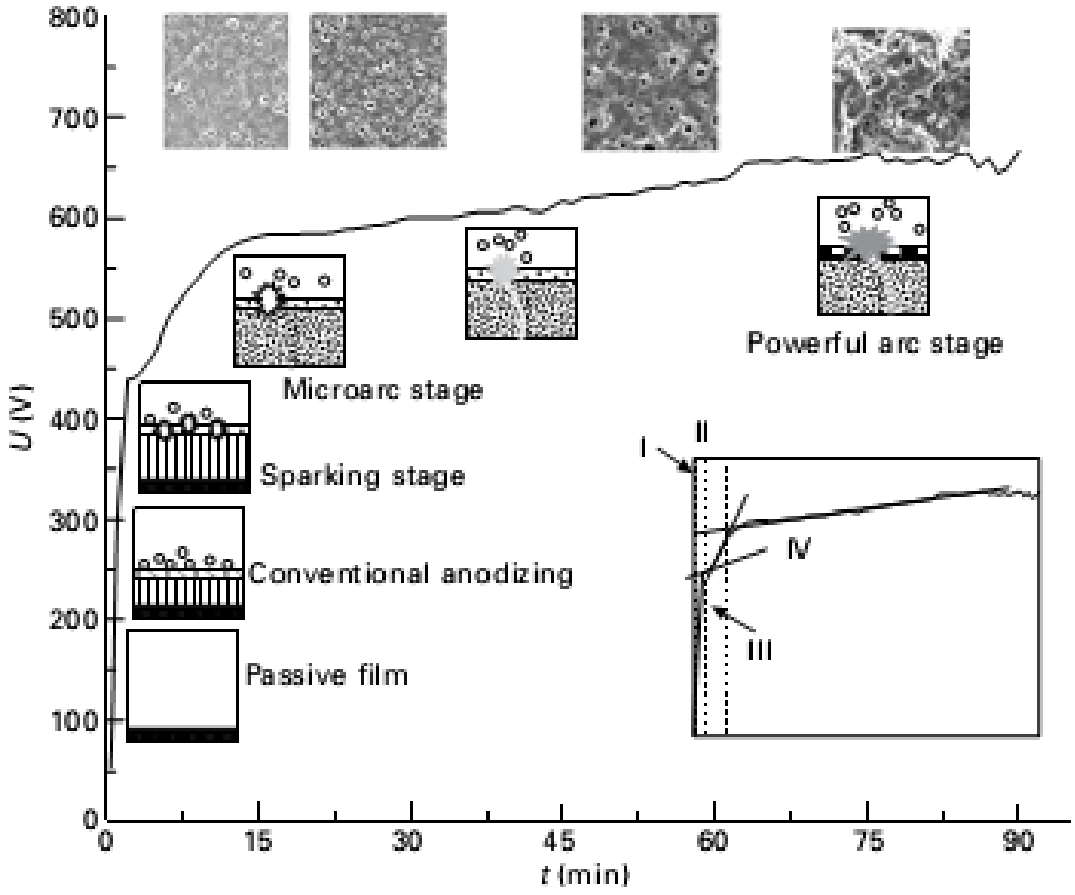

Fig. 2-3 Schematic of discharge phenomena and coating microstructure change during plasma electrolytic oxidation process [31]

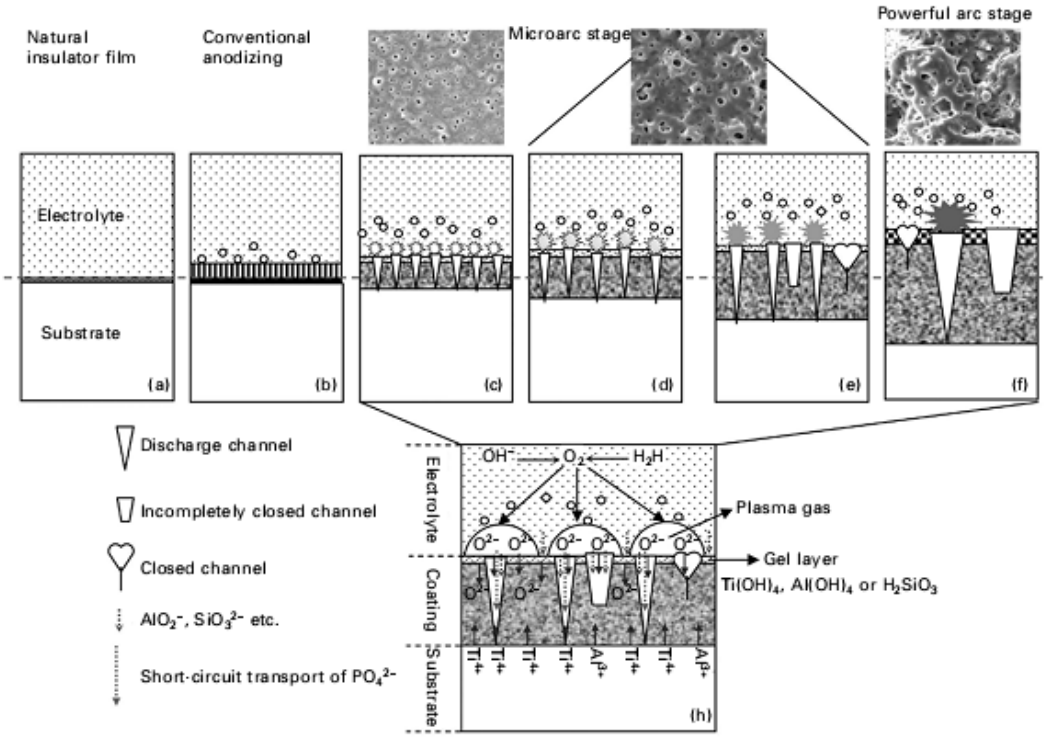

Fig. 2-4 Schematic of chemical reaction and structural changes during plasma electrolytic oxidation process of titanium alloy [31]

2.5. Effect of electrochemical parameters

2.5.1. H_3PO_4 and Ca-(and P-) based electrolytes

Electrolyte containing phosphorus such as phosphoric acid (H_3PO_4) can introduce phosphorus to the oxide films. As we have known that phosphorus is a basic component of the human bone, thus, phosphorus based electrolyte can produce porous oxide layer making easy to growth tissue into implants [32]. The oxide layer containing Ca and/or P leads to osseoinduction of new bones and becomes bioactive [33].

Song and colleagues [12] argued that the porous oxide films were fabricated on commercially pure titanium (CP-Ti) by applying a 20 mA/cm^2 current for 120 s in the 1M H_3PO_4. Fig. 2-5 showed that the oxide films increased the surface roughness and they may enhance osseointegration because of mechanical interlocking through bone growth in pores. XPS spectra in Fig. 2-6 showed that the TiP_2O_7 appeared on the oxide films (ANO-P). The shape of the Ti 2p2/3 peaks of the films was asymmetric due to mix

of Ti^{4+} and Ti^{3+} peaks. Moreover, the O 1s spectra showed the peak width of the oxide films (ANO-P) was broader than the as-received (AS-R) because of a P-O peak originated from the TiP_2O_7 structure.

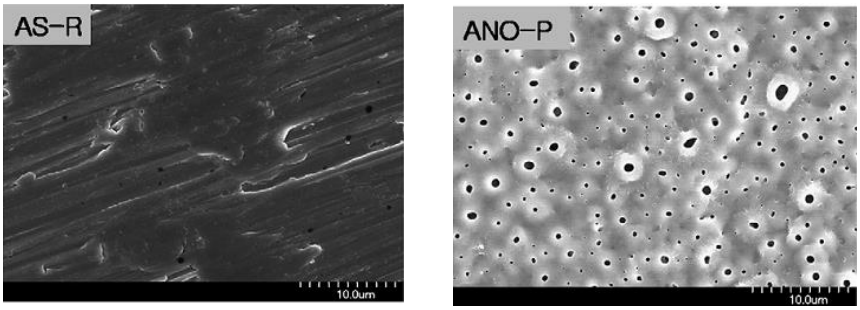

Fig. 2-5 SEM images of the as-received (AS-R) and as anodically oxidized (ANO-P) specimen surfaces [12]

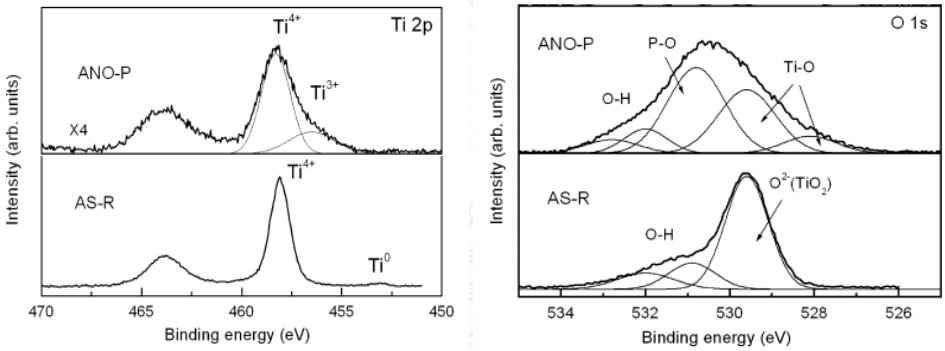

Fig. 2-6 Narrow scan XPS spectra of the Ti 2p and O 1s peak and their deconvoluted peaks fitted using the Gaussian fitting method [12]

Souza and colleagues [34] reported that the CP-Ti was anodized using Ca- and P-based electrolytes. Both 150 and 300 mA/cm^2 was applied for 100 s. The both sample layers are porous, as shown in Fig. 2-7(a-b). The pore size, the average roughness and layer thickness increases with the current density. Cracks were observed in all the layer area. The wide scan XPS spectra (Fig. 2-8) showed the main peaks of Ti, O, C, Ca and P appear at the anodic layer, in accordance with EDS results (Fig. 2-7(c)). The Ti 2p doublet spectra were similar for reference Ti, 150 and 300 mA/cm^2 samples. The TiO_2 on the reference Ti can be attributed to the native oxide layer. However, the O 1s of the anodized films differ from the reference Ti. In the

anodized films, the O 1s spectra is shifted to higher binding energies, indicating that the oxygen bonds can be present in compounds such as hydroxyl groups (Ti=OH, Ti-OH) and/or phosphates (P-O) other than TiO_2. The present of Ca and P, this can be assigned to Ca and P in calcium phosphate molecules not in hydroxyapatite.

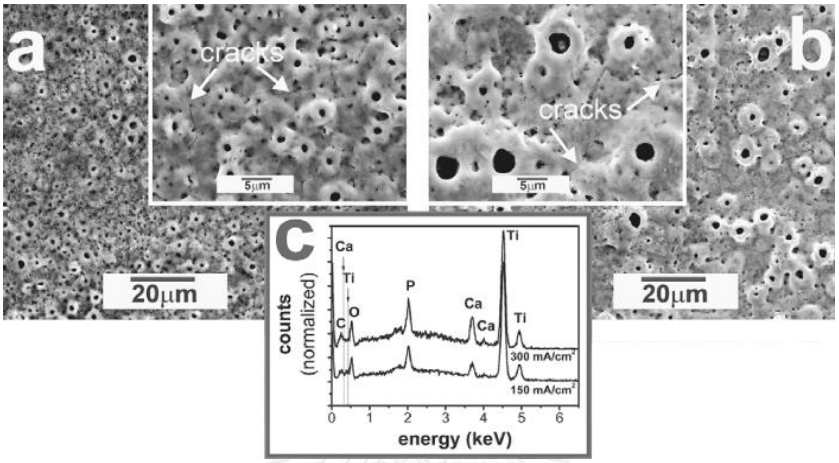

Fig. 2-7 SEM of the anodized films formed at (a) 150, (b) 300 mA/cm^2 and (c) EDS spectra [34]

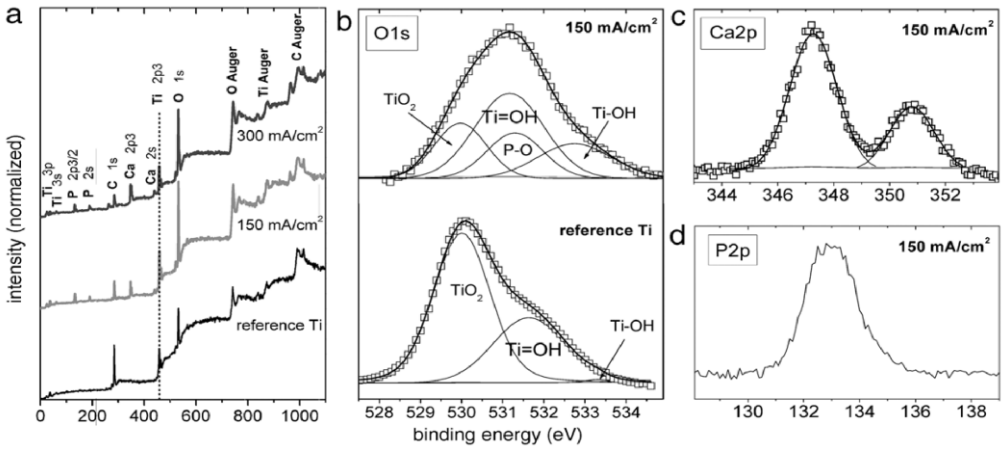

Fig. 2-8 XPS spectra of the reference Ti and the anodized films formed in Ca- and P-based electrolytes using the current densities 150 and 300 mA/cm^2 : (a) survey; (b) O 1s; (c) Ca 2p; (d) P 2p [34]

2.5.2. Ti-6Al-4V as working electrode

Masahashi and colleagues [35] reported that the anodized films on Ti-6Al-4V was prepared by anodization in a sulfuric acid electrolyte ranging from 0.02-1.2 M with a current density of 50 mA/cm^2 for 0.5 h. The pore size and roughness increase with the sulfuric acid concentration because the dissolution of the anodized films is accelerated. The Ti 2p spectrum of the anodized films is dominated by species in the Ti^{4+} and Ti^{3+} oxidation state. The O 1s XPS as shown in Fig. 2-9(a, d) is asymmetrical with a shoulder peak extending towards higher binding energies, which is attributed to hydroxyl groups. The deconvolution of O 1s XPS results in primary TiO_2 with a small amount of Al_2O_3 and vanadium oxides. The Al 2p (b, e) is composed of Al_2O_3 and another component assuming to be present as hydroxide. The V $2p_{3/2}$ (c, f) is considered of being two components of V_2O_5 and VO_2. Moreover, the intensity of the Al 2p and V $2p_{3/2}$ XPS become high with decreasing sulfuric acid concentration in the electrolyte. It is implied that the anodized films is composed of TiO_2, Al_2O_3, V_2O_5 and VO_2.

Lewandowska and colleagues[36] studied the chemical composition of the anodized films formed on Ti-6Al-4V alloy by galvanostatic method in 7% H_2SO_4 at 19 ^{o}C at a constant current density up to maximum final voltages of 12-100V and the anodized films were sputtered through the films. Fig. 2-10(a) shows the Ti 2p XPS signals from a signal for TiO_2 up to those for Ti metallic after sputtering. Fig. 2-10(b) presents the Al 2p signal during sputtering through the films; from a signal Al_2O_3 up to this for metallic Al. It is indicated that the anodized films consist of TiO_2 and Al_2O_3. However, vanadium was not be detected within the films.

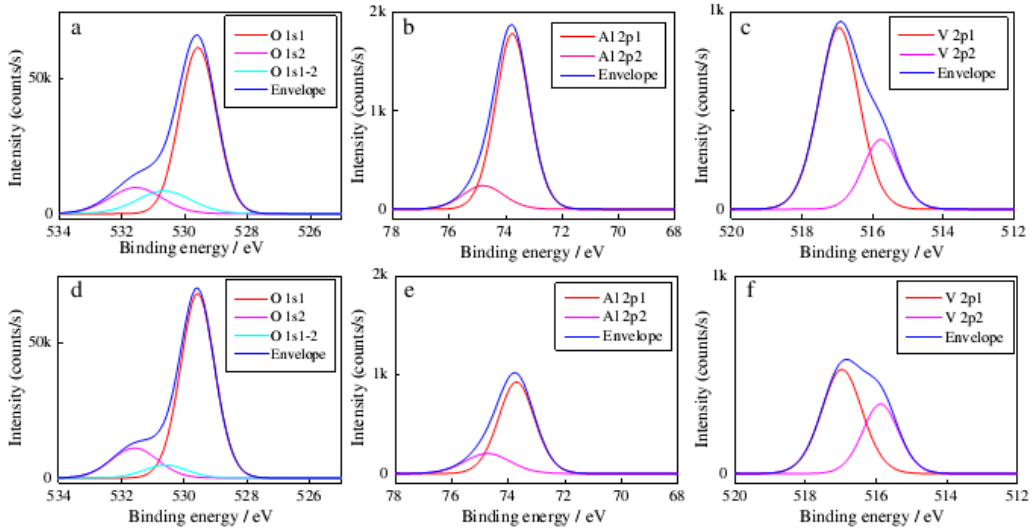

Fig. 2-9 O 1s (a, d), Al 2p (b, e) and V $2p_{3/2}$(c, f) XPS spectra of the annealed anodic oxides prepared in an electrolyte of 0.1 M (a–c) and 1.2 M (d–f) sulfuric acid [36]

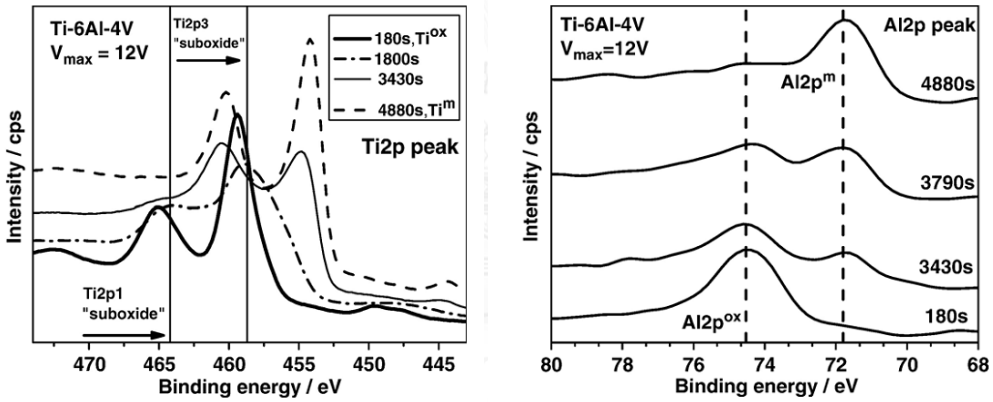

Fig. 2-10 Change in shape and position of the (a) Ti 2p and (b) Al 2p XPS peak with sputtering for an anodic oxide film covered Ti-6Al-4V sample [36]

2.5.3. Applied low voltage

Several works reported that the anodized films were produced at high current density or high voltage. However, there were disadvantages such as high energy, high expenses and dangerous. Therefore, the low current density and low voltage were considered to produce the anodized films in order to solve these problems.

Ibrahim and colleagues [19] reported that the anodic oxide film formed on CP-Ti in NaOH solutions at -0.5 V and 1.2 V. The composition from the XPS spectra of the passive oxide film consists of TiO_2 and a mixture of suboxides of Ti_2O_3 and TiO. Nevertheless, the surface morphology did not change after anodization.

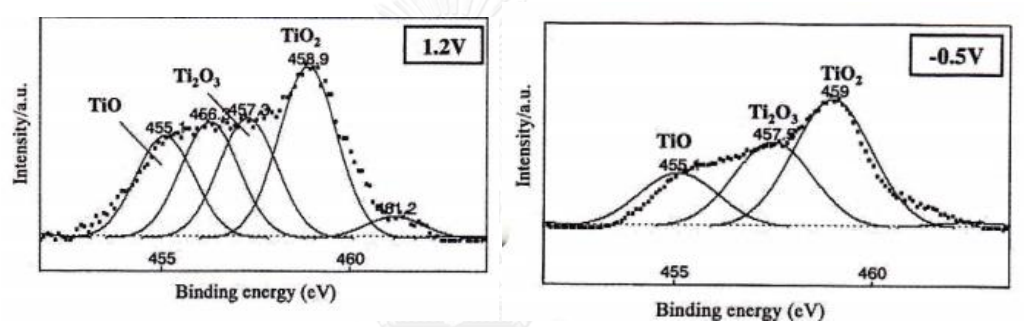

Fig. 2-11 XPS spectra of the anodized films formed at 1.2 V and -0.5 V in NaOH [19]

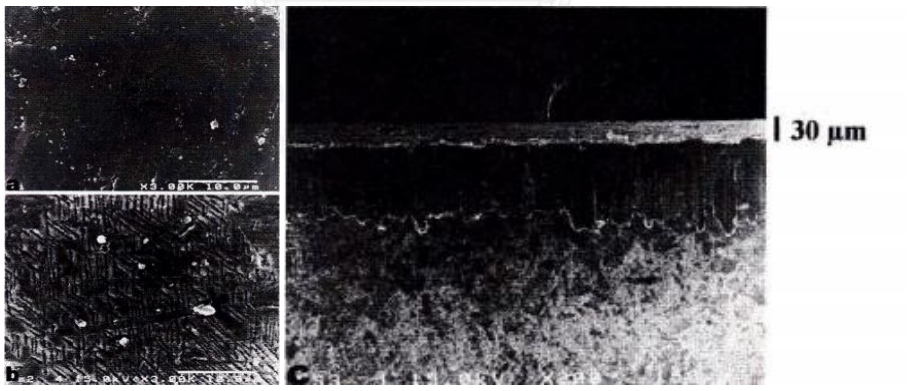

Fig. 2-12 Surface morphology of Ti before and after anodization [19]

2.5.4. Galvanostatic and potentiostatic method

Quintero et al. [37] studied the effect of electrochemical parameters on the morphology and chemical compositions of anodic films obtained on CP Ti, in both galvanostatic and potentiostatic mode in 1.5 M H_2SO_4/0.3 M H_3PO_4 as an electrolyte in order to find the better control of morphology and properties of the anodic films.

Fig. 2-13 a) shows the curves of anodizing process for galvanostatic mode in three different regions. The region I, potential linearly increases, corresponding to an insulating films formation. The region II, the slope of curve deceases. In this region, the formation of sparks and gas evolution on the anodic films begins, resulting in porous films formation. In the region III, the potential remains constant until the end of process. Fig. 2-13 b) shows the anodizing process of the anodic films formed by potentiostatic mode. The region I, the current density increases instantaneously, where an insulating films is formed. The region II, the current density decreases. When the anodizing potential is equal or higher than 100 V, there are both the formation of sparks on surface and the evolution of gas in the system start. In region III, the current slowly decrease [37].

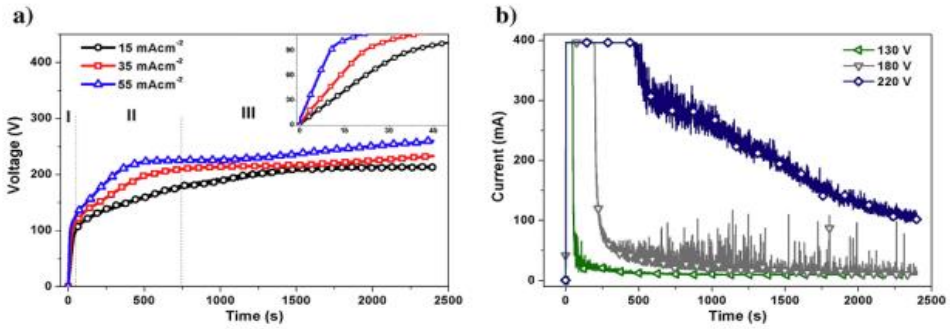

Fig. 2-13 Anodizing process of the anodic films formed by a) galvanostatic mode and b) potentiostatic mode [37]

The anodic films formed by galvanostatic mode applied current density of 15 mA/cm^2 that the potential reached to around 215 V and the anodic films formed by potentiostatic mode applied potential of 220 V was compared in order to understand the effect of potential on the change in surface morphology and chemical composition.

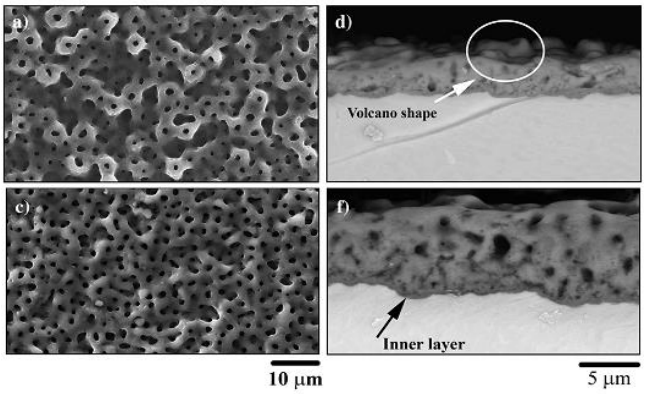

Fig. 2-14 Surface morphology and cross-section of (a, b) the anodic films formed at 15 mA/cm^2 reached to potential of 215 V and (c, d) the anodic films formed at 220 V [37]

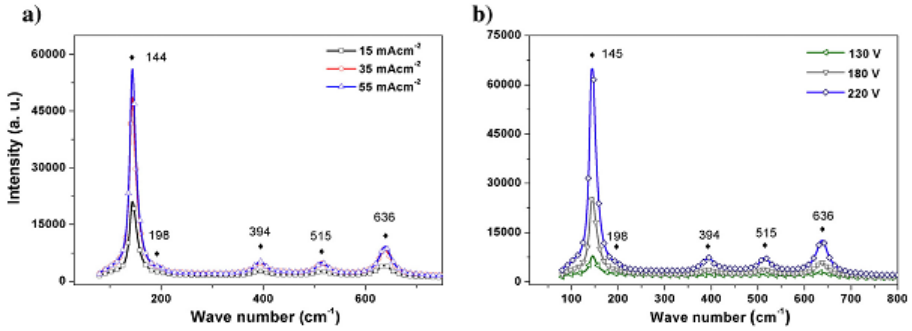

Fig. 2-15 Raman spectra of the anodic films formed by a) galvanostatic mode and b) potentiostatic mode [37]

Fig. 2-14 showed that the anodic films formed at 220 V shows uniform circular pores similar to a volcano with average diameter and thickness are higher than the anodic films formed at 15 mA/cm^2 reached to potential of 215 V. Moreover, the incorporation of phosphorus of the anodic films formed by potentiostatic mode (5.20 %) is higher than in galvanostatic mode (4.19 %). It may be because of higher thickness of the anodic films. While, the porosity of the anodic films formed at 15 mA/cm^2 reached to potential of 215 V (14.02 %) have more porosity than the anodic films formed at 220 V (11.63 %) [38]. The Raman spectroscopy showed that the anatase TiO_2 phases were observed at wave number of 144 cm^{-1}, 198 cm^{-1}, 394 cm^{-1}, 515 cm^{-1} and 636 cm^{-1} as shown in Fig. 2-15 [38]. Therefore, it is not clear which potentials from

galvanostatic mode or potentiostatic mode influence the changes in the surface morphology and chemical composition [38].

2.6. Improving Hydrophilicity by UV irradiation

2.6.1. Basic principles of UV induced hydrophilicity on TiO_2 surfaces

There are two mechanisms of UV irradiation enhancing hydrophilicity on TiO_2 surface. The first mechanism is through the formation of oxygen vacancies and the second is through the removing hydrocarbon on the TiO_2 surface. The band gab energy of TiO_2 is 3.2 eV and 3.0 eV for anatase, rutile and brookite, respectively. When the TiO_2 films absorbs UV light which have energy more than band gap energy of TiO_2. This energy excites the electrons of the valence band of TiO_2 and promotes these electrons to the conduction band. Therefore it creates pairs of the negative-electrons (e^-) and the positive-holes (h^+). The electrons tend to reduce the Ti^{4+} to Ti^{3+} and the holes react with the bridging site oxygen and oxygen atom is released, resulting in oxygen vacancies. Then water molecule can replace oxygen vacancy and absorb hydroxyl group and induce hydrophilicity on the TiO_2 films [21,22].

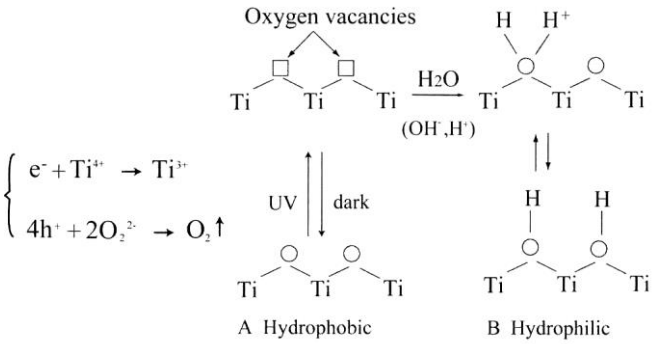

Fig. 2-16 Effect of UV-induced hydrophilicity due to oxygen vacancy formation on TiO_2 surface [21]

Another one is through the removing hydrocarbon. The schematic of mechanism for UV-induced hydrophilicity on TiO_2 is shown in Fig. 2-17 [23]. In the top of Fig. 2-17, the TiO_2 film shows hydrophobic property because of a monolayer of adsorbed hydrocarbon molecules as shown by thin black symbols. When the UV was irradiated on the TiO_2 surface, the coverage of adsorbed hydrocarbon will slowly

decrease, probably near zero because it was decomposed by photocatalytic activity [23,24]. Then the water was adsorbed on the surface films. Therefore the TiO_2 film shows hydrophilic property after UV irradiation because of removing hydrocarbon.

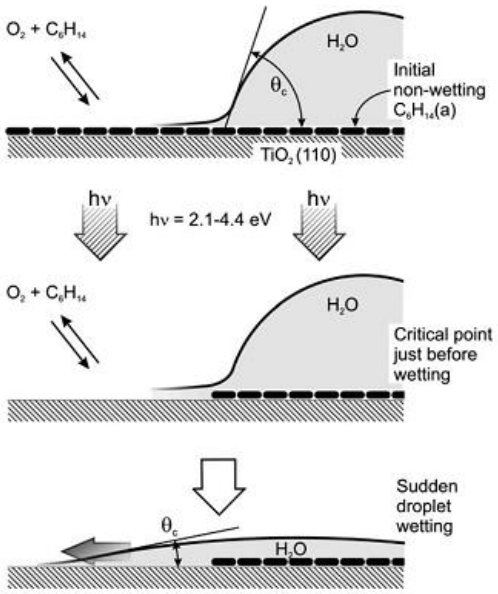

Fig. 2-17 Schematic interpretation of UV induced hydrophilicity due to removed hydrocarbon on TiO_2 [23]

2.6.2. Surface characterization after UV irradiation

Han et al. [22] has shown that the UV irradiation on MAO enhanced the hydrophilicity due to the conversion of Ti^{4+} to Ti^{3+} and the generation of oxygen vacancies. The micro-arc oxidized (MAO) titania was irradiated by UV for 0.5 h to 2 h. Fig. 2-18 shows only the intensity of O 1s peak at 532.8 eV becomes strong after UV irradiation, especially in the case of irradiation for long time. It is suggested that the increasing intensity of O 1s peak at 532.8 eV is not related with TiO_2. The percentage area of C 1s at 288.9 eV was not change after UV irradiation as shown in Table 2-1. It is suggest that the content of O-C=O was not change after UV irradiation. It is indicated that the increasing intensity of O 1s peak at 532.8 eV is important factor to generate Ti-OH groups on the TiO_2 surface after UV irradiation.

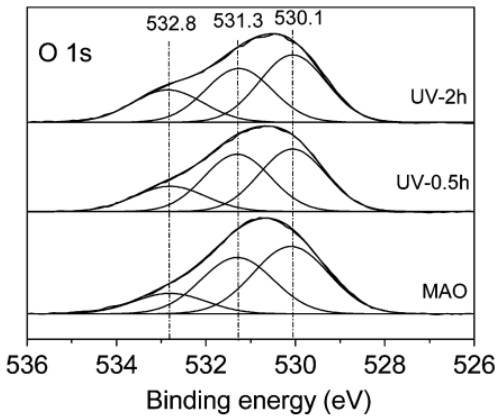

Fig. 2-18 O 1s XPS spectra of the MAO, UV-0.5 h and UV-2 h coatings [22]

Table 2-1 Percentage areas of the decovoluted peaks in the O 1s XPS spectra and percentage area of the deconvoluted 288.9 eV peak in C 1s XPS spectra of the MAO, UV-0.5 h and UV-2 h coatings [22]

Sample	Percentage areas of the deconvoluted peaks in O1s XPS spectra			Percentage area of the deconvoluted 288.9 eV peak in C1s XPS spectra
	530.1 (eV)	531.3 (eV)	532.8 (eV)	
MAO coating	47.7	38.4	13.9	5.4
UV-0.5 h coating	42.6	39	18.4	6.2
UV-2 h coating	43.4	34.7	21.9	5

Guillemot et al. [39] suggested that increase in Ti 2p3/2 at lower binding energy and in O 1s at higher binding energy is defect surface. The full-width at half-maximum (fwhm) of Ti 2p peak showed Ti^{4+} affected by annealing temperature. The broadening peak may be TiO_2 structure is induced lattice vibrations by thermal and Ti^{3+} defects may be generated on the surface.

Zhao et al. [40] indicates that the oxygen is essential in the hydrophilic reactions. They supposed that adsorbed oxygen could catch photoexcited holes, and promoted the separation of electron–hole pair, which was favorable to the conversion of the surface hydrophilicity. The O^{2-} decreased and the hydroxyl group increased after UV irradiation because UV irradiation generated defect surface. Therefore, the binding

energy of Ti shift to lower binding energy and the binding energy of O shift to higher binding energy.

Masahashi and colleagues [16] prepared the anodized films on CP-Ti by galvanostatic method until the conversion voltage reached from 80-220 V using 0.1 mass% sulfuric acid as an electrolyte. The annealed oxides showed low contact angles less than 10 ^{o} after UV illumination. The Ti 2p XPS reveals that the surface is composed of titanium oxide and the symmetrical shape of the Ti 2p suggests that reduced Ti^{3+} ions are not present in the oxides. The oxides show an asymmetric O 1s at approximately 530.5 eV is ascribed to oxygen in TiO_2 and a shoulder band on the higher binding energy side at approximately 532.4 eV of the main peak due to the adsorption of hydroxyl groups. This suggests that the surface of the annealed oxide interacts strongly with the hydroxyl groups and also show hydrophilic property.

Table 2-2 Peak position (eV) and percentage contents of the surface species on TiO_2 thin films before (a) and after (b) UV irradiation [16]

	Ti^{4+}		Ti^{3+}		TiO_2	
	Position	%Area	Position	%Area	Position	%Area
a	459.7	90.1	458.4	9.9	530.8	65.0
b	459.7	85.8	458.4	14.2	530.8	59.3

OH		H_2O & C–O	
Position	%Area	Position	%Area
531.8	27.9	533.1	7.1
531.8	34.1	533.1	6.6

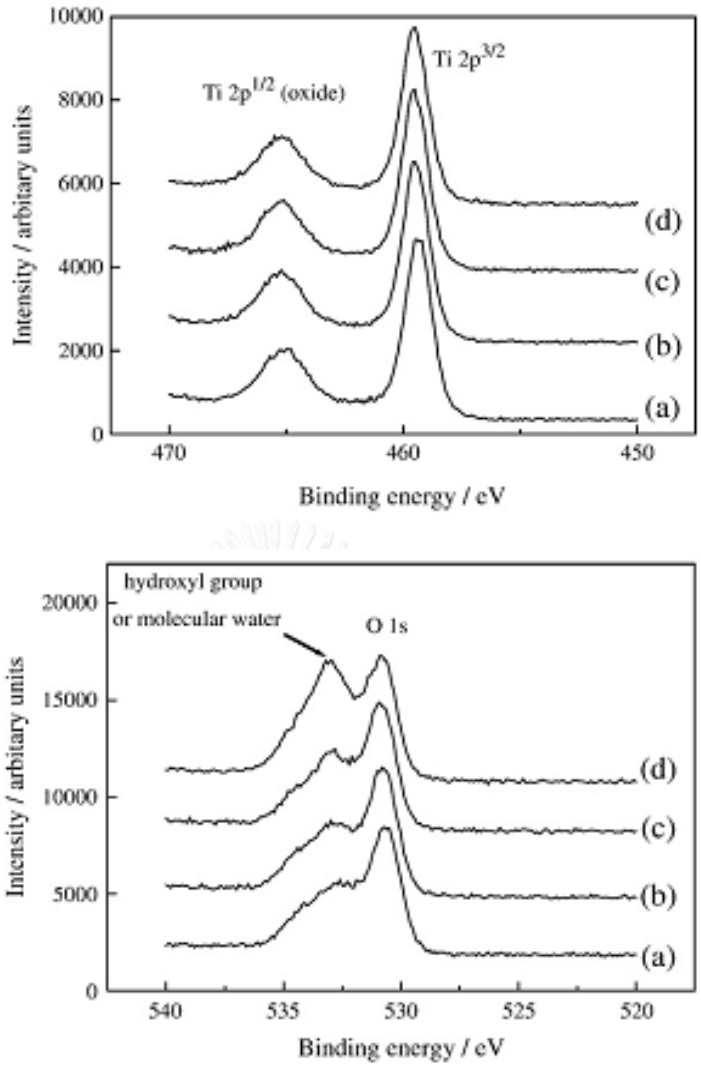

Fig. 2-19 Ti 2p and O 1s XPS spectrum of the annealed oxides for the following conditions: before illumination (a), under UV illumination for 5 min (b), for 30 min (c), and for 1h (d) [16]

UV irradiation could also enhance hydrophilicity of the anodized films via formation of oxygen defects on the film surface as shown in Fig. 2-20. A small portion of the trapped hole may react with TiO_2 itself, breaking the bond between the lattice titanium and oxygen ions by the coordination of water molecules at the titanium sites. The coordinated water molecules release a proton for charge compensation, and then a new OH group forms, resulting in the increase in the number of OH groups on the surface and directly results in the increase of hydrophilicity [41].

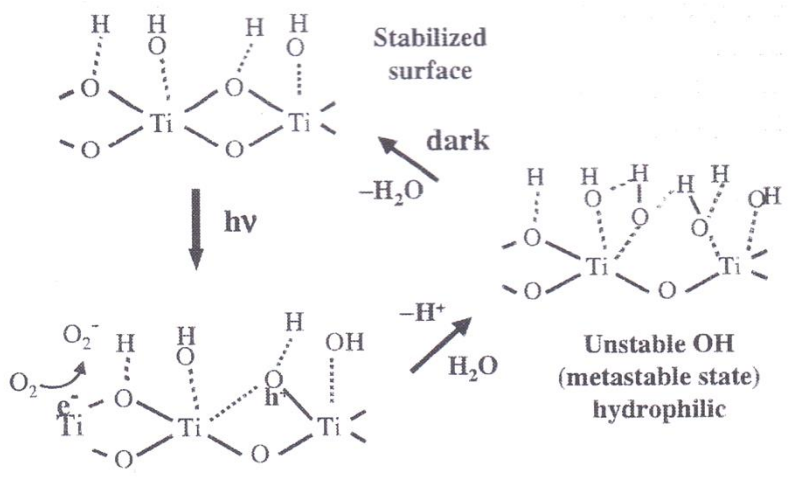

Fig. 2-20 Photocatalytic activity of TiO_2 [41]

Aita et al. [24] suggest that UV irradiation enhances bioactivity on titanium surface due to UV-catalytic progressive removal of hydrocarbons from the TiO_2 surface as shown in Fig. 2-21. The acid-etched surface required only 1 h UV treatment, while the machined surface required 48 h for decreasing in contact angle to 0°. The 0° contact angle of H_2O maintain on the surface for 7 days in the dark. The Ti $2p_{3/2}$ peak was slightly shifted to a higher binding energy for the acid-etched surface compared with the machined surface. It is may indicated that the acid-etched surface is covered by a thicker oxidized layer. XPS spectra of the acid-etched titanium surface revealed that the C 1s peak decrease with increase of UV irradiation time, whereas Ti 2p and O 1s peaks increase. Moreover, the shoulder peaks such as Ti^{3+} or Ti were not appeared in the lower binding energy. It is indicated that titanium substrates were fully oxidized to form stoichiometric TiO_2 and a decrease of percentage of carbon with an increase of UV irradiation time was due to photocatalytic removal of hydrocarbons.

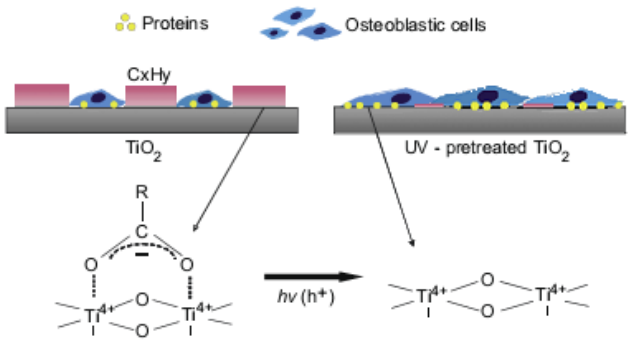

Fig. 2-21 Schematic description of a protein adsorption, and attachment and spread of osteoblasts enhanced by UV irradiation on TiO_2 [24]

Fig. 2-22 shows that the intensity of the peak at 3433 cm^{-1} (-OH stretching vibration) decreased after UV irradiation. It is indicated that the –OH bonding was partly decomposed because of UV irradiation. Moreover, the very weak peak at 3000 cm^{-1} (CH_2 and CH_3 groups stretching vibration), 1660, 1563 and 1446 cm^{-1} (C-O stretching and COO vibrations) and 1275 and 1350 cm^{-1} (C-O stretching vibration) were eradicated by UV irradiation. It was suggested that the peak intensity of carbon-based organics decreased rapidly after UV irradiation. Therefore, UV irradiation could remove the organics in the films by photochemical reaction and photoexcited thermal effect [42].

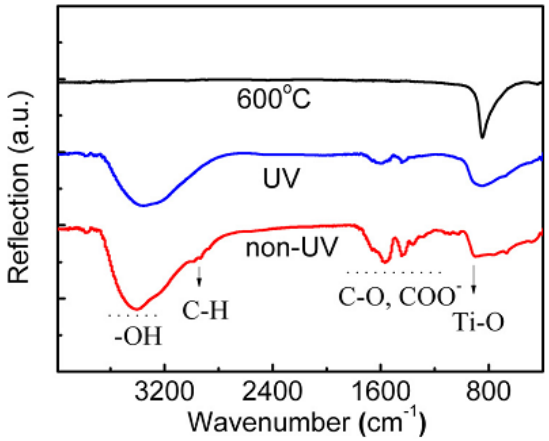

Fig. 2-22 FTIR spectra of TiO_2 non-UV films, UV films and 600 °C-films [42]

The intensity of peaks at 3089 and 3068 cm^{-1} (benzene peak) decreased after UV irradiation. The peaks at 2360 and 2320 cm^{-1} (CO_2) and 1640 cm^{-1} (H_2O) increased

as the reaction progressed. The broad absorption in the range of 3800-3500 cm^{-1} increased. It is indicated that the interacting hydroxyl groups regenerated and adsorbed molecules on the surface. The peak of the bending vibration of adsorbed water increased in the 1750-1500 cm^{-1} range. At the same time, a small peak at 3740 cm^{-1} (the isolated hydroxyl bands) increased. These results indicate that some adsorbed surface species molecules are released from the adsorption sites but probably remain on the TiO_2 sample surface by water incorporation. In addition, the new bands at 1587, 1491 and 1254 cm^{-1} appeared after UV irradiation. These results indicate that weakly adsorbed phenol was formed as the reaction progress, which led to the progressive deactivation of the catalyst in the gas-solid system [43].

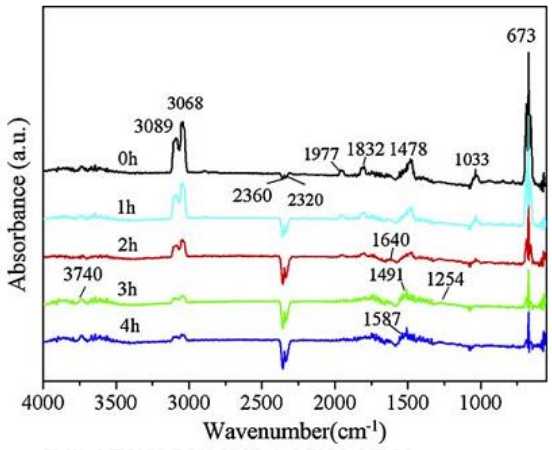

Fig. 2-23 IR spectra of the photocatalytic degradation of benzene on the TiO_2 microballs under 0, 1, 2, 3 and 4 h UV irradiation [43]

The absorption peaks of 600 and 529 cm^{-1} (Ta-O-Ta and Ta-O stretching) shift to higher wavenumber after UV irradiation as a result of densification of the films. A broad band in the 800-1000 cm^{-1} range is due to suboxides TaO and TaO_2. This peak is dispersed after UV irradiation. The broad band in the 3100-3400 cm^{-1} range shows the dehydration and dehydroxylation of the polymers within the film before and after UV irradiation [44].

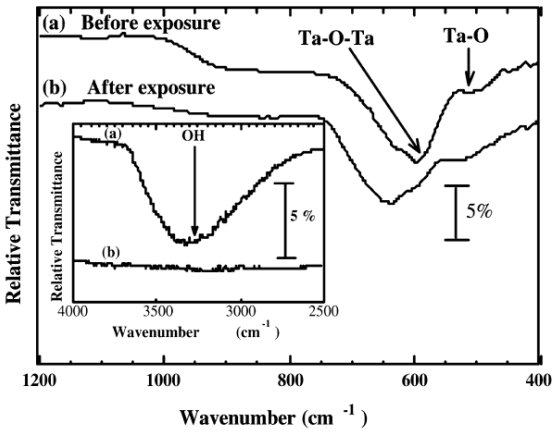

Fig. 2-24 FTIR spectra of the films before and after UV irradiation and the insert picture shows, a) films before UV irradiation and b) films after UV irradiation [44]

After UV irradiation, the intensity peak at 1681 cm^{-1} (C=O, carbonyl group) decreased due to bond breakage at carbonate site with the elimination of carbon monoxide/carbon dioxide. Moreover, the presence of TiO_2 nanoparticles in sample lead to a decrease in intensity of the peaks at 436 cm^{-1} (Ti-O-Ti band), 650 cm^{-1} (Ti-O band) and 1681 cm^{-1} (C=O band) [45].

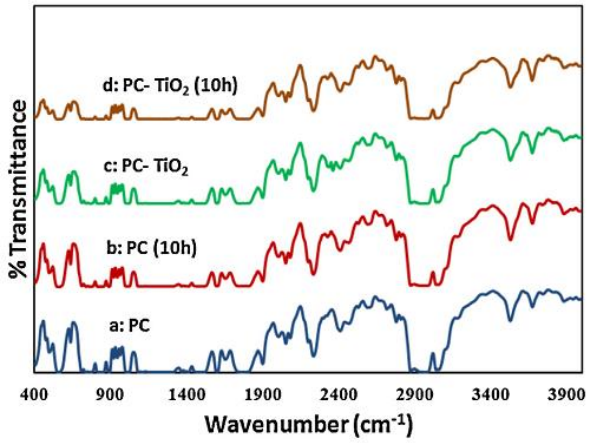

Fig. 2-25 FTIR spectra of a) bare PC, b) PC irradiation for 10 h, c) PC-TiO_2 nanocomposite (1 wt%) and d) PC-TiO_2 nanocomposite (1 wt%) irradiation 10 h [45]

After UV irradiation, the water contact angle of PC–TiO_2 nanocomposite decreased. The surface energy increased. The SEM images showed the surface roughness of PC-TiO_2 nanocomposite increase. Moreover, the oxygen content also increase after UV irradiation observed by XPS. Therefore, the water contact angle

decrease due to both the increment of oxygen content and surface roughness. The low contact angle of solid surface is due to the high surface energy resulting in hydrophilicity[45].

Table 2-3 Contact angle and surface energy of the films after UV irradiation [45]

Material and Treatment time	Contact angle (°)	Total surface energy ($mN\,m^{-1}$)
PC, PC–TiO_2	92, 90	43.66, 44.57
PC, PC–TiO_2 4 h irradiation	48, 41	59.66, 63.57
PC, PC–TiO_2 6 h irradiation	40, 28	62.23, 69.53
PC, PC–TiO_2 8 h irradiation	31, 20	66.57, 73.26
PC, PC–TiO_2 10 h irradiation	29, 16	68.43, 75.43
PC, PC–TiO_2 15 h irradiation	26, 12	69.90, 77.95

Han et al. reported that the morphology and grain size of the MAO coating after UV irradiation did not change as shown in Fig. 2-26 [22].

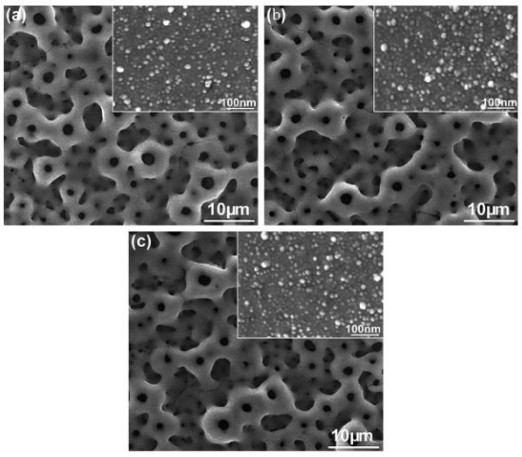

Fig. 2-26 Surface morphologies of the MAO (a) before UV and after UV (b) 0.5 h and (c) 2 h [22]

2.7. Improving OH groups on the anodized films

2.7.1. Ethanol Oxidation

The kinetics of the ethanol oxidation reaction are improved by the greater availability of OH^- ions in solution and/or a higher OH^- coverage of the electrode surface [46]. Therefore, the formation of Ti-OH groups of the anodized films is formed after ethanol treatment as following ethanol oxidation [46]:

$$CH_3CH_2OH + 3OH^- \rightarrow CH_3CO_{ads} + 3H_2O + 3e \quad (1)$$

$$OH^- \rightarrow OH_{ads} + e \quad (2)$$

$$CH_3CO_{ads} + OH_{ads} \rightarrow CH_3COOH \quad (3)$$

$$CH_3COOH + OH^- \rightarrow CH_3COO^- + H_2O \quad (4)$$

Ethanol oxidation is determined by the degree of CH_3CO_{ads} and OH_{ads} coverage. OH_{ads} adsorbed on the electrode is important for ethanol oxidation. OH_{ads} adsorbed on the electrode will take the place of CH_3CO_{ads} if the concentration of OH^- is too high, so OH_{ads} is available in excess and CH_3CO_{ads} is insufficient at the electrode surface [46].

CHAPTER 3

EXPERIMENTAL PROCEDURE

3.1. Materials

The detail of the chemical using in this work shows inTable 3-1.

Table 3-1 Chemical used in this work

Chemical	Company	MW (g/mol)	Density (g/cm^3)
HF	Riedel-de Haen	20.01	1.14
H_3PO_4 85%	Merck	98	1.71
MCPM, 85% purity	Sigma-Aldrich	252.07	-
Glycerol 99%	Sigma-Aldrich	92.09	1.25
Ethanol 99.5%	Sigma-Aldrich	46.07	0.79
Ti-6Al-4V	K V M Heating Element Co., Ltd.		
Implant	Nobel biocare		

3.2. The anodized films preparation

3.2.1. The working electrode preparation

Ti-6Al-4V plates were used as a working electrode. The Ti-6Al-4V with a size of 1 × 8 × 20 mm was drilled and polished with SiC paper. After that, it was washed by reverse osmosis water in an ultrasonic bath for 15 minutes and dried at room temperature. Ti-6Al-4V plate was connected with the Cu wire and glass tube by glue. Prior to the anodization, the working electrode was etched in 1 M HF for 1 minute in order to remove the native oxide films on the surface and finally washed in reverse osmosis water.

3.2.2. The electrolyte preparation

The two different types of electrolytes were prepared in this study. One was the 1M H_3PO_4 solution and the another one was 1M MCPM (the mono-calcium phosphate monohydrate ($Ca(H_2PO_4).H_2O$; MCPM)) solution. The MCPM electrolyte was prepared by adding analytical grade MCPM (Sigma-Aldrich) in reverse osmosis water. The electrolyte was stirred with a magnetic stirrer at elevated temperature (60-80 ^{o}C) for 2 h to enhance the dissolution of calcium phosphate. After cooling the calcium phosphate suspension to room temperature, the membrane filter was used to filter out the suspension. This filtered solution was used as electrolyte. The pH of electrolyte was about 2.

3.2.3. The anodization

The two different equipment were set up for preparing the anodized films at low and high conditions. The anodizing apparatus at low current density or voltage was set with an Ag/AgCl reference electrode, Pt-counter electrode and Ti-6Al-4V as a working electrode. The three electrode cells were set as shown in Fig. 3-1. According to the set-up, the anodized films were performed with current density of 0.25-2 mA/cm^2 or voltage of 2-10 V, for 30 min for both types of electrolytes (1 M H_3PO_4 or 1 M MCPM) at room temperature. The electrochemical behavior was measured by a potentiostat-galvanostat (Methrom, Autolab, PGSTAT30) connected to a computer and operated by the GPEs program. After anodization, the anodized films formed on the Ti-6Al-4V surface was rinsed with reverse osmosis water and dried at room temperature. The anodized films were kept in desiccator.

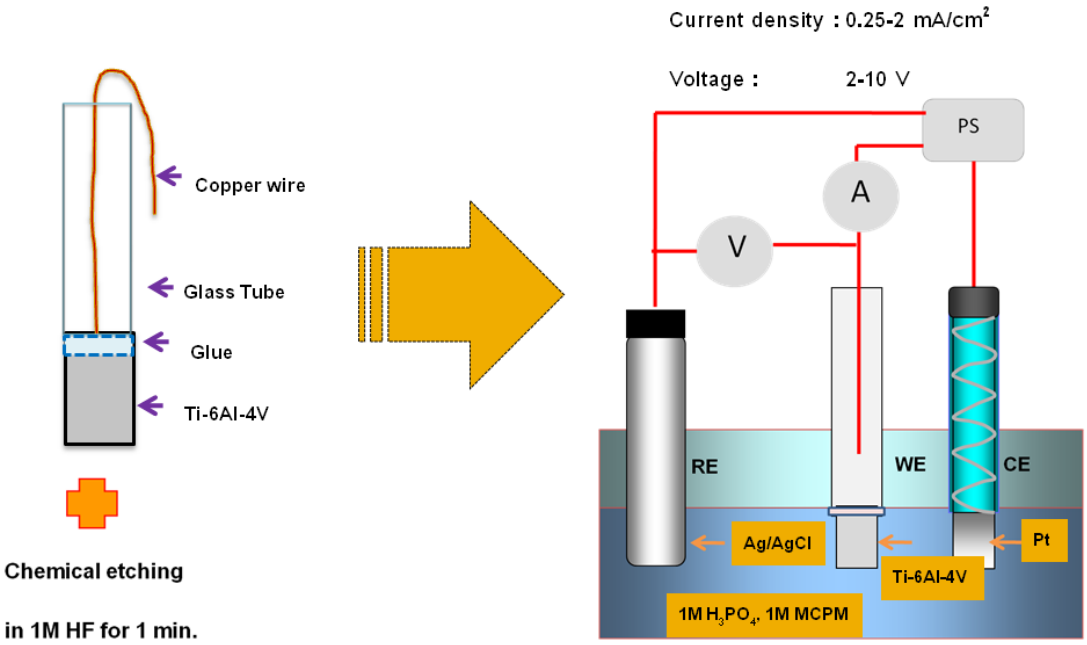

Fig. 3-1 Anodizing process at low current density or voltage

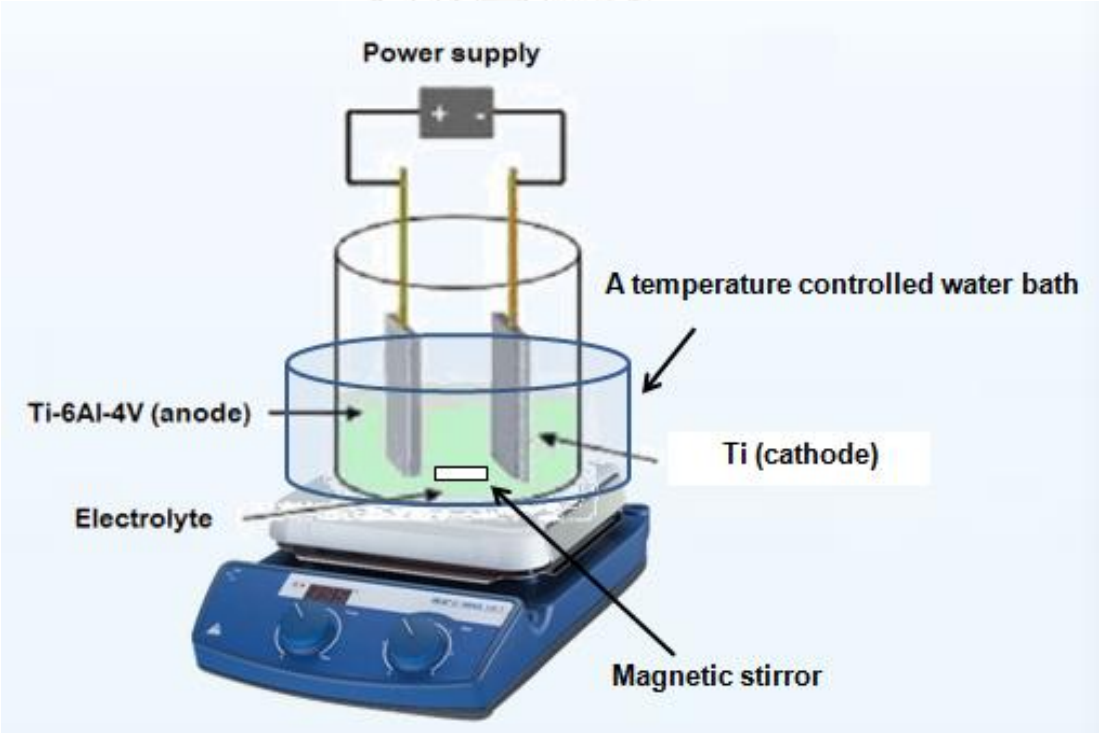

Fig. 3-2 Anodizing process at high current density or voltage

For anodizing process at high current density or voltage as shown in Fig. 3-2, a DC power supply was used as a power source. An ammeter and volmeter were used to measure current and voltage respectively during the anodizing process. The electrochemical cell consisted of a glass beaker placed in a temperature controlled water bath and the electrolyte was stirred with a magnetic stirrer. A CP-Ti plate was used as cathode. The Ti-6Al-4V as working electrode was connected to the power supply and immersed in the electrolyte. Anodization was performed in either 1M H_3PO_4 or the monocalcium phosphate monohydrate ($Ca(H_2PO_4).H_2O$; 1M MCPM) solution at the current densities of 20-80 mA/cm^2 or initial voltage of 20-150 V for 30 min. Then the sample was rinsed with the reverse osmosis water to clean up in the final step and kept in desciccator.

3.3. The anodized films and the TiUnite dental implant characterizations

3.3.1. Contact angle measurement

The hydrophilicities of the different surfaces were determined by measuring the contact angles with one drop of reverse osmosis water using contact angle meter (CAM_PLUS Tantec).

The contact angle of the sample before and after UV irradiation for 2, 4, 8 and 24 h was observed using the sessile drop method with a 5 μL distilled water and contact angle meter (Model: Simage03, Excimer Inc, Kanagawa, Japan).

Numerical data are presented as the mean ± standard deviation (SD), derived from the indicated number of independent repeats. Statistical analysis was performed by SPSS V.13 software. Significant differences in the contact angles were determined by one-way analysis of variance (ANOVA) and followed by Bonferroni post hoc tests for multiple comparisons. A p-value of < 0.05 was considered to be significant.

3.3.2. Scanning electron microscopy (SEM)

The SEM (JSM-6480LV (JEOL) and the SEM (KEYENCE VE-9800) were used for morphological analysis. The SEM mode with an acceleration voltage of 15 kV was selected for SEM analysis.

3.3.3. X-ray photoelectron spectroscopy (XPS)

X-ray photoelectron spectroscopy (XPS; AXIS ULTRA^{DLD}, Kratos analytical, Manchester UK.) was used for surface species analysis. The spectra were collected using a monochromatic Al K_α radiation at 1.4 keV. In all cases, the X-ray photoelectron spectra were referenced to the C 1s peak at binding energy = 285 eV.

The chemical species on the anodized films surface before and after UV irradiation and the TiUnite dental implant were examined by X-ray photoelectron spectroscopy (XPS; JPS-9000SX, JEOL Ltd.). Al K_α X-rays (1486.6 eV) was used as an X-ray source. The obtained XPS spectra were corrected to the C 1s at binding energy of 284 eV.

3.3.4. Fourier Transform Infared Spectroscopy (FT-IR)

The functional groups of the films were measured by Fourier Transform Infared Spectrometer (Thermo Scientific Nicolet 6700 FT-IR spectrometer and JASCO FT/IR-4100) in Attenuated Total Reflection (ATR) mode using a diamond plate.

3.3.5. X-ray diffraction (XRD)

The phase components of the anodized films and the TiUnite dental implant were analyzed by X-ray diffraction (XRD; RINT 2200 Ultima III diffractometer, Rigaku Corp., Tokyo, Japan).

3.3.6. Raman spectroscopy

The crystalline phases in the anodized films and the TiUnite dental implant were performed using Raman spectroscopy with a LabRAM HR 320 (Horiba/Jobin Yvon).

3.4. Surface energy

For study about surface energy, the water contact angle and glycerol contact angle were used. The Owens-Wendt theory was used to calculate surface energy as shown in Eq. 1 and 2 [47].

$$1 + \gamma_l \cos\theta = 2[(\gamma_s^d \gamma_l^d)^{1/2} + (\gamma_s^p \gamma_l^p)^{1/2}] \quad (1)$$

$$\gamma^t = \gamma_s^d + \gamma_s^p \quad (2)$$

Where γ_l is the surface tension of liquid.

γ^p_s and γ^d_s are the polar and dispersion terms of solid surface energy, respectively.

γ^p_l and γ^d_l are the polar and dispersion terms of liquid surface tension, respectively.

In this study, the water and glycerol were used as polar liquid with specific surface tension as shown in Table 3-2 [47].

Table 3-2 Surface tension parameters for test liquids [47]

	Dispersive component (γ_l^d) (mN/m)	Polar component (γ_l^p) (mN/m)	Total (γ_l^t) (mN/m)
Water	21.8 ± 3	51	72.8
Glycerol	37 ± 4	27	64

3.5. UV irradiation

The UV light treatment was performed using 9 W lamp (Toshiba, Japan); (λ = 254 nm). The samples were placed at 15 cm distance from the UV source. Irradiation times were for 2, 4, 8 and 24 h and the samples were stored in the dark until the hydrophilicity convert to hydrophobicity.

3.6. Ethanol treatment

The surface treatment of Ti-6Al-4V plate was prepared by galvanostatic method. The Ti-6Al-4V plate etched in 1M HF was used as working electrode, Pt plate was used as counter electrode and Ag/AgCl was used as reference electrode. The 1M H_3PO_4 was used as electrolyte. The working electrode was anodized at a constant current density of 2 mA/cm^2 for 0.5 h. After the anodizing process, the anodized film was cleaned and dried at room temperature. The obtained anodized film was defined as Ano 1.

The direct anodizing process for Ti-6Al-4V in 1M H_3PO_4 electrolyte with addition of ethanol of 6% v/v, 18% v/v and 30% v/v, the current density was set to 2 mA/cm^2 for 0.5 h. The other electrical parameters were the same as those used for preparing the Ano 1 specimen. The obtained specimen was denoted as Ano mix.

To combine anodized films with the ethanol treatment, the Ti-6Al-4V plate was first treated by galvanostatic method in 1M H_3PO_4 electrolyte as mentioned above, and then the Ano 1 specimen was further treated by the galvanostatic method at 2 mA/cm^2 in 1M H_3PO_4 electrolyte with addition of ethanol of 6% v/v, 18% v/v and 30% v/v. The anodizing parameters in this solution were the same as those for preparing Ano mix specimen. The obtained specimens were designated as Ano 2.

3.7. Experimental diagrams

(1) TiUnite dental implant characterizations

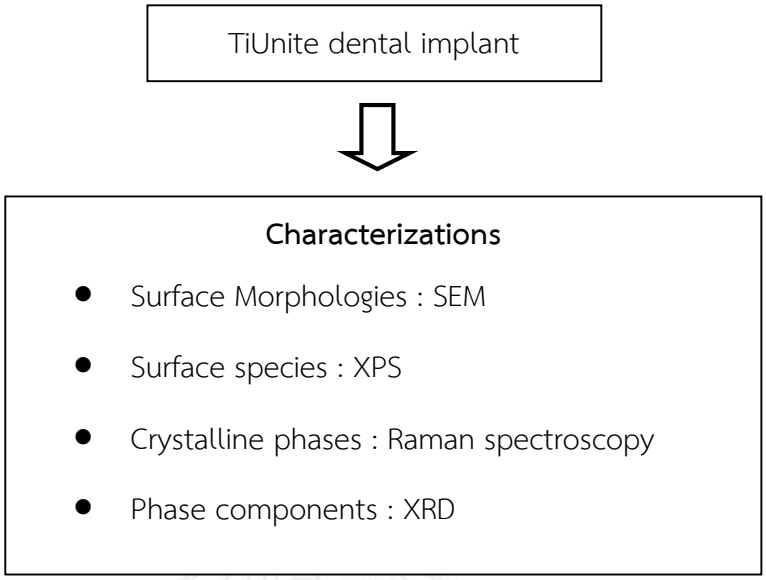

Fig. 3-3 TiUnite dental implant characterizations

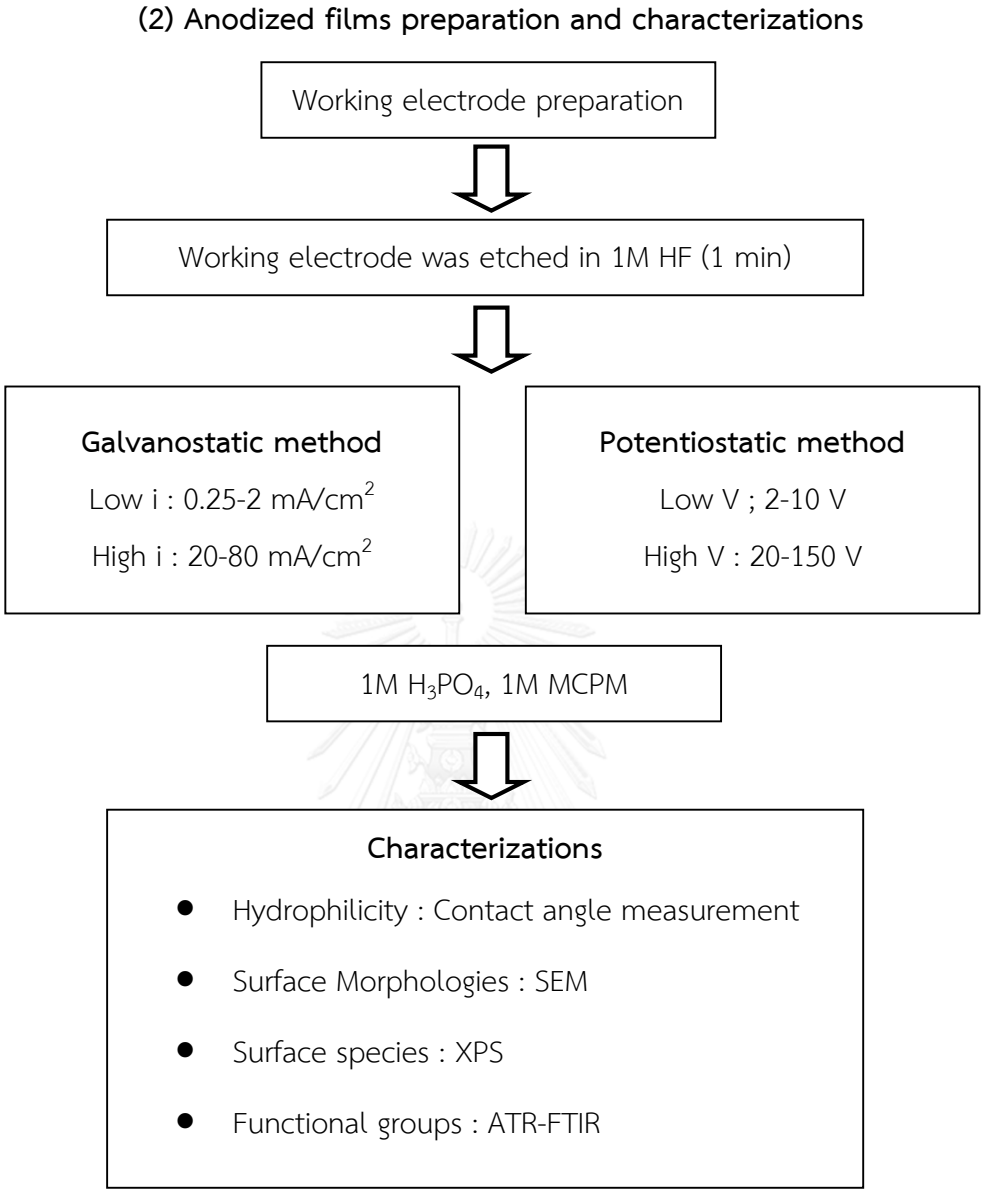

Fig. 3-4 Flow chart of the anodized films preparation

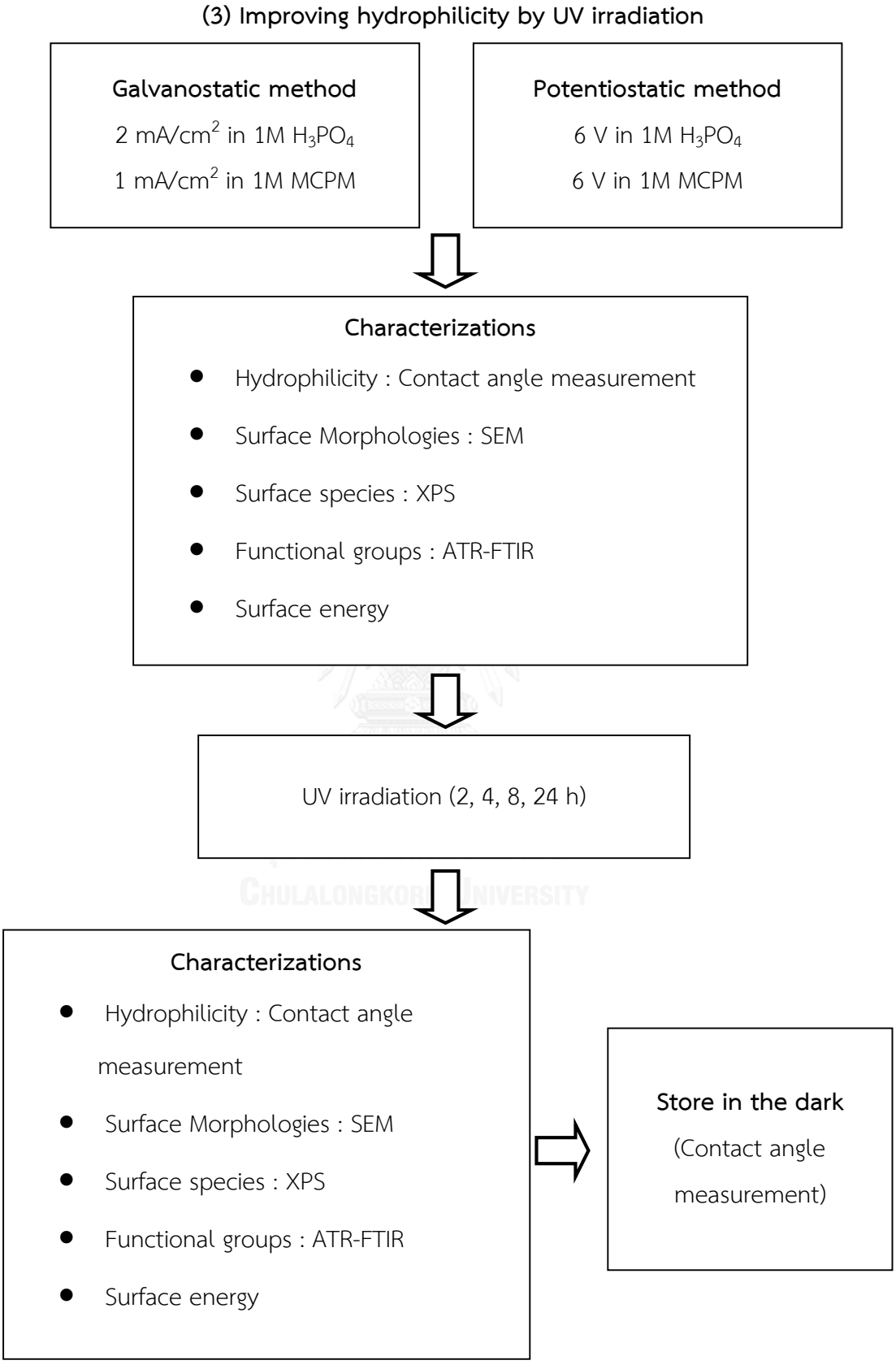

Fig. 3-5 Flow chart of the improving hydrophilicity by UV irradiation

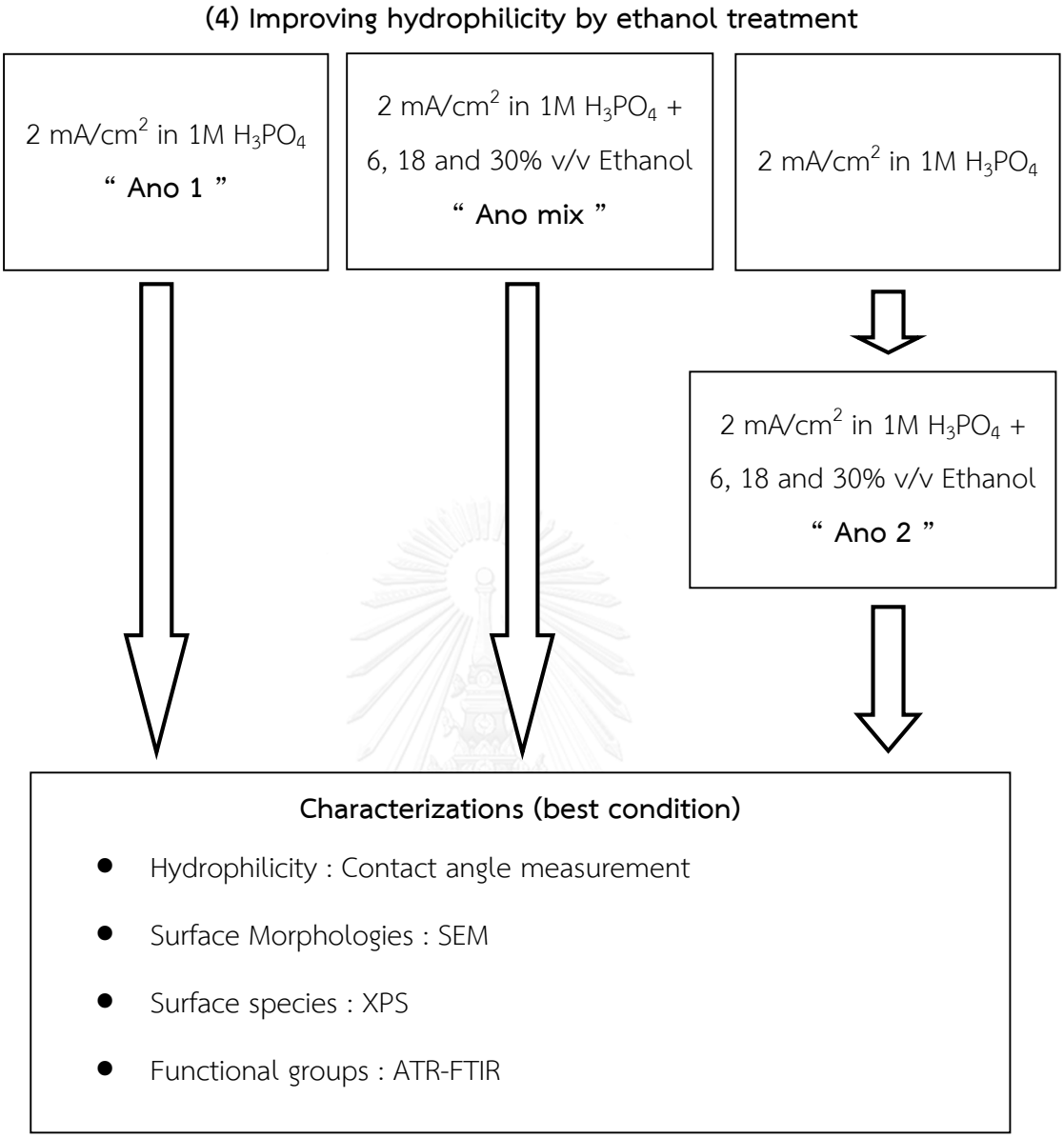

Fig. 3-6 Flow chart of the improving hydrophilicity by increasing OH groups

CHAPTER 4
RESULTS AND DISCUSSIONS

4.1. Dental implant characterization

4.1.1. The basic information of the NobelReplace™ Conical Connection RP (TiUnite dental implant)

TiUnite (5.0 mm × 16 mm, Nobel Biocare, Göteborg, Sweden) was purchased from the company as shown in Fig. 4-1. It was made from titanium grade 4. The plasma electrolytic oxidation (anodization) was used to modify surface resulting in the formation of titanium oxide [48].

Fig. 4-1 NobelReplace™ Conical Connection RP (TiUnite, 5.0 mm × 16 mm)

4.1.2. Surface characterization of TiUnite dental implant

The TiUnite dental implant showed porous surface due to breakdown phenomenon during anodizing process [49]. Pore size was around 0.5 - 4 μm, some areas elongated to 10 μm as shown in Fig. 4-2.

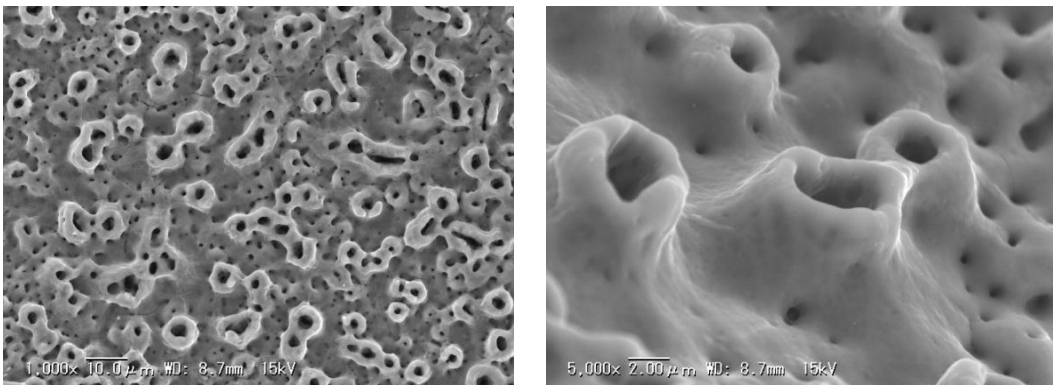

Fig. 4-2 Surface morphology of TiUnite dental implant (a) 1000X and (b) 5000X

Fig. 4-3 shows the XPS spectra of TiUnite dental implant. The results show that the Ti doublet peaks of Ti 2p1/2 and Ti 2p3/2 of the implant appeared at 464.3 eV and 458.3 eV. These Ti 2p peaks was deconvoluted corresponding to TiO_2.

O 1s spectra of implant as shown in Fig. 4-3 (b) show main peak close to 533.30 eV. This O 1s spectrum was deconvoluted to O^{2-}, OH^- and H_2O at 529.4 eV, 531.2 eV and 533.3 eV, respectively.

C 1s spectra of implant as shown in Fig. 4-3 (c) represent a singlet peak at 284 eV. C 1s spectrum was deconvoluted to hydrocarbon and organic adsorbates at 283.1 eV, 284.1 eV and 285.95 eV. These carbon peaks is not important composition of the oxide films but they are contamination from the absorbed organic carbon during sample handing [50]. These results show similar features with TiUnite implant of Kang et al. work [49].

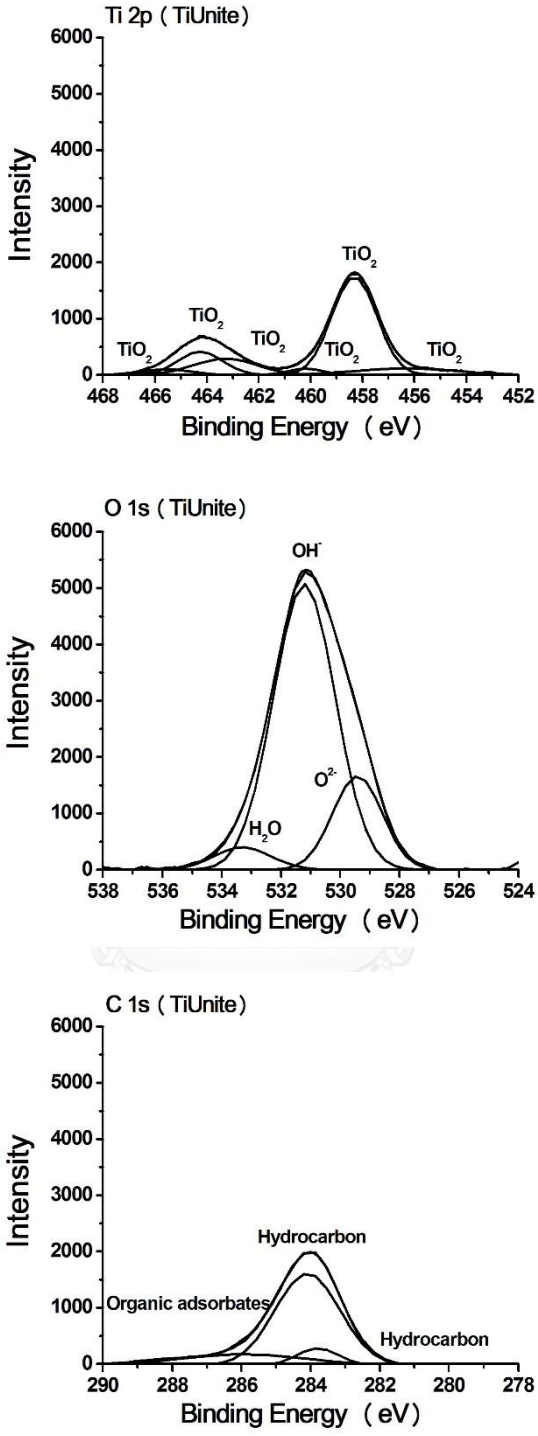

Fig. 4-3 XPS spectra of the TiUnite dental implant

These results are confirmed by XRD pattern. The XRD patterns of the TiUnite dental implant are shown in Fig. 4-4. The TiUnite dental implant surfaces crystalline phase of anatase is observed corresponding to JCPDS # 00-021-1272. This result suggests that the TiO_2 layers that are formed during plasma electrolytic oxidation.

Moreover, these findings were confirmed by Raman spectroscopy. The Raman spectra of the TiUnite dental implant were shown in Fig. 4-5. The TiUnite dental implant is tetragonal anatase structured TiO_2. The anatase TiO_2 (the space group D^{19}_{4h} ($I4_1/amd$)) has six Raman active vibrations: $A_{1g} + 2B_{1g} + 3E_g$ [38,51,52]. The peak at ~ 145 cm^{-1} (correspond to E_g), ~ 198 cm^{-1} (correspond to E_g), ~ 395 cm^{-1} (correspond to B_{1g}), ~ 514 cm^{-1} (correspond to $A_{1g} + B_{1g}$) and ~ 635 cm^{-1} (correspond to E_g) modes of anatase TiO_2 are observed.

The vibration dynamics of anatase is shown in Fig. 4-6 [53]. In anatase, only A_{1g} vibration mode is predicted to be the oxygen vibration, the B_{1g} vibration mode is Ti atom vibration and the remaining vibrations are mixes of both O atom and Ti atom vibration. The narrows showed the displacement of the corresponding atoms. E_g are the double degenerated vibrations, the narrow showed only one of the possible displacement geometries. The length of the arrows is the amplitude of vibration [53]. A and B is one dimensional symmetries and E is two dimensional symmetries. The subscript "g" is "gerade" indicating the symmetry with respect to inversion and the subscript "1" indicates the singlet state [54] (the spin of two electrons have antiparallel (paired), the two spin momenta cancel each other and there is zero net spin) [55]. In addition, the A_{1g}, B_{1g} and E mode is caused by anti-symmetric bending vibration, symmetric bending vibration and symmetric stretching vibration of O-Ti-O, respectively [56].

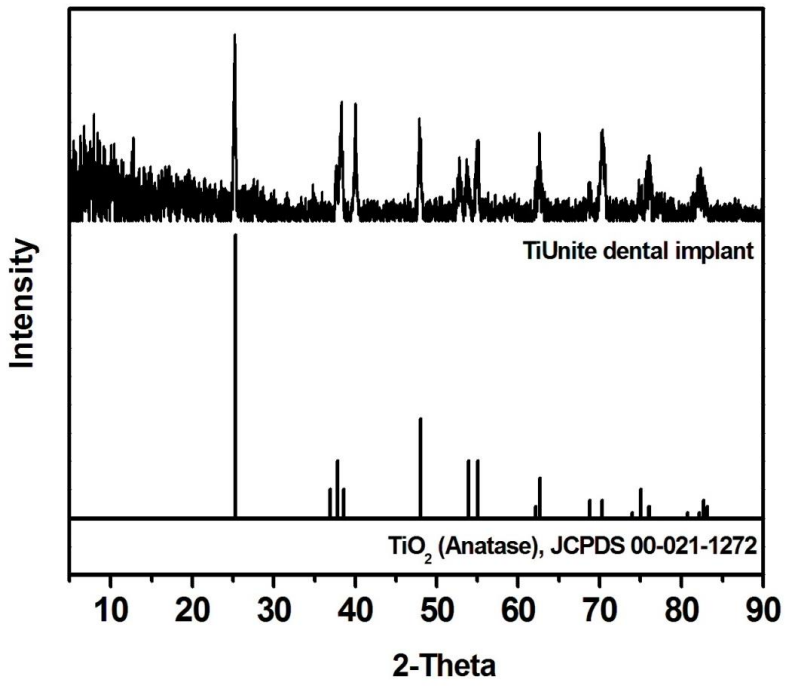

Fig. 4-4 XRD pattern of the TiUnite dental implant

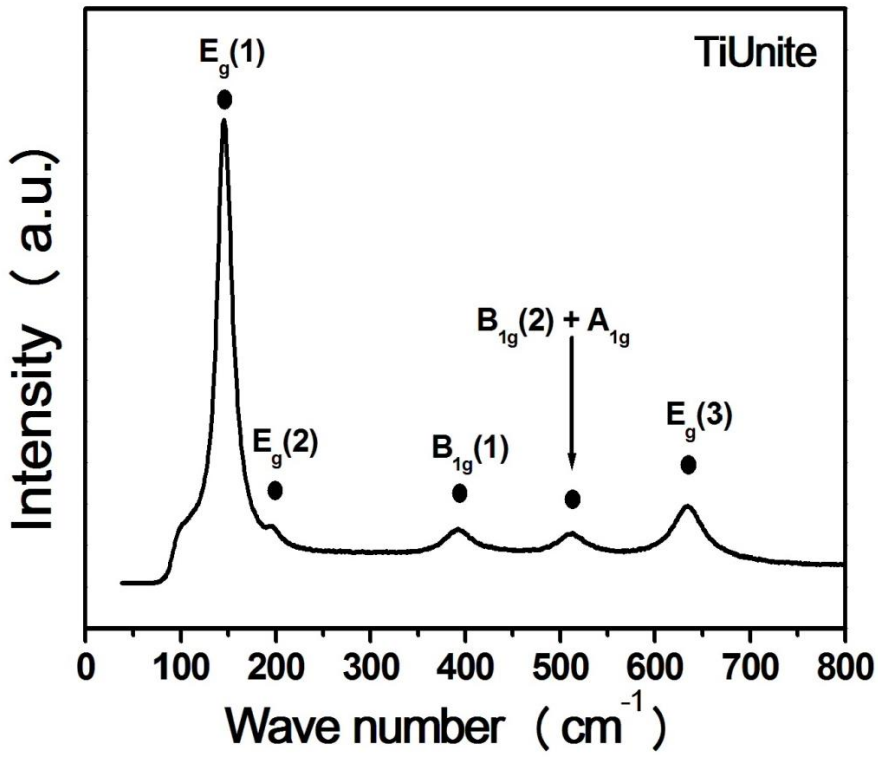

Fig. 4-5 Raman spectra of TiUnite dental implant

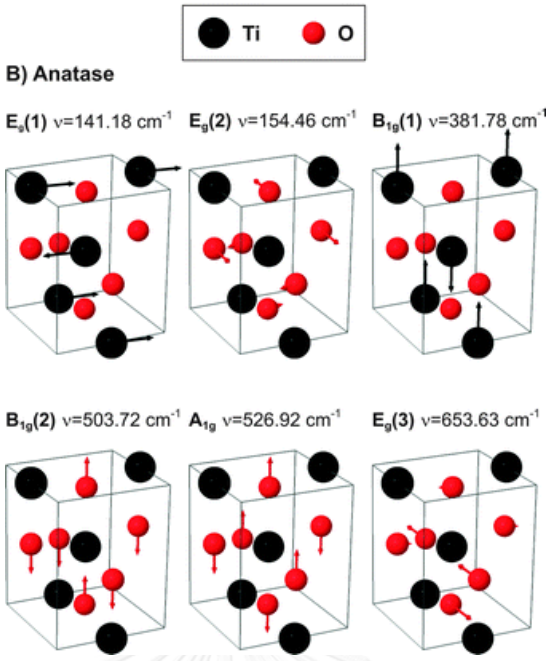

Fig. 4-6 Scheme of Raman active atomic vibrations of anatase [53]

It is well known that the surface properties of titanium implants are important factors for successful osseointegration. The surface characterizations are essential for a better understanding of the role of surface properties on osseointegration. Various surface modification techniques have been developed in order to improve their clinical permanence. Therefore, the surface characterizations of the commercial implant were used as reference in this study.

4.2. Effect of anodizing conditions on hydrophilicity of the anodized films

The passivation behavior of metal and alloys shows in the polarization diagram as shown in Fig. 4-7. The potential increased, so the current density increased according to normal dissolution behavior until a critical value (i_{crit}). This point starts to form the passive films, which occurs at potentials higher than primary passive potential (E_{pp}). Beyond this point, the current density decreased to a residual current (i_{pass}). At higher potentials (E_t) breakdown of the passive film might occur with an increase in anodic activity and form the transpassive state [57].

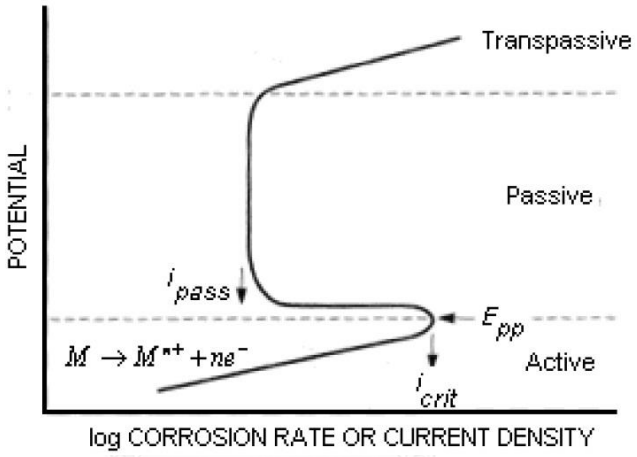

Fig. 4-7 Schematic polarization diagram displaying the change from active corrosion to passive behavior and to transpassive state [57]

It is indicated that the applying a current density or voltage in the passive state, it is possible to grow the oxide layer on the titanium alloys in order to protect the surface from oxidation. Karambakhsh reported that the i_{pass} of the anodized films on Ti-6Al-4V in different solutions around 0.053-0.069 $\mu A/cm^2$ [58]. Therefore, the low current densities of 0.25-2 mA/cm^2 applied in this work can perform the passive oxide films on the Ti-6Al-4V.

4.2.1. Effect of anodization current (Galvanostatic method)

4.2.1.1. Anodizing process

The anodizing process of the anodized films formation obtained at constant current (galvanostatic method) could be explained by the potential vs. time curve as shown in Fig. 4-8. The curve showed three different regions [37]. In the first region, the potential linearly increased corresponding to the formation of an insulating thin film. The second region, the slope of the curve decreased and the potential continued to increase to critical potential value. In this region, the evolution of oxygen on the film surface began. The third region, the potential remains stable until the end of process because there was no space on the surface of Ti-6Al-4V to form the film corresponding to corrosion resistance.

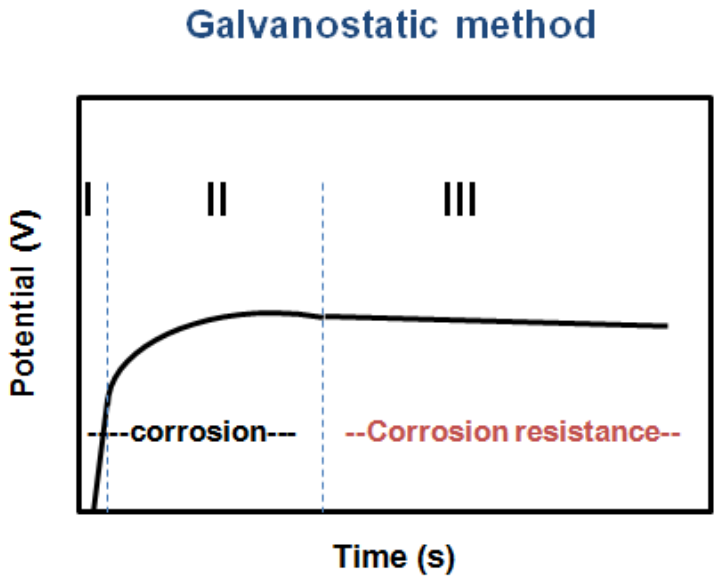

Fig. 4-8 Curve of the anodizing process of the anodized films formed by galvanostatic method

4.2.1.2. Hydrophilicity of the anodized films

Fig. 4-9 showed the contact angle of Ti-6Al-4V before and after anodization at different current density. The contact angle of untreated Ti-6Al-4V surface was about 84.7°. The contact angle of the anodized films formed at low current density of 0, 0.25, 1 and 2 mA/cm^2 in 1M H_3PO_4 decreases to 75.9°, 72.4°, 79.1° and 69.9°, respectively. The contact angle of the anodized films formed at high current density of 5, 20 and 80 mA/cm^2 in 1M H_3PO_4 decreased to 48.3°, 41.5° and 45.3°, respectively. Using of 1M MCPM as an electrolyte, the contact angle of the anodized films formed at low current density of 0, 0.25, 1 and 2 mA/cm^2 decreased to 81.3°, 70.8°, 66.9° and 73°, respectively. The contact angle of the anodized films formed at 5, 20 and 80 mA/cm^2 decreases to 24.3°, 17.2° and 21.7°, respectively. From these results, it is indicated that the contact angle of the anodized films formed at high current densities in 1M MCPM were lower than those of in 1M H_3PO_4. It may be due to high composition of Ca in the anodized films formed at high current densities resulting in high hydrophilicity. For the galvanostatic method, the anodized films formed at low current density of 2 mA/cm^2 in 1M H_3PO_4 and 1 mA/cm^2 in 1M MCPM and at high current density of 20 mA/cm^2 in either 1M H_3PO_4 or 1M MCPM displayed the lowest contact angle in each group resulting in the highest hydrophilicity. The contact angle of the anodized films applied at both low and high current density significantly decreased after anodization ($p<0.05$) compared to the untreated Ti-6Al-4V. However, the anodized films formed at low current density, there are no significant difference ($p>0.05$) in the water contact angle compared to the films formed without current density. The contact angle of the anodized films formed at high current density significantly decreased in comparison with the anodized films formed at low current density. The results of contact angle suggested the successful enhancing in hydrophilicity on the anodized films via galvanostatic method ranging from 5-80 mA/cm^2 in either 1M H_3PO_4 or 1M MCPM.

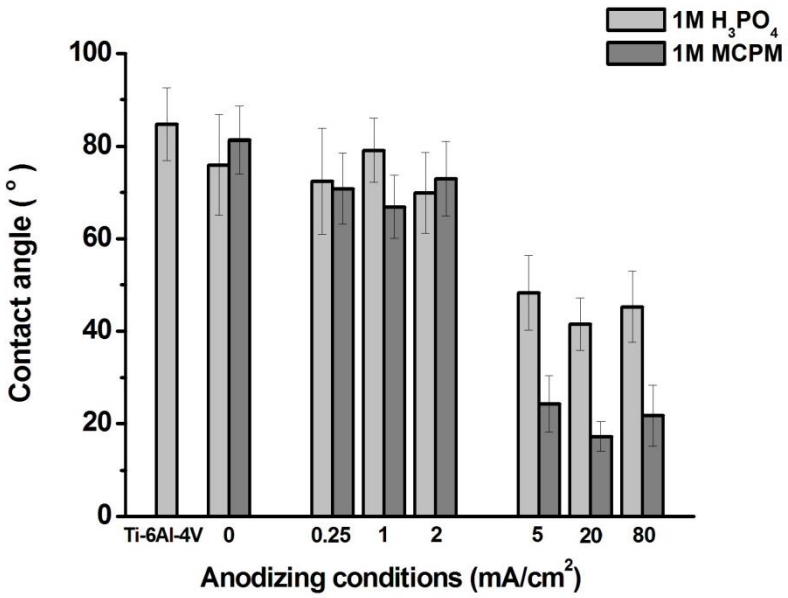

Fig. 4-9 Contact angle of the untreated Ti-6Al-4V and the anodized films applied different current density in either 1M H_3PO_4 or 1M MCPM

4.2.1.3. The morphology of the anodized films

After the anodizing process, the Ti-6Al-4V surface morphology has clearly changed especially the anodized films formed at high current density as shown in Fig. 4-10.

The anodized films formed at high current densities showed porous surface with non-homogeneous pores. However, no any pore was observed in the anodized films formed at low current densities of 0.25-2 mA/cm^2. The anodized films formed at high current density showed porous surface because it is increasing in electric current at high current densities resulting in a wide pore formation due to stronger electric sparks taking place on the nearby anode surface of the growing layers. When an electric spark occurs, the temperature is high enough to melt the oxide layer. These sparks was also the main reason for pore formation. After the sparks disappeared, the melted regions solidified in the adjacent electrolyte. These frequent melting and solidifying phenomena made the layers roughened [59]. However, no electrical sparking occurred at low current densities due to the low electric current passing the electrochemical cell. Therefore, no pore occurred on the anodized films formed at low current

densities. The porous surface might be one of the factors enhancing the hydrophilicity to the anodized films.

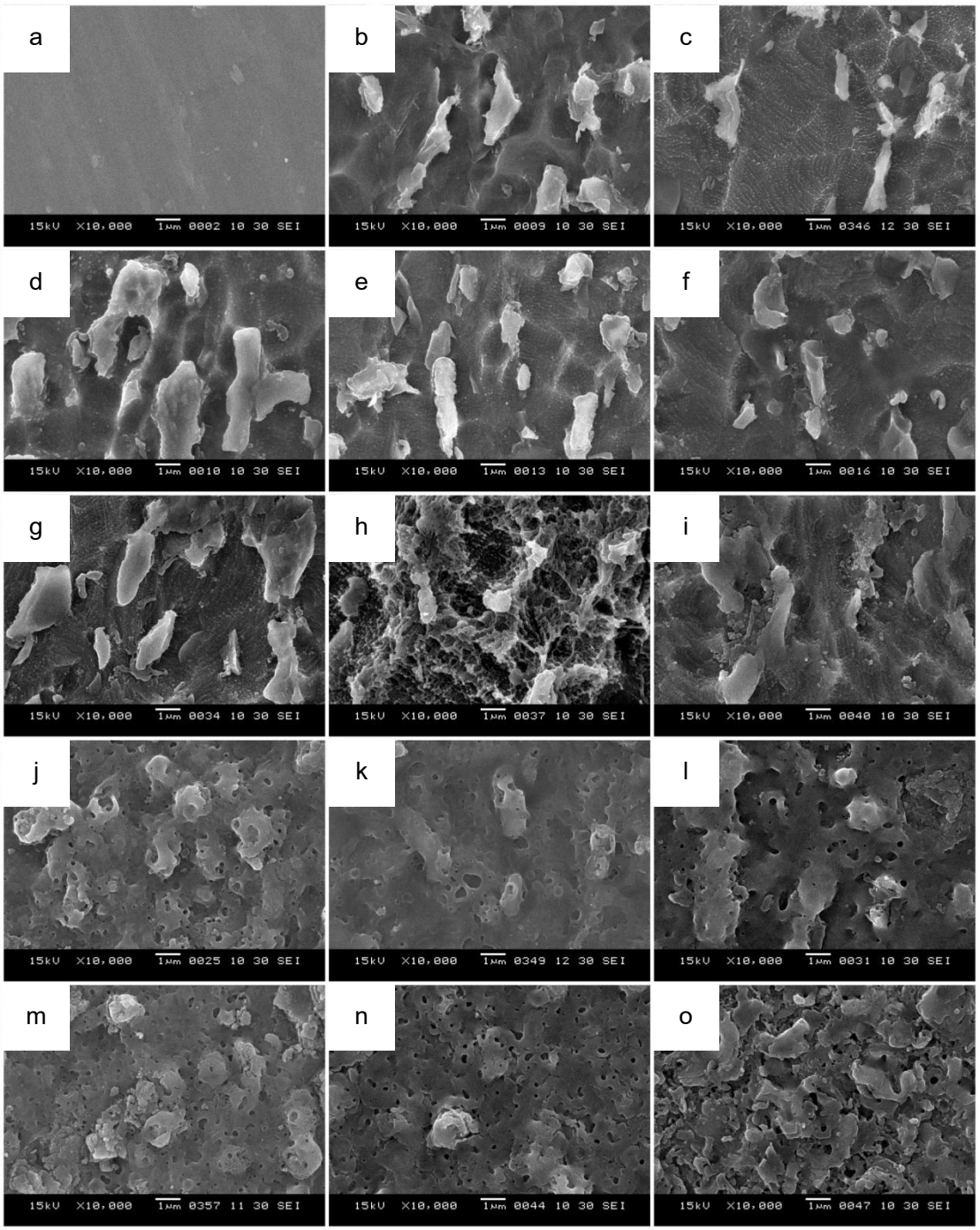

Fig. 4-10 SEM micrographs of (a-c) the Ti-6Al-4V untreated and the films formed without current density, (d-f) the anodized films formed at 0.25, 1 and 2 mA/cm^2 in 1 M H_3PO_4, (g-i) 0.25, 1 and 2 mA/cm^2 in 1 M MCPM, (j-l) 5, 20 and 80 mA/cm^2 in 1 M H_3PO_4 and (m-o) at 5, 20 and 80 mA/cm^2 in 1 M MCPM, respectively

4.2.1.4. The chemical species of the anodized films

The Ti 2p and O 1s narrow XPS spectra of the untreated Ti-6Al-4V and the anodized films show in Fig. 4-11, Fig. 4-12, Fig. 4-13, Fig. 4-14, and Fig. 4-15. The Ti 2p spectra of the untreated Ti-6Al-4V, the films formed without current and the anodized films formed at low current density of 0.25-2 mA/cm^2 provide clear evidence that the chemical species not only consist of TiO_2, but there are additional oxide species such as Ti_2O_3, TiO or Ti at lower binding energy. The peak positions can be attributed to the oxidation state +IV for TiO_2, +III (Ti_2O_3), +II (TiO) and 0 (Ti metal) [25]. However, the Ti 2p spectra of the anodized films formed at high current density of 5-80 mA/cm^2 in both electrolytes present only TiO_2. The O 1s spectra of the untreated Ti-6Al-4V present O^{2-} (the titanium oxide) as a main peak and co-exist with OH^- (hydroxide). The O 1s spectra of the films formed without current and the anodized films formed at low current density present O^{2-} (the titanium oxide) as a main peak and co-exist with OH^- (hydroxide) and H_2O (adsorbed water). However, the O 1s spectra of the anodized films formed at high current density of 5-80 mA/cm^2 in both electrolytes present OH^- (hydroxide) as a main peak and co-exist with H_2O (adsorbed water). The C 1s spectra has clearly distinguishable contributions from hydrocarbon species generated from sample handing [50]. The data do not show. From the SEM micrographs and the XPS results, it is indicated that the present of hydroxide, adsorbed water and porous surface on the anodized films formed at 5-80 mA/cm^2 in both electrolyte could improve the hydrophilicity to the anodized films.

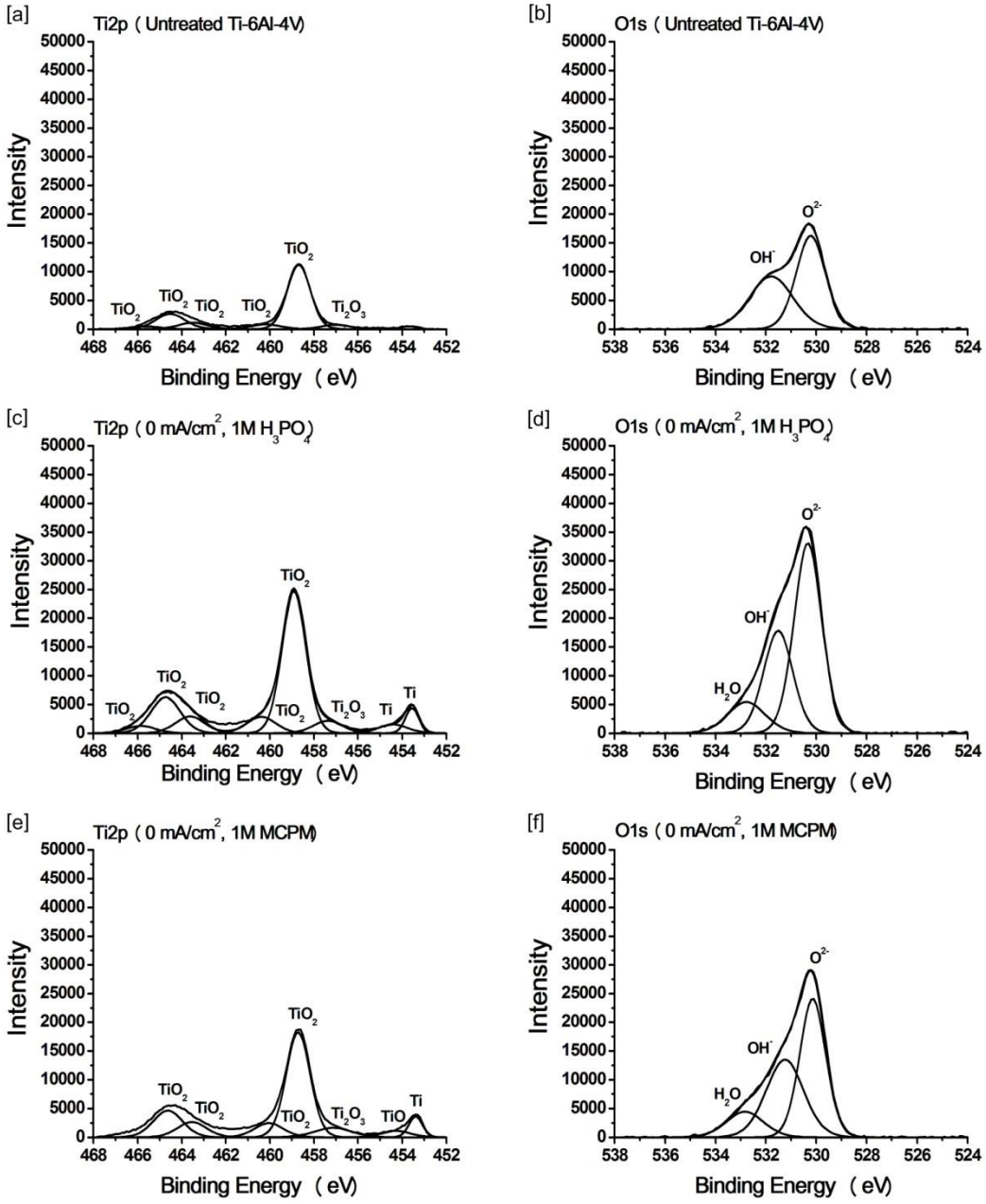

Fig. 4-11 Ti2p and O1s XPS spectra of the untreated Ti-6Al-4V and the films formed without current in either 1M H_3PO_4 or 1M MCPM

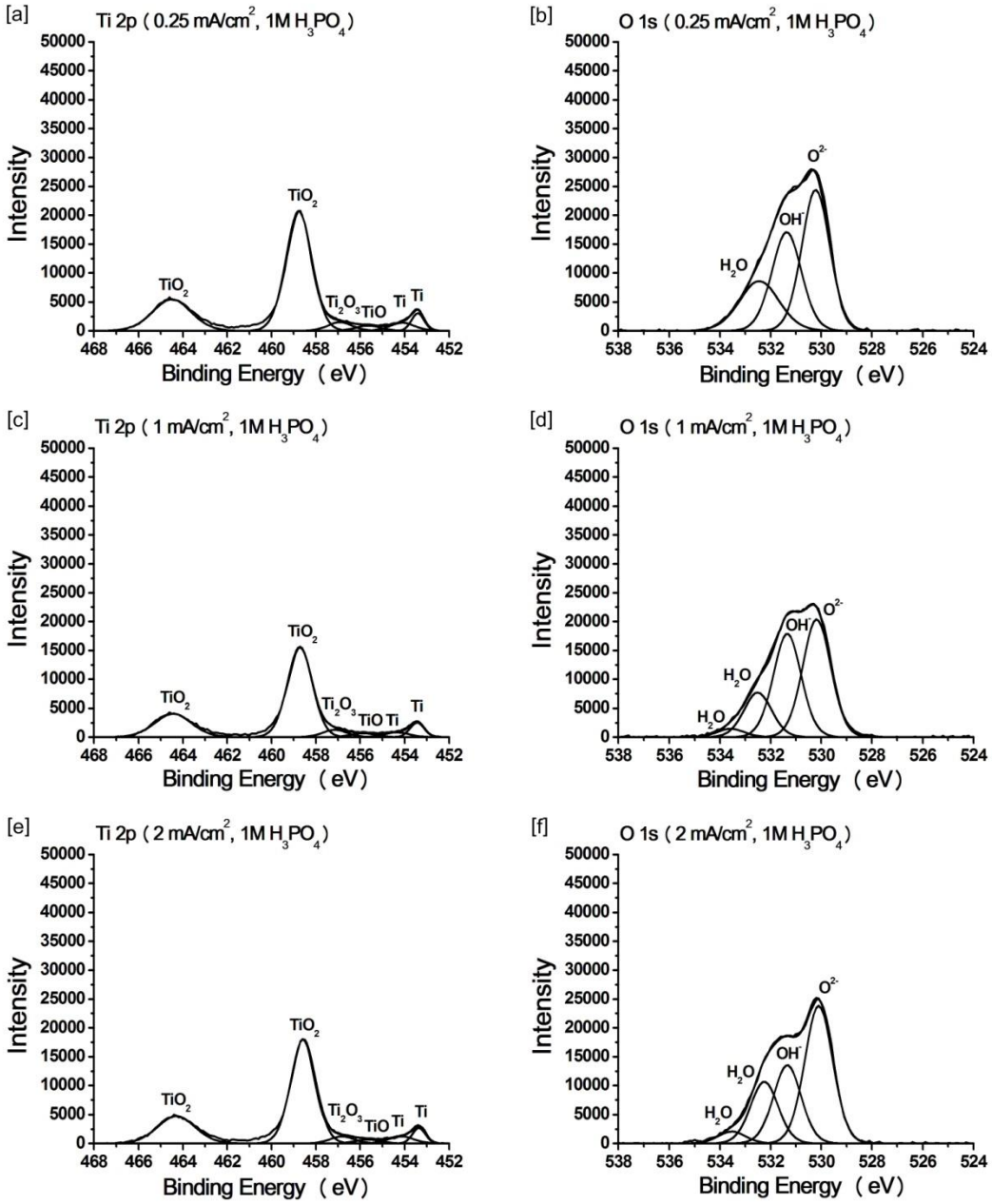

Fig. 4-12 Ti2p and O1s XPS spectra of the anodized films formed at 0.25, 1 and 2 mA/cm^2 in 1M H_3PO_4

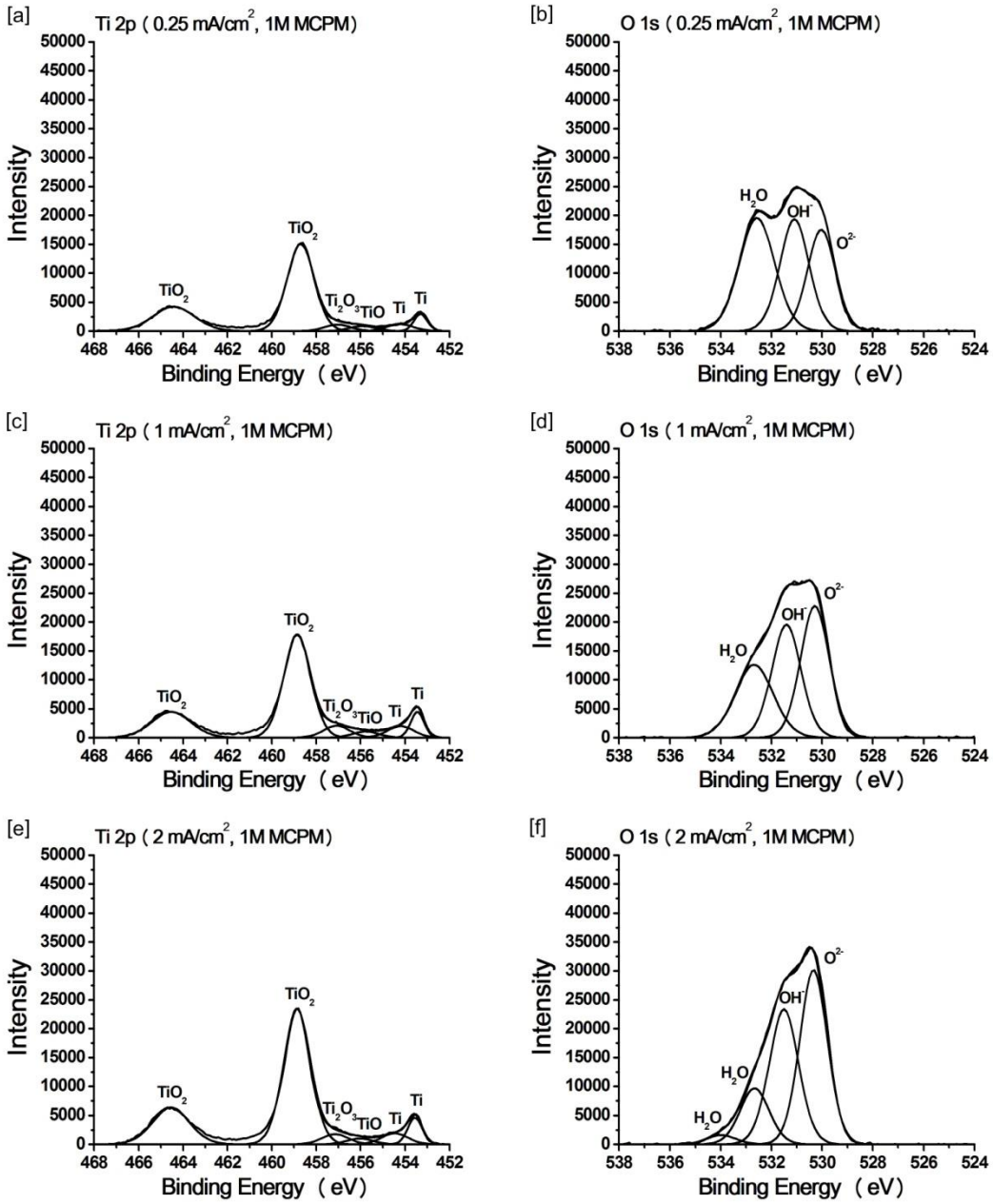

Fig. 4-13 Ti2p and O1s XPS spectra of the anodized films formed at 0.25, 1 and 2 mA/cm^2 in 1M MCPM

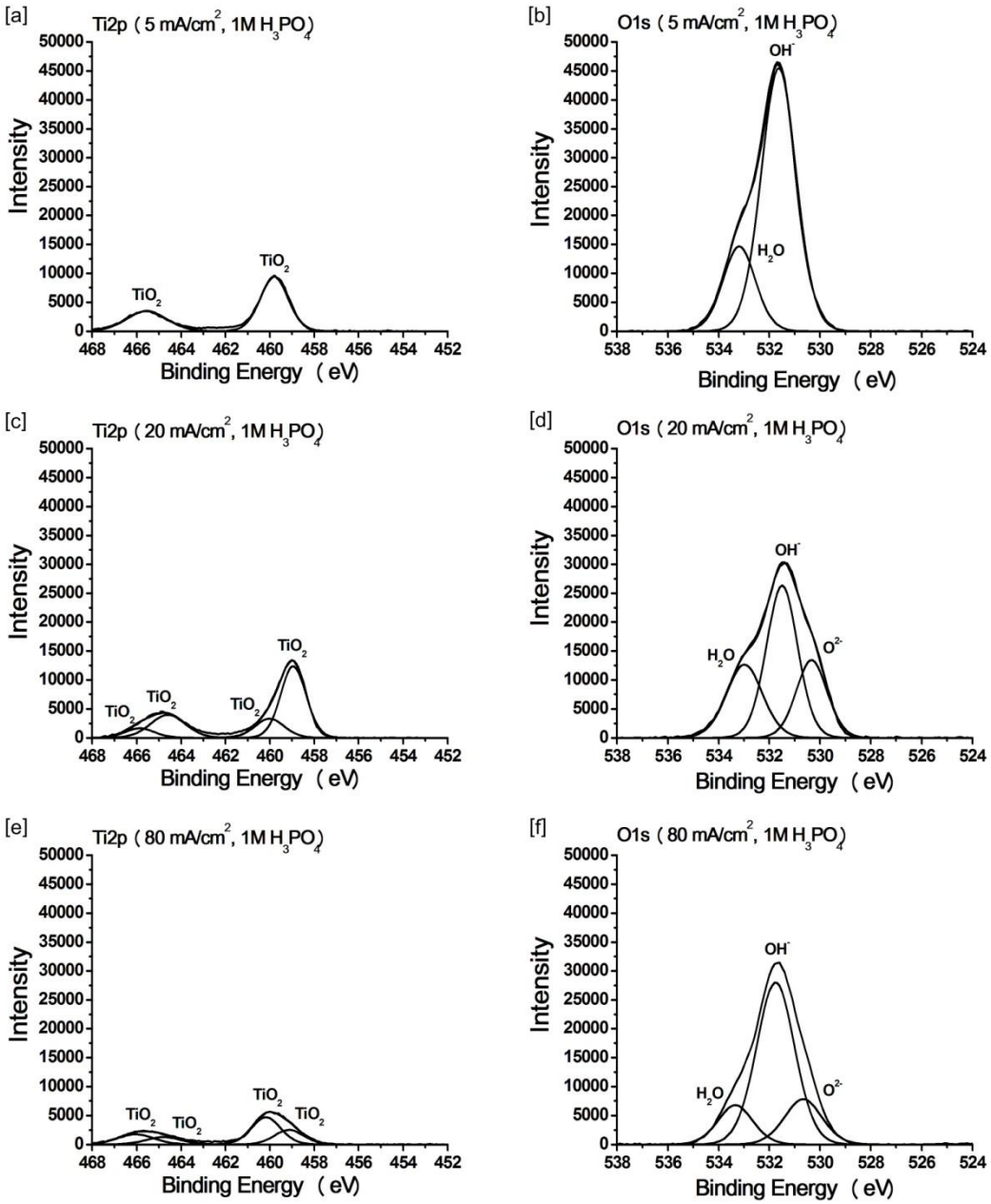

Fig. 4-14 Ti2p and O1s XPS spectra of the anodized films formed at 5, 20 and 80 mA/cm^2 in 1M H_3PO_4

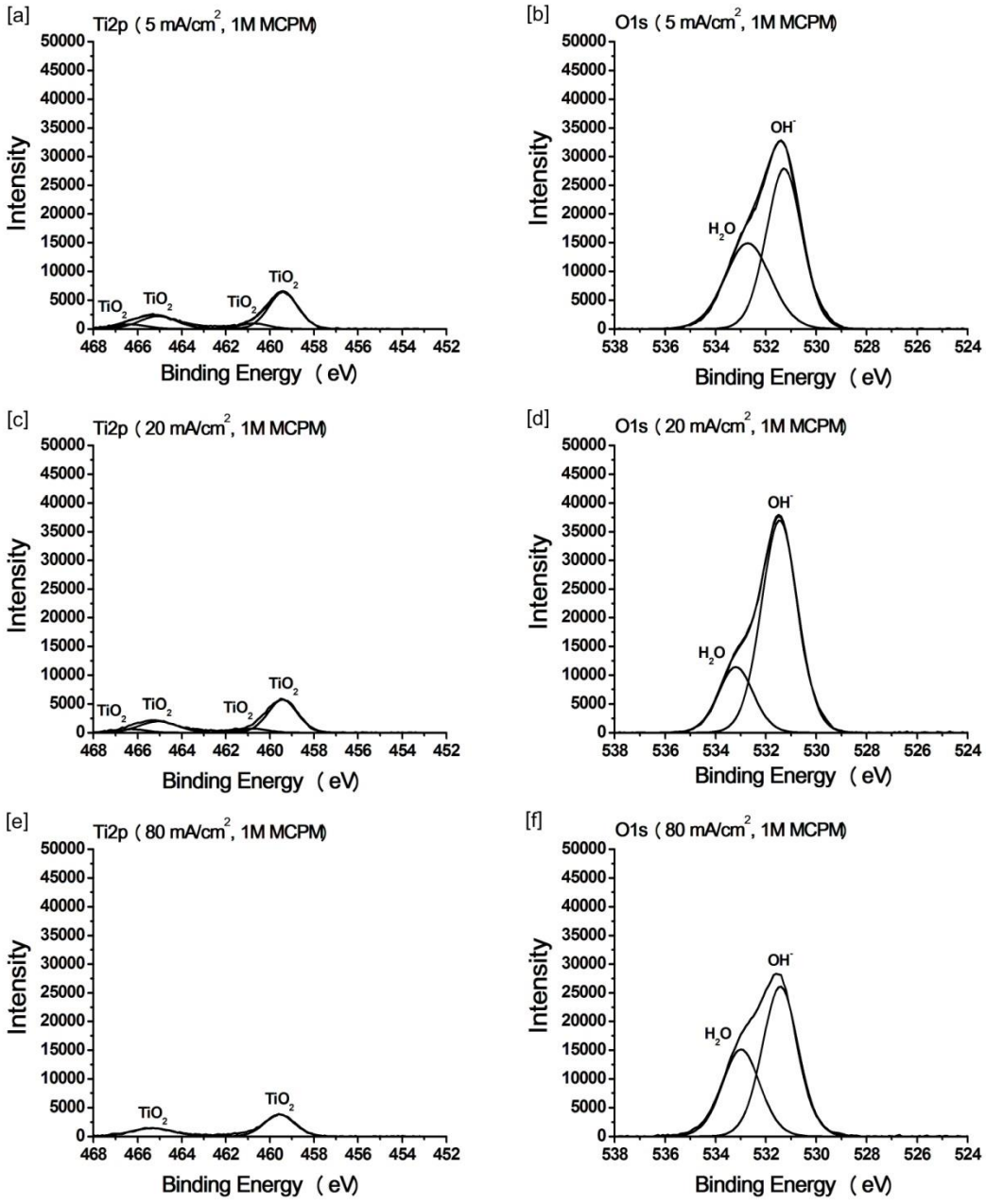

Fig. 4-15 Ti2p and O1s XPS spectra of the anodized films formed at 5, 20 and 80 mA/cm^2 in 1M MCPM

4.2.1.5. ATR-FTIR spectra of the anodized films

Fig. 4-16 and Fig. 4-17 show the FTIR spectra of the Ti-6Al-4V before and after anodization at low current density and high current density. It is observed that the FTIR spectra of the untreated Ti-6Al-4V and the films formed without current and the anodized films formed at low current density of 2 mA/cm^2 in 1M H_3PO_4 and 1 mA/cm^2 in 1M MCPM showed small peak of OH group. However, there was increase intensity of OH group in the anodized films formed at 20 mA/cm^2 in either 1M H_3PO_4 or MCPM. The FTIR spectra of the anodized films formed at 20 mA/cm^2 in 1M H_3PO_4 at 2788 cm^{-1} and 1531 cm^{-1} are assigned to the stretching and bending vibrations of OH group respectively. The FTIR spectra of the anodized films formed at 20 mA/cm^2 in 1M MCPM at 3752 cm^{-1} and 1599 cm^{-1} are assigned to the stretching and bending vibrations of OH group respectively. These FTIR results confirm the hydroxyl groups from XPS results. Therefore, the high hydrophilicity of the anodized films formed at high current density in either 1M H_3PO_4 or 1M MCPM may result from the hydroxyl groups on the porous surface.

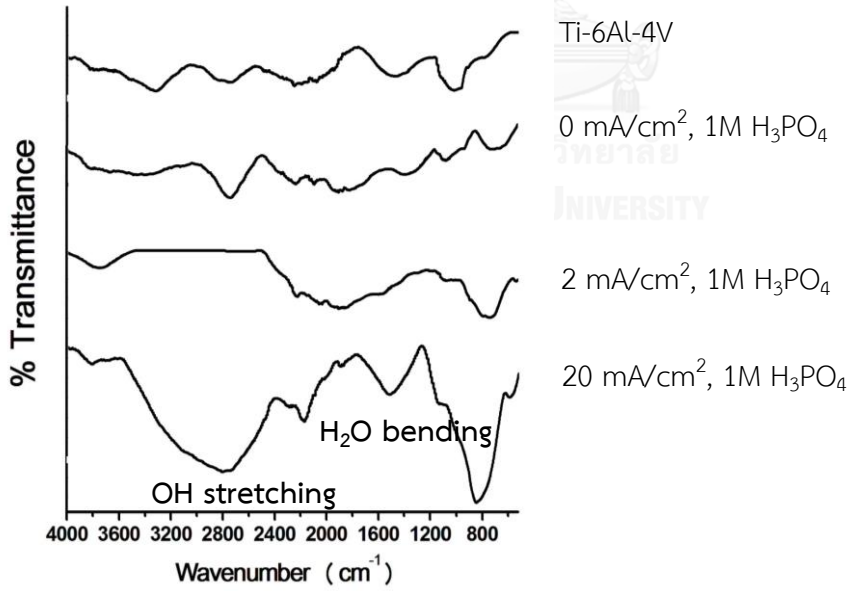

Fig. 4-16 ATR-FTIR spectra of the untreated Ti-6Al-4V, the films formed without current and the anodized films formed at 2 and 20 mA/cm^2 in 1M H_3PO_4

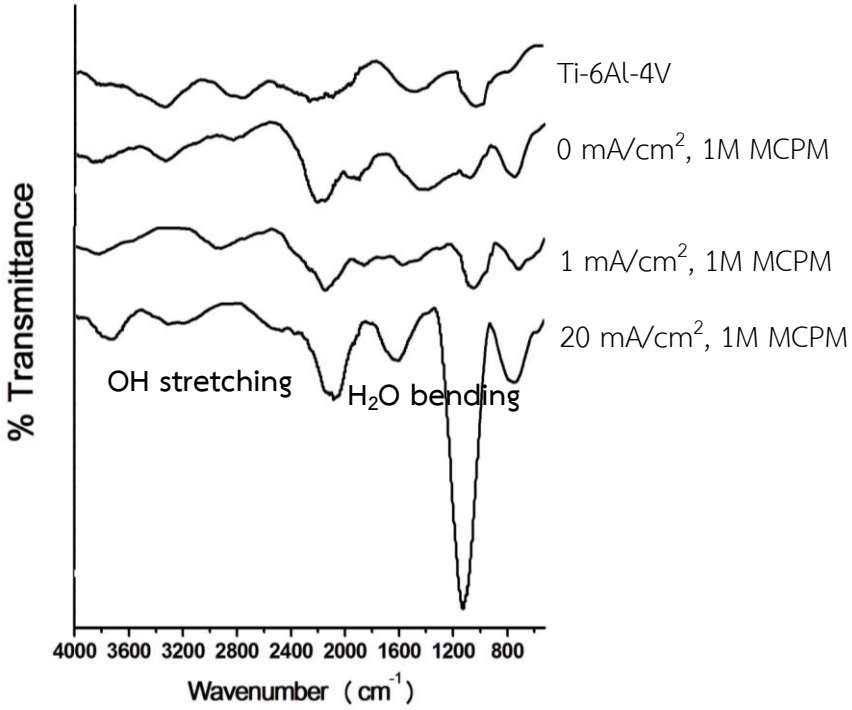

Fig. 4-17 ATR-FTIR spectra of the untreated Ti-6Al-4V, the films formed without current and the anodized films formed at 1 and 20 mA/cm^2 in 1M MCPM

4.2.2. Effect of anodization voltage (Potentiostatic method)

4.2.2.1. Anodizing process

Fig. 4-18 showed the anodizing process of the anodized films formation obtained at constant voltage (potentiostatic method). The current vs. time curve was used to explain the anodizing process. The curve showed three different regions [37]. At the first region, there was high current corresponding to the formation of insulating thin films. In second region, the current decreased and the evolution of oxygen began. In the third region, the current exhibited small variations until the end of process due to corrosion resistance.

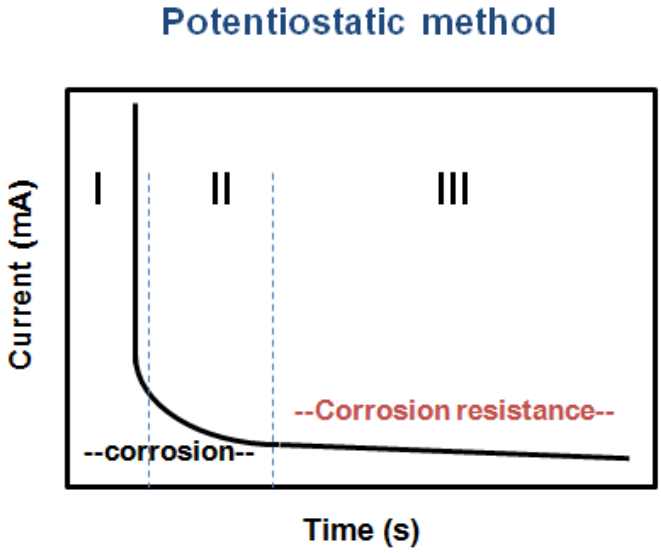

Fig. 4-18 Curve of the anodizing process of the anodized films formed by potentiostatic method

4.2.2.2. Hydrophilicity of the anodized films

Fig. 4-19 showed the contact angle of Ti-6Al-4V before and after anodization at different voltage. The contact angle of untreated Ti-6Al-4V surface is about 84.7°. The contact angle of the anodized films formed at low voltage of 0, 2, 4, 6 and 8 V in 1M H_3PO_4 decreased to 75.9°, 52.3°, 50.5°, 49.2° and 54.8°, respectively. The contact angle of the anodized films formed at high voltage of 5, 10, 50, 100 and 150V in 1M H_3PO_4 decreased to 48.8°, 48.5°, 46.4°, 59.7° and 37.9°, respectively. For the using 1M MCPM as an electrolyte, the contact angle of the anodized films formed at low voltage

of 0, 2, 4, 6 and 8 V decreased to 81.3°, 61.2°, 64.13°, 40.27° and 54.27°, respectively. The contact angle of the anodized films formed at high voltage of 5, 10, 50, 100 and 150V in 1M MCPM decreases to 50.9°, 52.9°, 51.6°, 50.5° and 26.2°, respectively. From these results, it is indicated that the contact angle of the anodized films formed at high voltage of 150 V in 1M MCPM were lower than those of in 1M H_3PO_4. It may be due to high composition of Ca in the anodized films resulting in high hydrophilicity. For the potentiostatic method, the anodized films formed at low voltage of 6V and at high voltage of 150V in either 1M H_3PO_4 or 1M MCPM are lowest contact angle in each group showing the highest hydrophilicity. The contact angle of the anodized films applied at low and high voltage significantly decreased after anodization ($p<0.05$) compared to the untreated Ti-6Al-4V and the films formed without current. The anodized films formed at both low and high voltages could enhance hydrophilicity to the films.

From the contact angle of the anodized films formed by galvanostatic method and potentiostatic method, the results showed that the best condition of the anodized films formation in low condition was 6V in 1M MCPM and in high condition was 20 mA/cm^2 in 1M MCPM. It is indicated that composition of Ca in the anodized films result in high hydrophilicity.

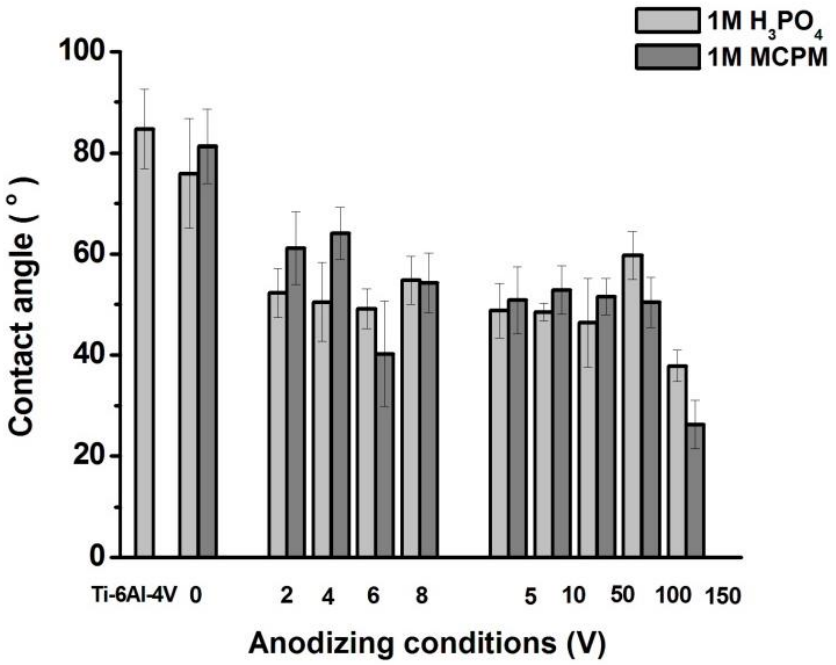

Fig. 4-19 Contact angle of the untreated Ti-6Al-4V and the anodized films formed at different voltage in either H_3PO_4 or MCPM

4.2.2.3. The morphology of the anodized films

SEM micrographs in Fig. 4-20, Fig. 4-21 and Fig. 4-22 showed the microstructure of the anodized films formed at low and high voltage. After the anodizing process, the Ti-6Al-4V surface morphology has clearly changed especially the anodized films formed at high voltage of 150V in 1M MCPM. The anodized films formed at 150V in 1M MCPM showed porous surface with non-homogeneous pores. However, the other anodized films showed rough surface. This porous and rough surface formation could be explained in the same way of galvanostatic method. From these results it is indicated that both rough and porous surface promoted better hydrophilicity on the anodized films and the porous surface showed the highest hydrophilicity behavior.

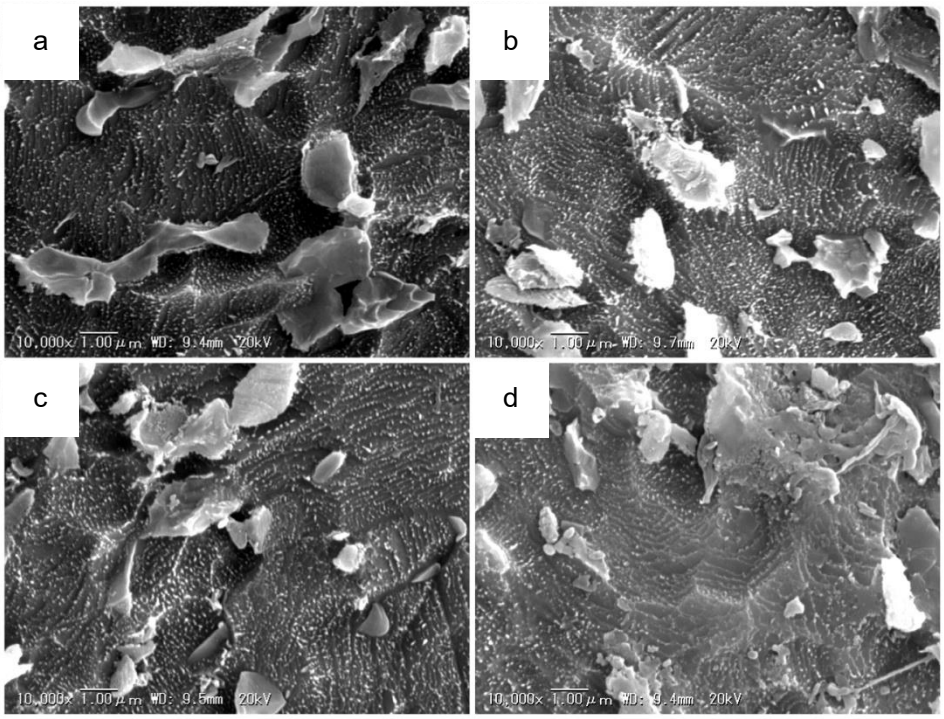

Fig. 4-20 SEM micrographs of the anodized films formed at 2, 4, 6 and 8 V in 1M H_3PO_4, respectively

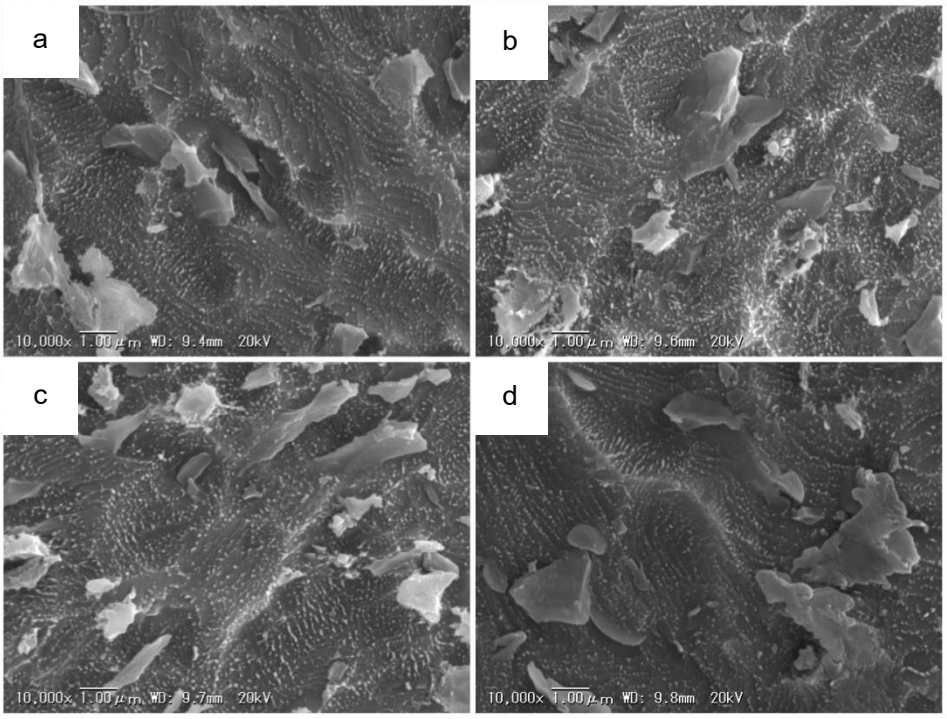

Fig. 4-21 SEM micrographs of the anodized films formed at 2, 4, 6 and 8 V in 1M MCPM, respectively

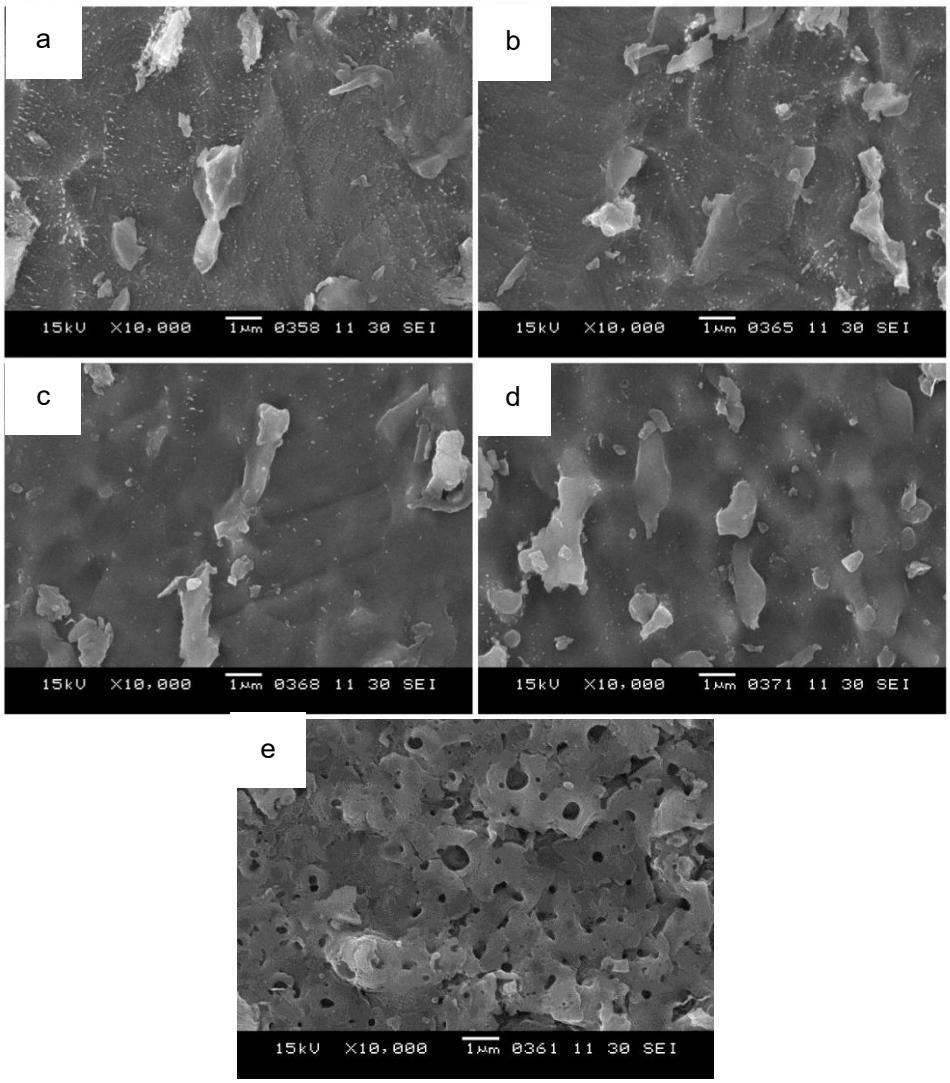

Fig. 4-22 SEM micrographs of the anodized films formed at 5, 10, 50, 100 and 150 V in 1M MCPM, respectively

4.2.2.4. The chemical species of the anodized films

The Ti 2p and O 1s narrow spectra of the anodized films formed at low V and high V show in Fig. 4-23, Fig. 4-24, Fig. 4-25 and Fig. 4-26. The Ti 2p spectra of all samples show TiO_2. The O 1s spectra of the anodized films formed at low V present O^{2-} (the titanium oxide) as a main peak and co-exist with OH^- (hydroxide) and H_2O (adsorbed water). However, the O 1s spectra of the anodized films formed at high V of 150 V shift to higher binding energy compared with those of low V. The anodized films formed at 10 and 150 V shift to higher binding energy compared with other conditions presenting OH^- as a main peak and co-exist with O^{2-} and H_2O for 10 V and co-exist only H_2O for 150 V as shown in Fig. 4-26. Although, the anodized films formed at 10 V composed of OH^- and co-exist with O^{2-} and H_2O and the morphology show roughness surface, its contact angle is higher than those of 150 V. These results indicated that the presence of both hydroxide and adsorbed water and porous surface on the anodized films formed at 150 V showed the highest hydrophilicity.

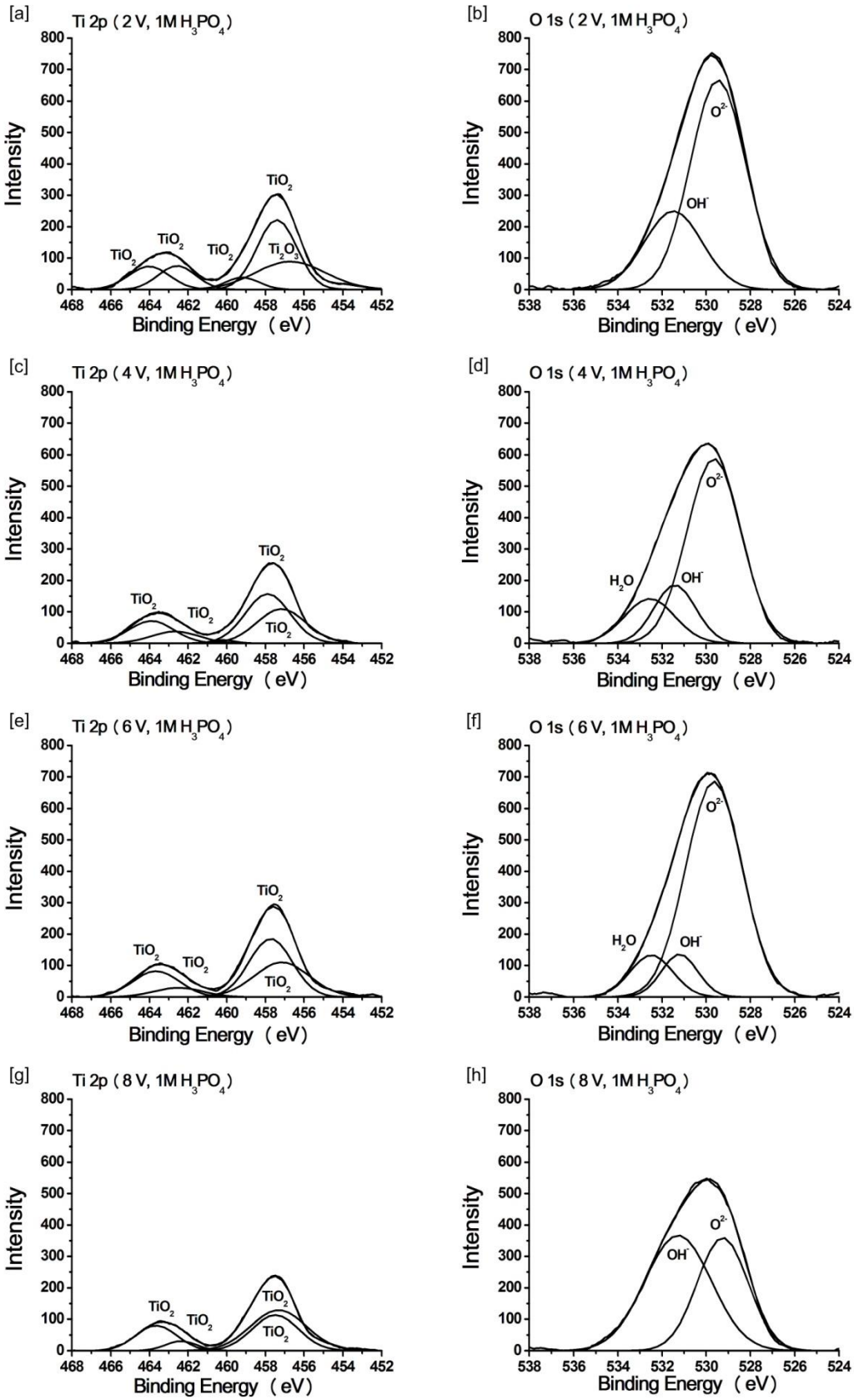

Fig. 4-23 Ti 2p and O 1s spectra of the anodized films formed at low V in 1M H_3PO_4

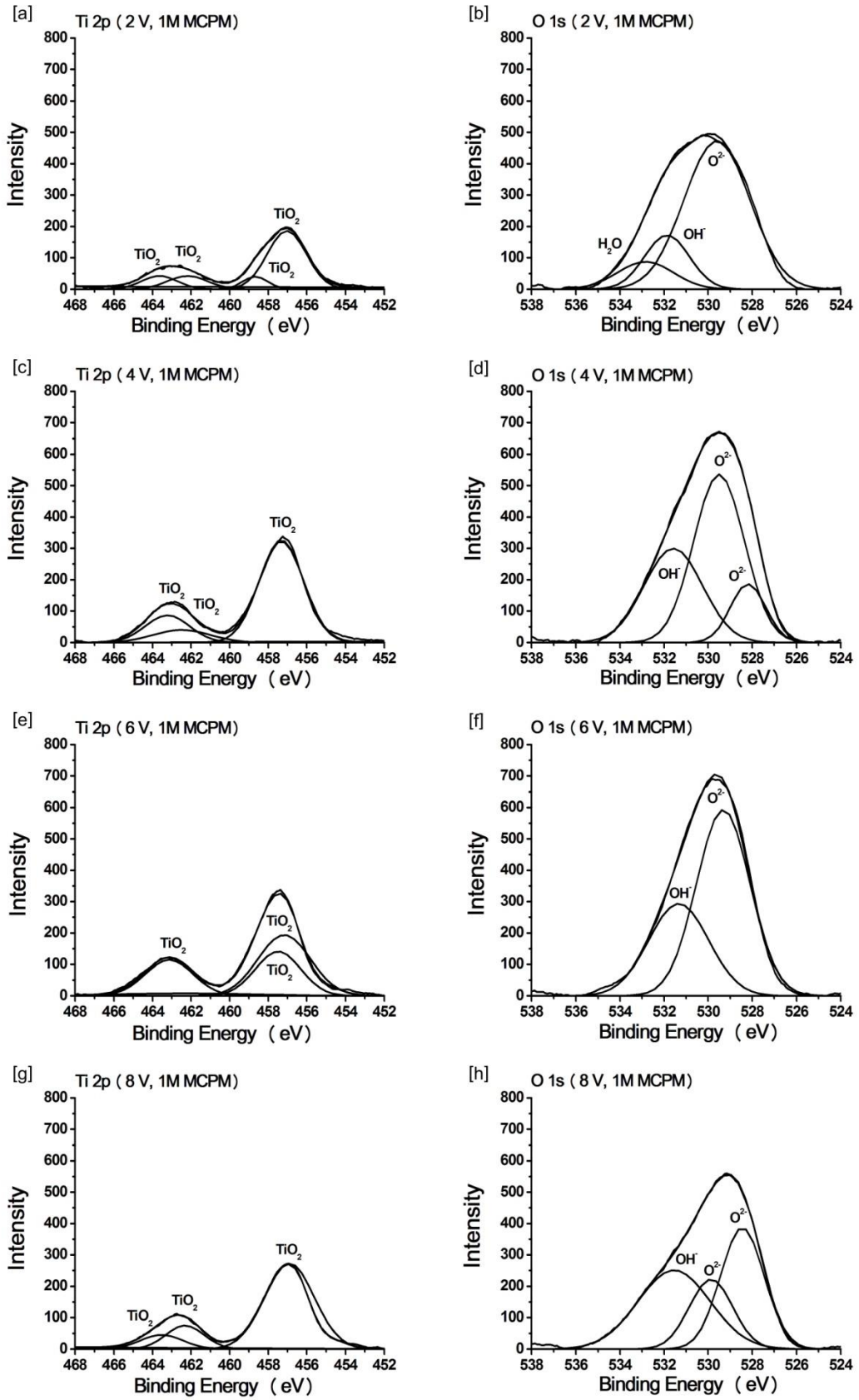

Fig. 4-24 Ti 2p and O 1s spectra of the anodized films formed at low V in 1M MCPM

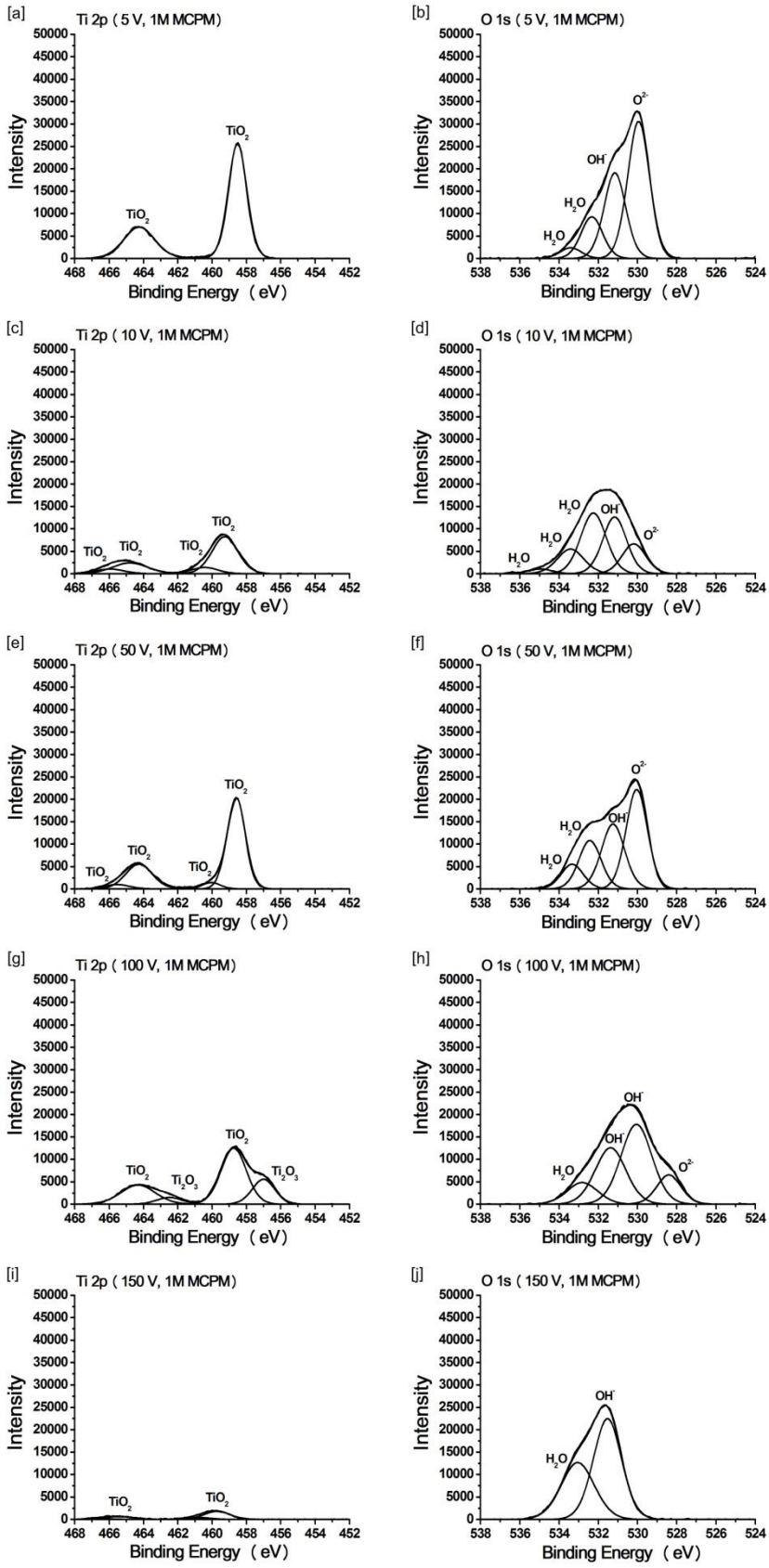

Fig. 4-25 Ti 2p and O 1s spectra of the anodized films formed at high V in 1M MCPM

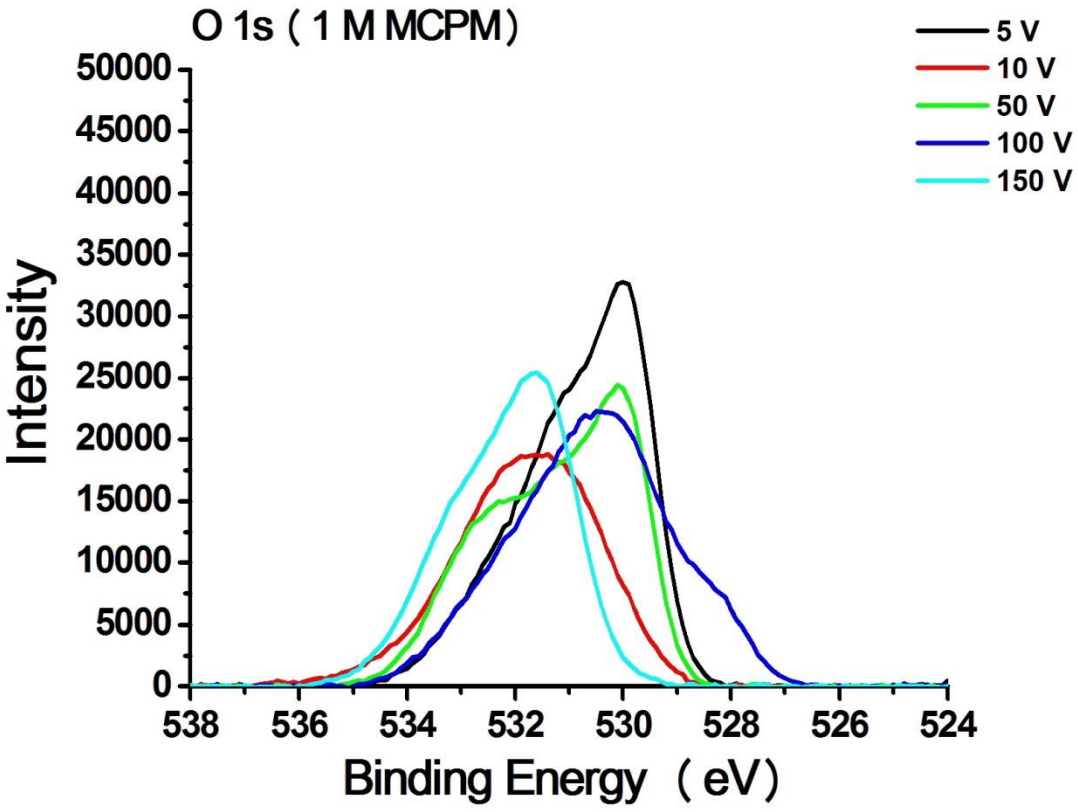

Fig. 4-26 O 1s spectra comparison of the anodized films formed at high V in 1M MCPM

4.2.2.5. ATR-FTIR spectrum of the anodized films

Fig. 4-27 showed the FTIR spectra of the anodized films formed at low voltage of 6V and high voltage of 150V in either 1M H_3PO_4 or 1M MCPM. It was observed that the FTIR spectra of the anodized films appear the OH group on the films surface. These FTIR results confirm the hydroxyl groups from XPS results. Therefore, the high hydrophilicity of the anodized films formed at high voltage of 150 V in 1M MCPM results from the hydroxyl groups on the porous surface.

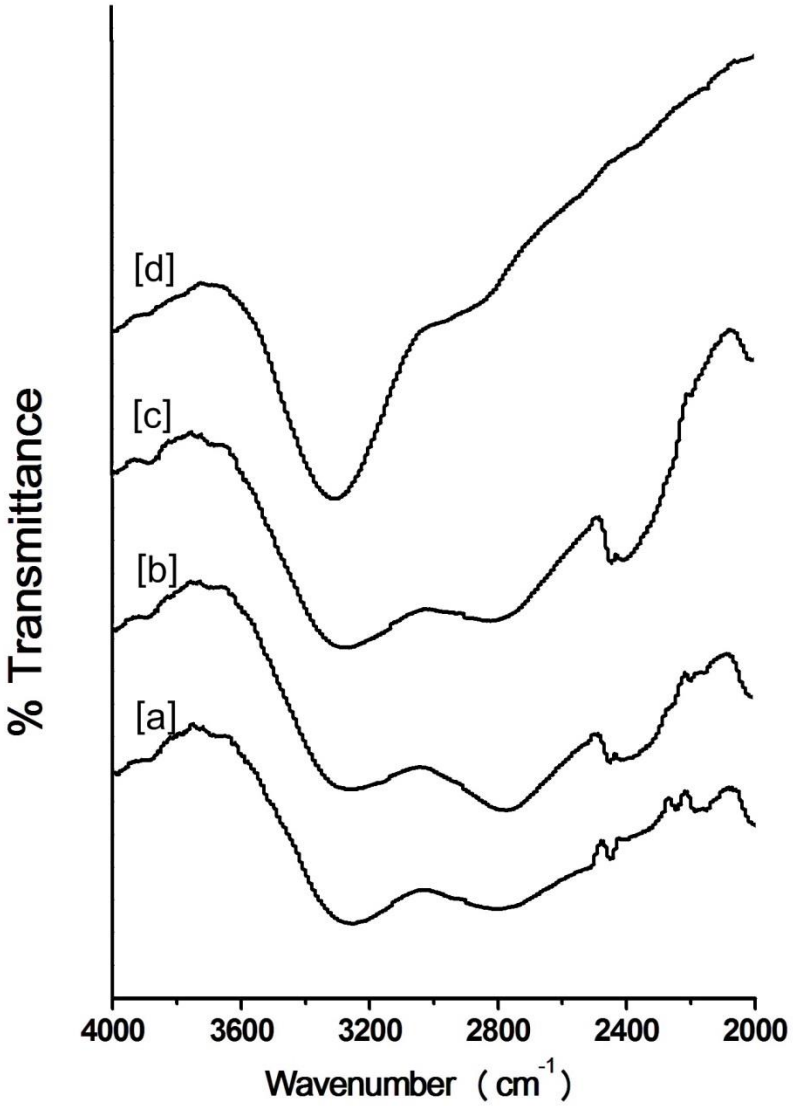

Fig. 4-27 ATR-FTIR spectra of the anodized films formed at (a) 6V in 1M H_3PO_4, (b) 6V in 1M MCPM, (c) 150 V in 1M H_3PO_4 and (d) 150 V in 1M MCPM

Discussion

The hydrophilicity of the anodized films formed by both galvanostatic method and potentiostatic method at low and high current densities or voltages was investigated. These results showed that the enhancing hydrophilcity of the anodized films formed at high current densities or voltages results from the porous surface and the hydroxyl groups on the films surface.

The porous surface was formed at high current density or high voltage. It is emphasized that the applied either high current or high voltage caused electrical sparks with high energy. High electrical current passed through the electrochemical cell and generated heat in the oxide layer resulting in melting and solidifying of the growing oxide layers in the surrounding electrolyte made the porous surface [60].

Fig. 4-28 showed the chemical reaction and structural changes during anodizing process. When the voltage reaches to breakdown voltage, the spark discharge occurred in some region resulting in a large number of small uniform micro-pores. After the voltage increased and reached to stable value, the number of spark decrease but their intensity increased resulting in rougher surface and increasing of the thickness. The porous films formation could be classified in three steps [31]. Firstly, when a large number of discharges were produced, the electron moved into the discharge channels rapidly due to high temperature and high pressure. The anionic components entered to these channels. At the same time, alloying elements of the substrate melted and diffused into the channels. Secondly, the oxide was solidified due to the rapid cooling of electrolyte. Therefore, the thickness increased in the area nearby the discharge channels. Finally, the gases were driven from the discharge channels resulting in holes with volcano shapes.

However, after applied low current density or low voltage, no electrical sparking occurred resulting in only roughness surface. Therefore, the applied high current or high voltage increases the opportunity to form porous surface and increase hydroxyl groups to the anodized films more than those of low current or low voltage resulting in higher hydrophilicity.

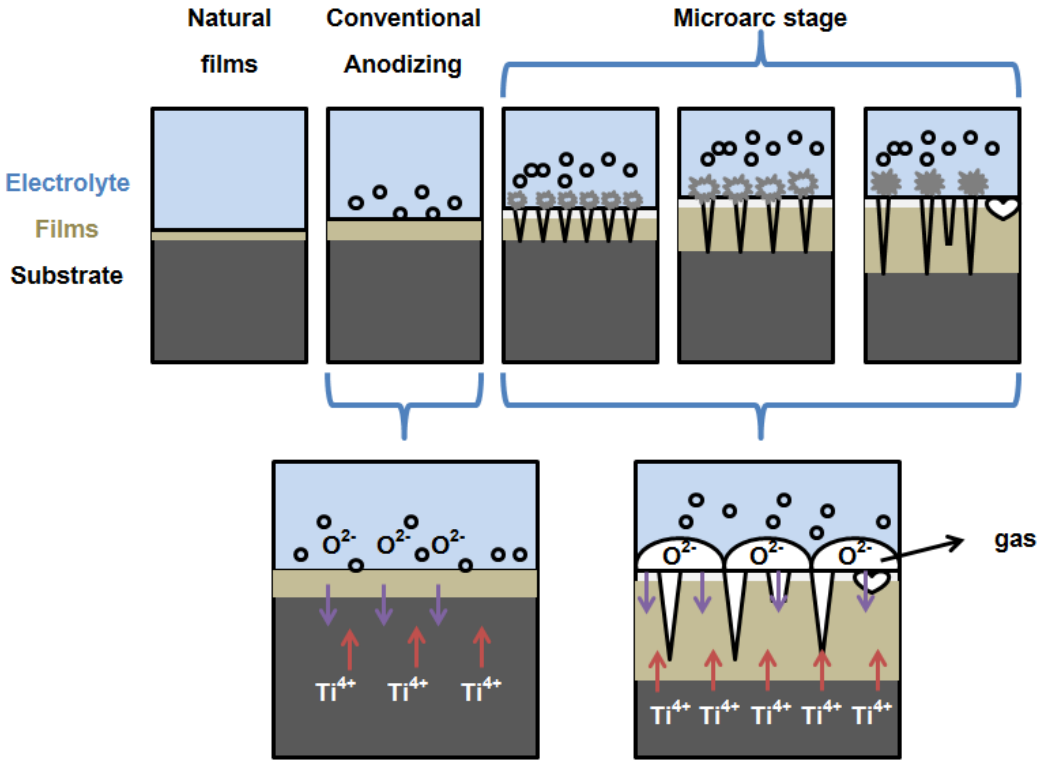

Fig. 4-28 Scheme of the chemical reaction and structural changes during anodizing process (this picture was modified from reference No. [31])

Fig. 4-10 showed the surface with different heights of the grains of the Ti-6Al-4V before and after anodization at low and high current density. A smooth surface was formed on the untreated Ti-6Al-4V. The grain structure showed large grain compared to the anodized films. The films formed without current densities and the anodized films formed at low current densities showed rough surface. The grain structure was smaller than those of the untreated Ti-6Al-4V. The anodized films formed at high current densities showed porous surface. The grain structure was obviously shown and it was smaller than those of anodized films formed at low current densities. These grains differed in height and surface shape; some areas were smooth, others were covered by pore. The grain size are in the order the untreated Ti-6Al-4V > the films formed without current density and the anodized films formed at low current densities or voltages > the anodized films formed at high current densities or voltages. It is indicated that the anodic current densities or voltages effect on the grain

orientation [61]. The grain size decreased with increasing of current density or voltage due to increasing of the thickness [61,62,63].

The mechanism of the grains formation was explained by phase diagram [64] and solidification process [65,66] as shown in Fig. 4-29 and Fig. 4-30. From the phase diagram of Ti-6Al-4V, At T_1, the liquid of Alloy C_0 starts solidification. The first solid has composition as C_{s1}. After that the T_1 was cooled to T_2, an outer shell of composition C_{s2} is formed surrounding C_{s1} due to inadequate diffusion on fast cooling, so a composition difference is created. The average composition of the solid composite at T_2 is somewhere between C_{s1} and C_{s2}:C_{s2^*}. The same situation continues throughout the process. Under equilibrium condition solidification completes at T_3. However, under non-equilibrium condition, the average composition of solid at T_3 is $C_{s3^*} < C_0$, indicating that solidification is not completed yet. Solidification actually ends when the average composition of solid equals C_0, i.e., at T_4.

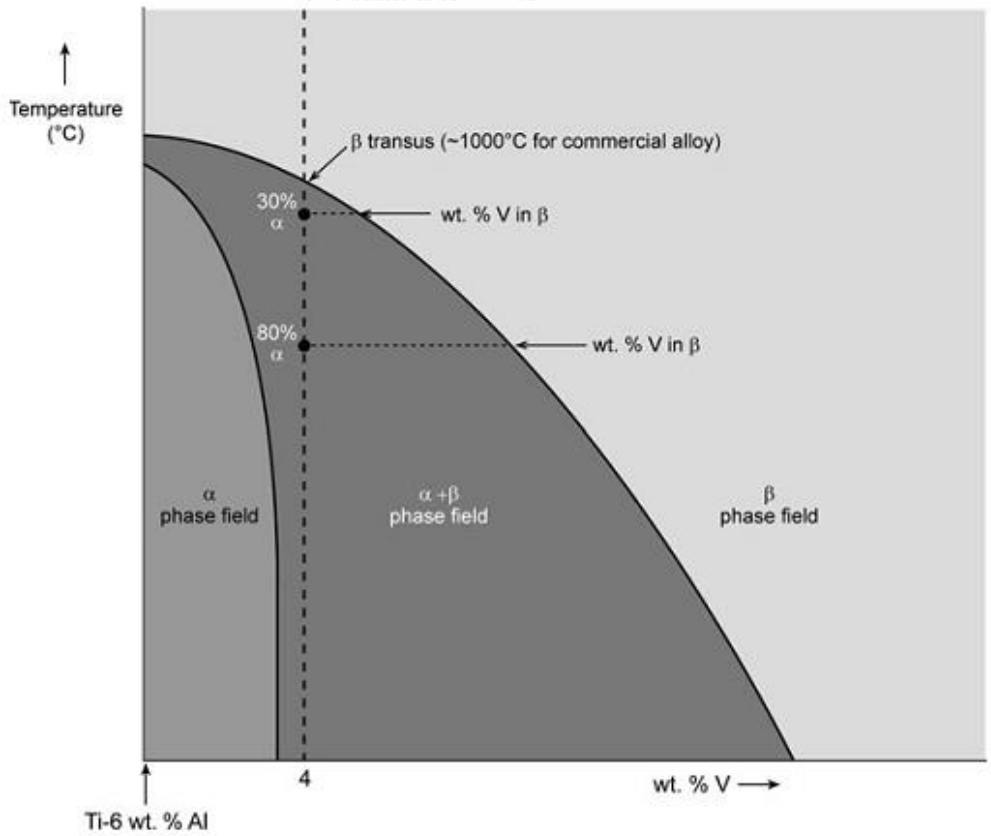

Fig. 4-29 Phase diagram of Ti-6Al-4V [64]

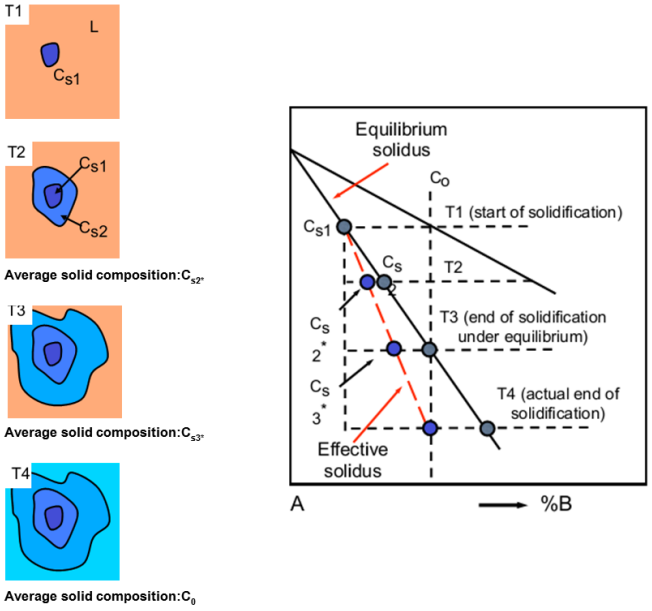

Fig. 4-30 Non-equilibrium solidification and cored structure formation [66]

Fig. 4-31 showed the different grain size on the anodized films surface due to atom orientations on each grain. The porous surface has small number of atoms in each grain but the number of the grain boundaries was very high. This grain formation could be explained by Fig. 4-32.

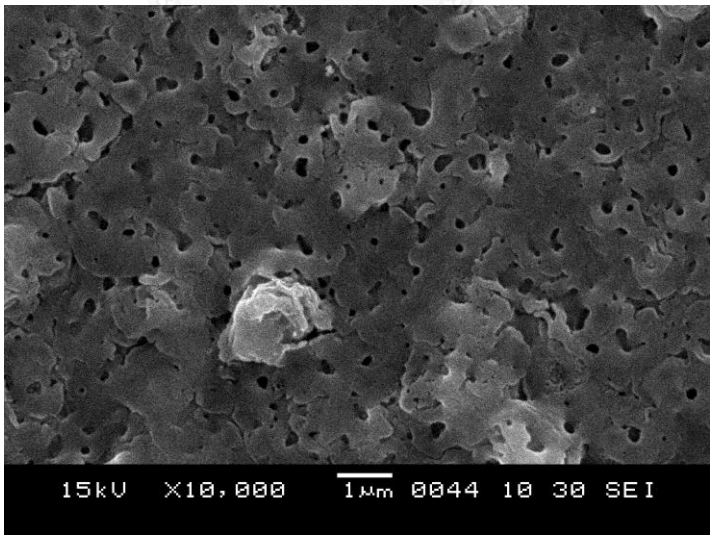

Fig. 4-31 SEM micrograph of the anodized films formed at 1 mA/cm^2 in 1M MCPM

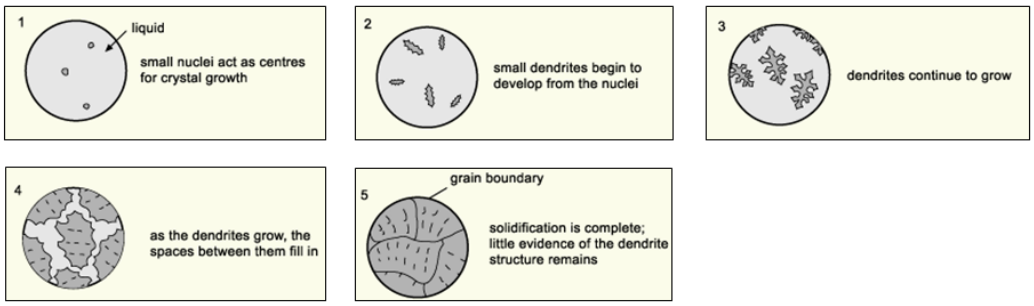

Fig. 4-32 Solidification of metal [67]

The crystals begin to grow and form grain boundaries from the nucleation point. At solidification temperature, the atoms of melted metal liquid begin to bond together and form crystals as a grain at the nucleation point. The size of grain depends on the number of nucleation points. The interface formed between grains is called grain boundary surface. These atoms have no crystalline due to disorder [65,67,68]. It is indicated that the fine grain structure of porous surface results from more nucleation points due to rapid cooling during anodizing process.

It has been reported that the nanograined titanium and its alloys can improve the corrosion resistance [26], the biological properties compared with coarse grained parts [26,27].

During anodizing process, the main reactions leading to oxidation at the anode [25] can be written as:

At Ti/Ti oxide interface: $Ti \rightarrow Ti^{2+} + 2e^-$

At Ti oxide/electrolyte interface:

$2\ H_2O \rightarrow 2\ O^{2-} + 4\ H^+$ (Oxygen ions react with Ti to form oxide)

$2\ H_2O \rightarrow O_2$ (gas) $+ 4\ H^+ + 4e^-$ (O_2 gas evolves or sticks at electrode surface)

At both interfaces: $Ti^{2+} + 2\ O^{2-} \rightarrow TiO_2 + 2e^-$

The anodized films formed at high current or high voltage exhibit a high hydrophilicity due to their porous surface and hydroxyl groups. Wenzel's theoretical model was used to describe the contact angle of rough surface. Wenzel's equation as follows:

$$\cos(\theta) = r(\gamma_{SV} - \gamma_{SL})/\ \gamma_{LV} = r\cos(\alpha)$$

where r is defined as the surface ratio, γ_{SV}, γ_{SL}, and γ_{LV} are the interfacial free energy per unit area of solid-vapor, solid-liquid, and liquid-vapor interfaces, respectively. α is the contact angle of a smooth area.

This equation indicated that the surface roughness enhances the hydrophilicity of a hydrophilic surface (θ<90°) and the hydrophobicity of a hydrophobic one (θ>90°) because r is always greater than 1 [60]. It is important to notice that the Wenzel equation is based on the assumption that the liquid penetrates into the roughness surface as shown in Fig. 4-33.

Moreover, the increase of hydroxyl groups on the TiO_2 films tends to make the hydrophilic surface because the hydroxyl groups can form hydrogen bond with water [69] as shown in Fig. 4-34.

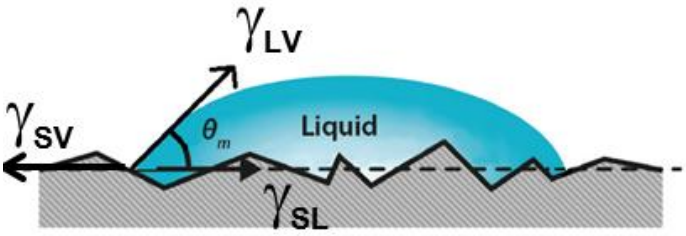

Fig. 4-33 Roughness surface induced hydrophilicity [60]

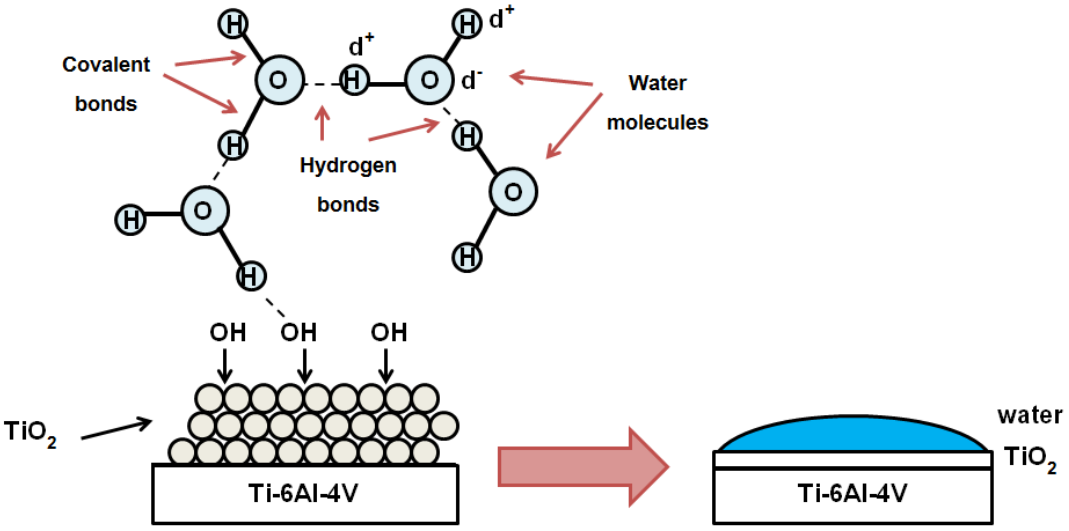

Fig. 4-34 Hydroxyl groups induced hydrophilicity to the films

4.3. Effect of UV irradiation on hydrophilicity of the anodized films

The anodized films formed at 2 mA/cm^2 in 1M H_3PO_4, 1 mA/cm^2 in 1M MCPM, and 6 V in either 1M H_3PO_4 or 1M MCPM were selected to enhance hydrophilicity by UV irradiation.

4.3.1. Surface characterizations of the anodized films formed at low current density and low voltage

The chemical species of the anodized films were characterized by XPS. The Ti 2p spectra show there are no differences in all samples. The TiO_2 appears on all samples as shown in Fig. 4-35. However, the O 1s shows the difference between the Ti-6Al-4V before and after anodization as shown in Fig. 4-36. The O 1s spectra of the untreated Ti-6Al-4V and the films formed without current density show O^{2-} as a main peak and co-exist with OH^- and/or H_2O. The O 1s spectra of the anodized films shift to higher binding energy and appear OH^- as a main peak and co-exist with O^{2-} and/or H_2O. It is indicated that the OH group was improved after anodization. These results were confirmed by the functional groups in ATR-FTIR results as shown in Fig. 4-37. It can be clearly seen that there are peaks in the range of 3000-3600 cm^{-1} (-OH stretching vibration) on all samples The surface morphology was enhanced after anodization as shown in Fig. 4-38. However, the contact angle of the anodized films, there are no significant difference ($p>0.05$) compared with the untreated Ti-6Al-4V as shown in Fig. 4-39.

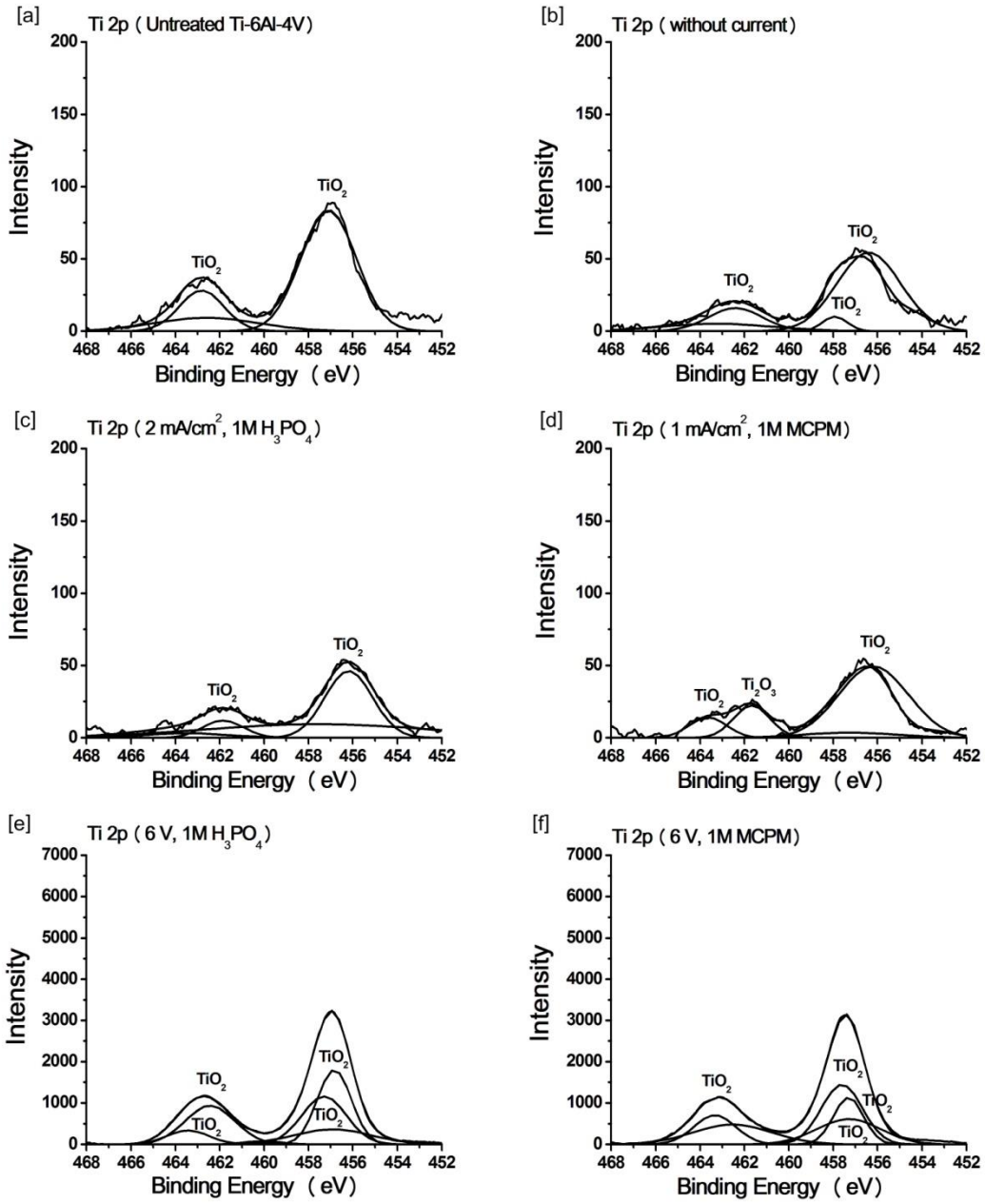

Fig. 4-35 Ti 2p spectra of the Untreated Ti-6Al-4V, the films formed without current and the anodized films formed at 2 mA/cm^2 in 1M H_3PO_4, 1 mA/cm^2 in 1M MCPM and 6 V in either 1M H_3PO_4 or 1M MCPM

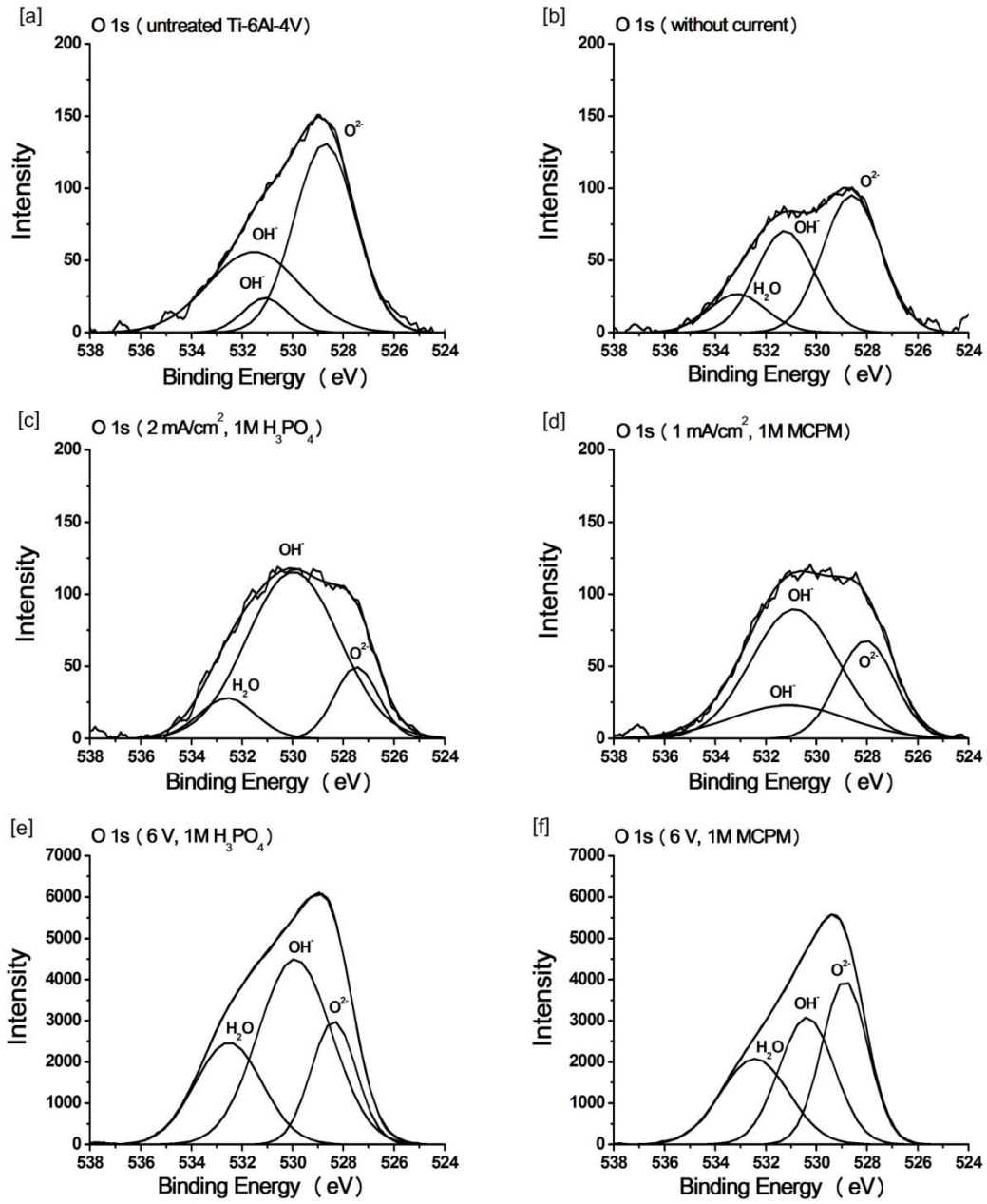

Fig. 4-36 O 1s spectra of the Untreated Ti-6Al-4V, the films formed without current and the anodized films formed at 2 mA/cm^2 in 1M H_3PO_4, 1 mA/cm^2 in 1M MCPM and 6 V in either 1M H_3PO_4 or 1M MCPM

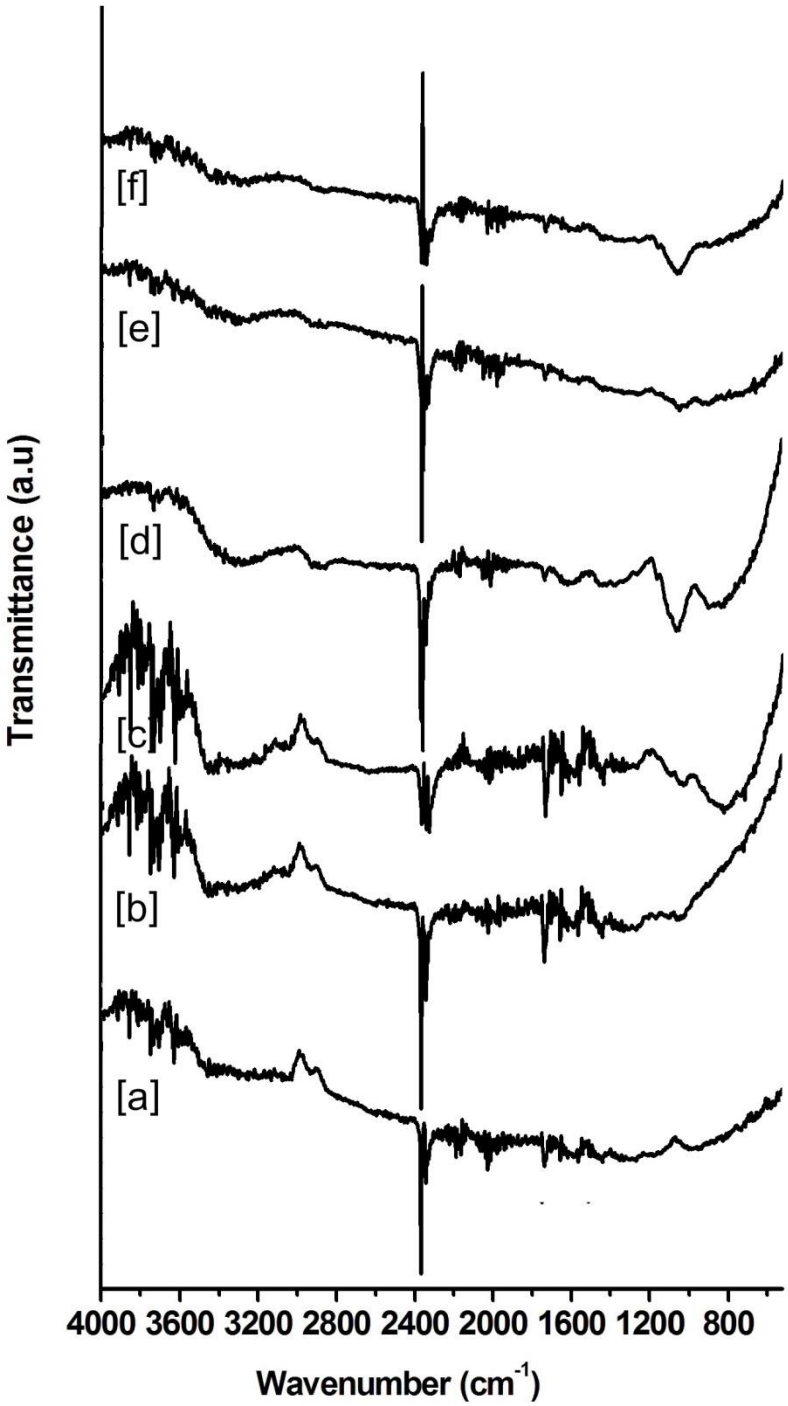

Fig. 4-37 ATR-FTIR spectra of (a) the Untreated Ti-6Al-4V, (b) the films formed without current and the anodized films formed at (c) 2 mA/cm^2 in 1M H_3PO_4, (d) 1 mA/cm^2 in 1M MCPM and (e, f) 6 V in either 1M H_3PO_4 or 1M MCPM

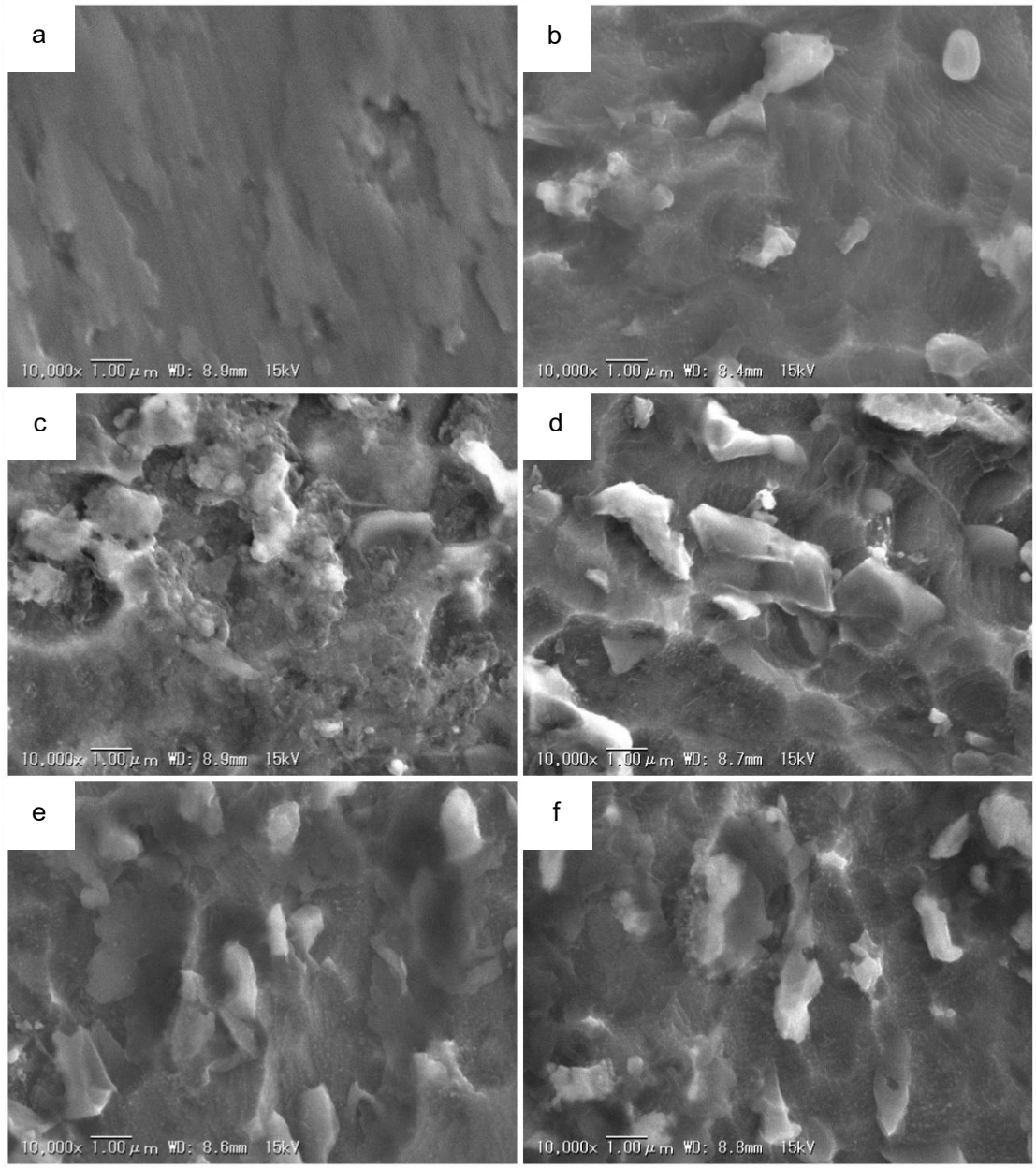

Fig. 4-38 Surface morphology of the (a) Untreated Ti-6Al-4V, (b) the films formed without current and the anodized film formed at (c) 2 mA/cm^2 in 1M H_3PO_4, (d) 1 mA/cm^2 in 1M MCPM and (e, f) 6 V in either 1M H_3PO_4 or 1M MCPM

Although, the chemical species and the surface morphologies were improved after anodization, the contact angle of the anodized films, there were no significant difference ($p>0.05$) compared to the untreated Ti-6Al-4V. It is indicated that the hydrophilicity of the anodized films did not enhance. Therefore, the UV irradiation was considered to improve hydrophilicity to the TiO_2 films.

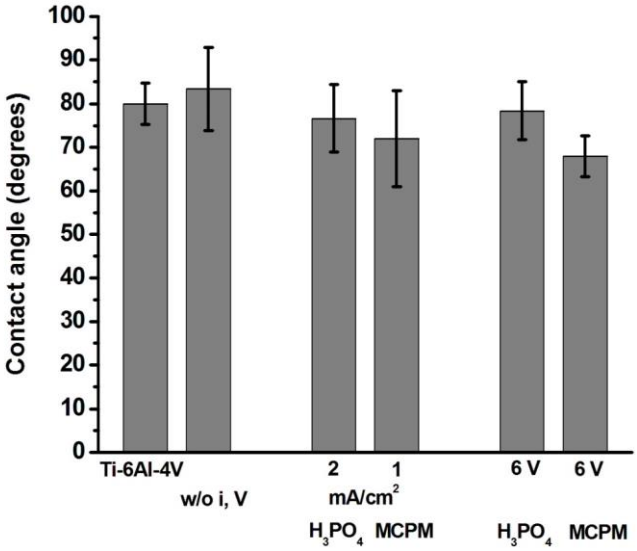

Fig. 4-39 Contact angle of the Untreated Ti-6Al-4V, the films formed without current and the anodized films formed at 2 mA/cm^2 in 1M H_3PO_4, 1 mA/cm^2 in 1M MCPM and 6 V in either 1M H_3PO_4 or 1M MCPM

4.3.2. UV induced hydrophilicity of the anodized films

The contact angle of the untreated Ti-6Al-4V decrease from 79.94° ± 4.71° to 53.48° ± 8.05°, the films formed without current decrease from 83.33° ± 9.51° to 47.39° ± 8.55°, the anodized films formed at 2 mA/cm^2 in 1M H_3PO_4 decrease from 76.61° ± 7.71° to 52.87° ± 10.23°, 1 mA/cm^2 in 1M MCPM decrease from 71.94° ± 10.94° to 27.86° ± 5.52° after UV irradiation for 24 h as shown in Fig. 4-40. At the same time, the contact angle of the anodized films formed at 6 V in 1M H_3PO_4 decrease from 78.35° ± 6.62° to 44.59° ± 7.29° and 6 V in 1M MCPM decrease from 67.99° ± 4.67° to 36.91° ± 5.83° as shown in Fig. 4-41. Therefore, the UV irradiation could enhance hydrophilicity to all samples. It is indicated that the anodized films formed at low

current density and low voltage could enhance hydrophilicity after UV irradiation for 24 h.

The contact angle of all samples increased after store in the dark for a week as shown in Fig. 4-40 and Fig. 4-41. It is indicated that the hydrophilicity converted to hydrophobicity after the samples were kept in the dark.

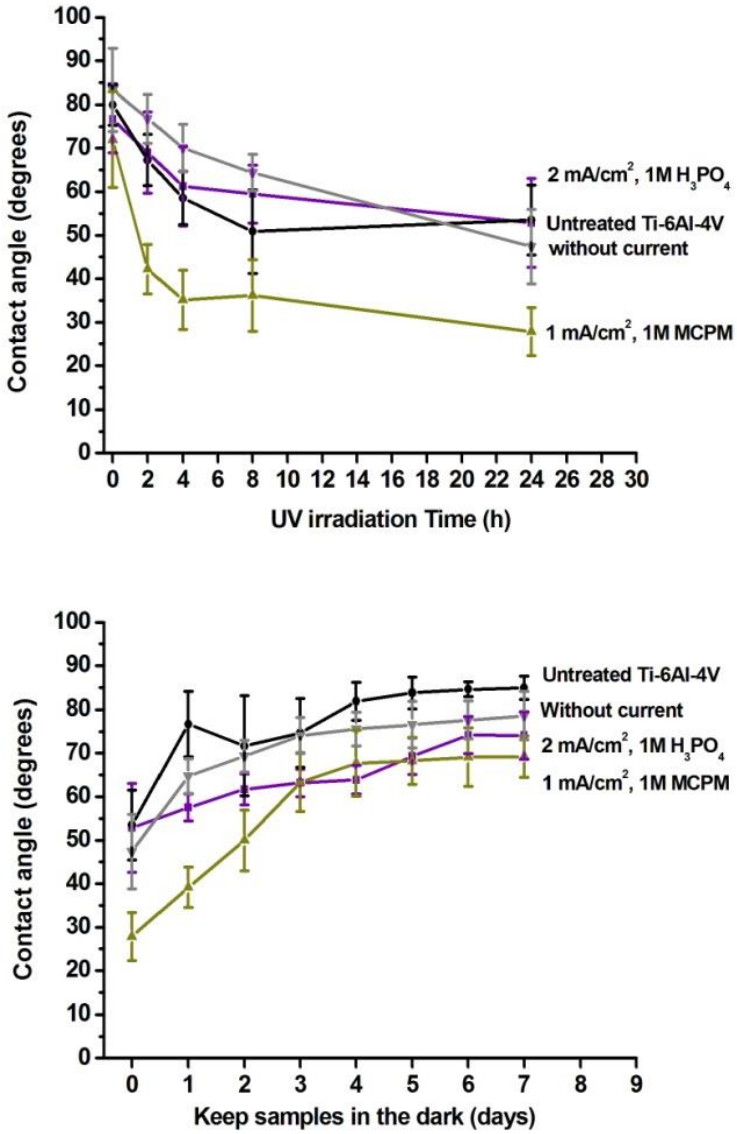

Fig. 4-40 Contact angle of the Untreated Ti-6Al-4V and the anodized film formed at 2 mA/cm^2 in 1M H_3PO_4, 1 mA/cm^2 in 1M MCPM and the films formed without current before and after UV irradiation and keep samples in the dark for a week

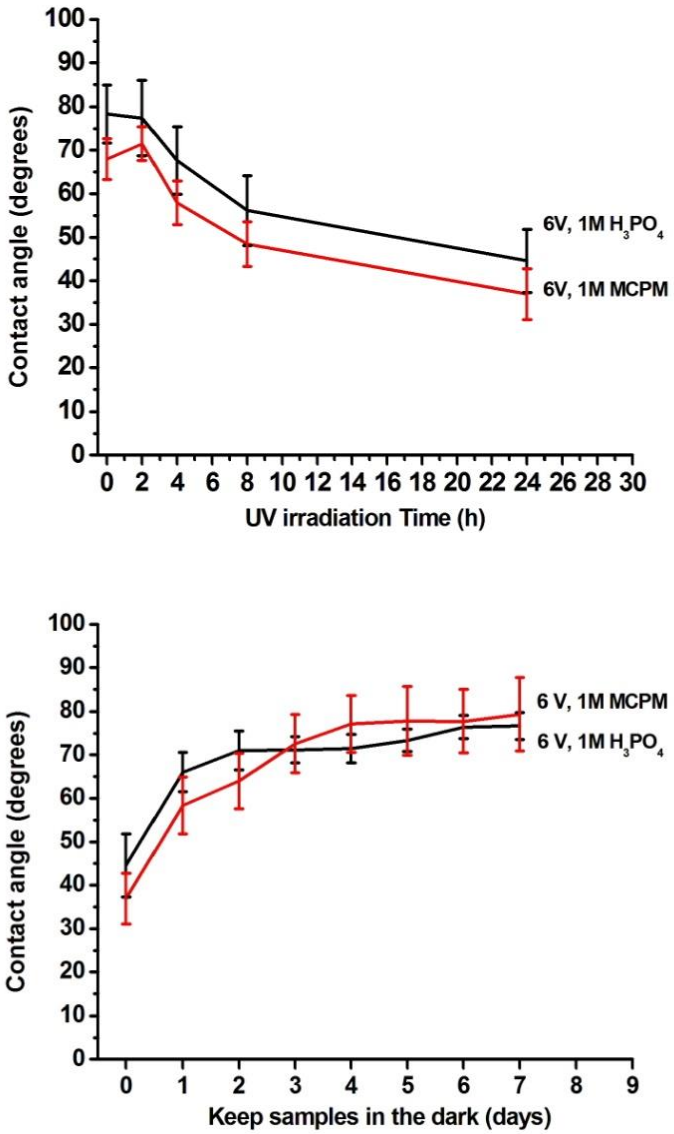

Fig. 4-41 Contact angle of the anodized film formed at 6 V in 1M H_3PO_4 and 6 V in 1M MCPM before and after UV irradiation and keep samples in the dark for a week

4.3.3. Surface chemical species of the anodized films after UV irradiation

The XPS spectra of Ti 2p, O 1s and C 1s are shown in Fig. 4-42. It revealed that the intensity of C 1s peak decreased, while the intensity of Ti 2p peak and O 1s peak increased after UV irradiation for 24 h. However, the position of the binding energy did not change. It is indicated that UV irradiation did not change the chemical species of the anodized films.

4.3.4. The functional group of the anodized films after UV irradiation

The functional groups of the films before and after UV irradiation were investigated by ATR-FTIR as shown in Fig. 4-43. After UV irradiation for 24 h, the peak of OH groups disappear at 3000 - 3600 cm^{-1}. It is indicated that the –OH group was not stable under UV irradiation. Moreover, the anodized films were heated at 80 ^{o}C in order to remove H_2O from the films surface. The result showed that the OH group appeared on the surface after heating at 80 ^{o}C. It is indicated that the OH group formed at the anodized films surface was not stable under UV irradiation for 24 h.

4.3.5. Surface morphologies of the anodized films after UV irradiation

The surface morphology of the untreated Ti-6Al-4V is smooth surface as shown in Fig. 4-44, the surface of the films formed without current is rough surface, while the surface of the anodized films is rough surface and show blue color (2 mA/cm^2, 1M H_3PO_4) and yellow color (1 mA/cm^2, 1M MCPM and 6 V in either 1M H_3PO_4 or 1M MCPM). The different color of the films appears. It may be because the different thicknesses of the films increase after anodization.

Compared with the surface morphology of the films before UV irradiation, the UV irradiation does not change the surface morphology as shown in Fig. 4-44. It is indicated that UV irradiation improves the hydrophilicity but the surface morphology did not change after UV irradiation corresponding with Han et al. [22,70].

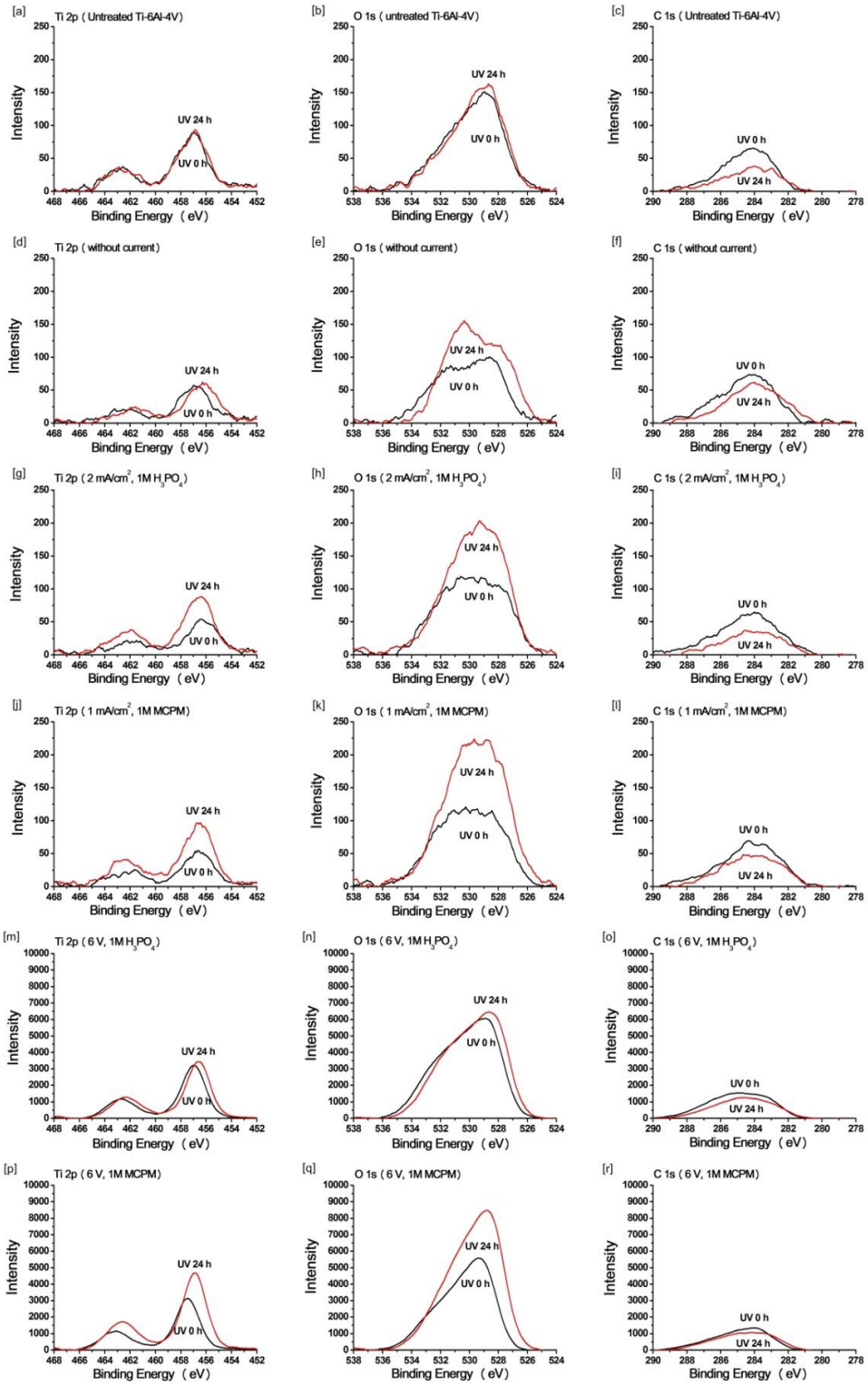

Fig. 4-42 XPS spectra of Ti 2p, O 1s and C 1s before and after UV irradiation of the untreated Ti-6Al-4V, the films formed without current and the anodized films formed at 2 mA/cm^2 in 1M H_3PO_4, 1 mA/cm^2 in 1M MCPM and 6 V in either 1M H_3PO_4 or 1M MCPM

[a] After UV irradiation 24 h

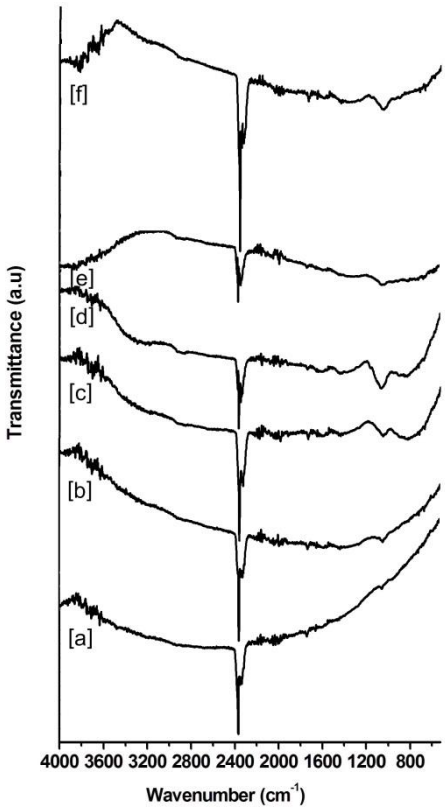

[b] After heat at 80°C

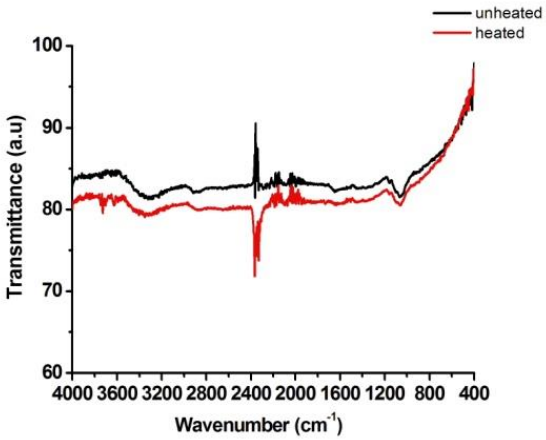

Fig. 4-43 ATR-FTIR spectra of (a) the Untreated Ti-6Al-4V, (b) the films formed without current and the anodized films formed at (c) 2 mA/cm^2 in 1M H_3PO_4, (d) 1 mA/cm^2 in 1M MCPM and (e, f) 6 V in either 1M H_3PO_4 or 1M MCPM [a] after UV irradiation 24 h, [b] after heat the anodized films formed at 1 mA/cm^2 in 1M MCPM at 80 °C

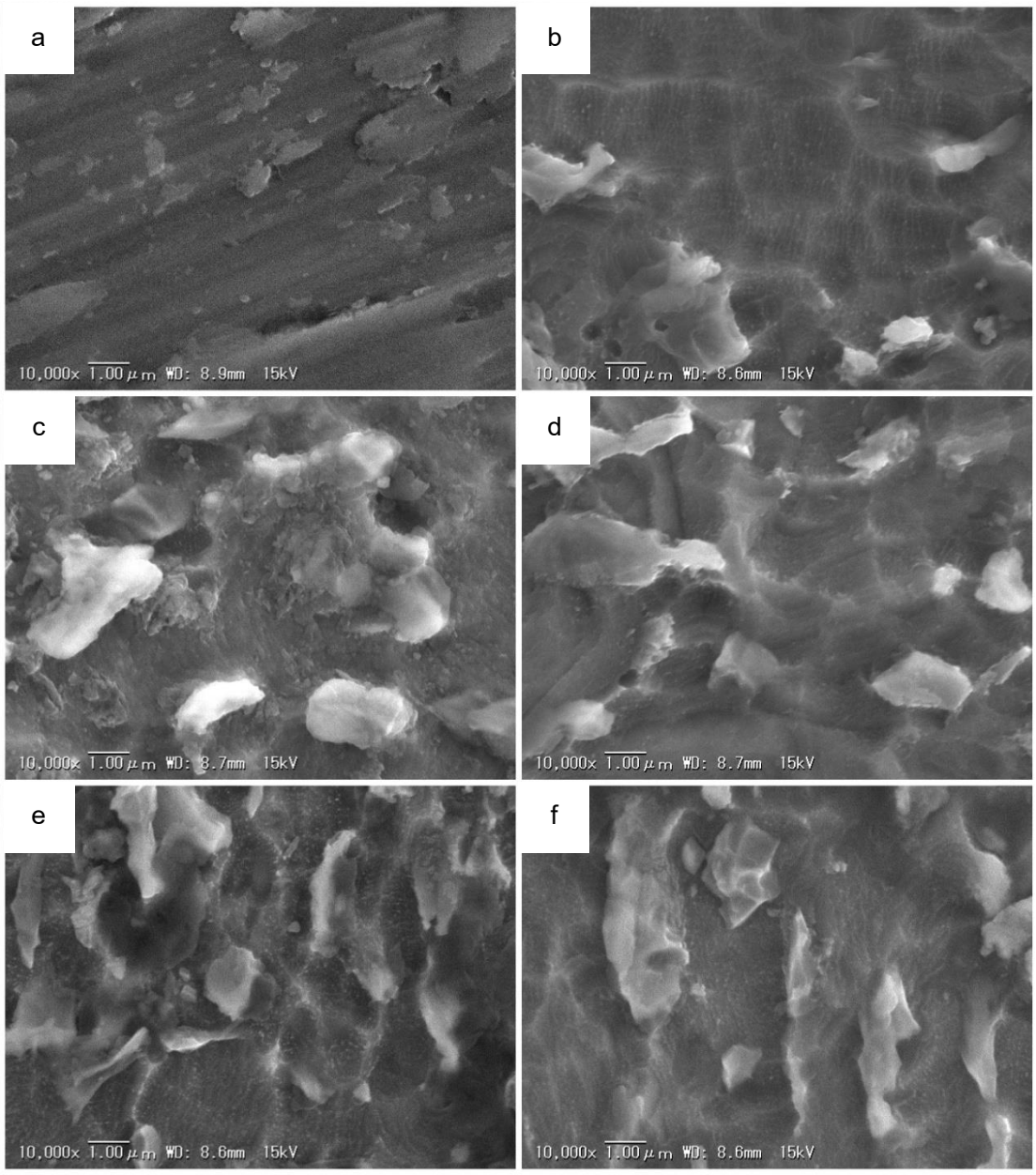

Fig. 4-44 Surface morphology after UV irradiation of (a) the untreated Ti-6Al-4V, (b) the films formed without current and the anodized films formed at (c) 2 mA/cm^2 in 1M H_3PO_4, (d) 1 mA/cm^2 in 1M MCPM and (e-f) 6 V in either 1M H_3PO_4 or in 1M MCPM

4.3.6. Surface energies of the anodized films after UV irradiation

Hydrophilicity and surface energy are important factor to understand the biological performance on the biomaterial surfaces such as protein adsorption and cellular adhesion [13]. Fig. 4-45 show the averaged contact angles of the untreated Ti-6Al-4V, the films formed without current and the anodized films formed at 2 mA/cm^2 in 1M H_3PO_4, 1 mA/cm^2 in 1M MCPM and 6 V in either 1M H_3PO_4 or in 1M MCPM before and after UV irradiation. The results show that both contact angle of H_2O and glycerol decreased after UV irradiation.

The contact angle is inversely proportional to the surface energy. These changes can be explained by Owense-Wendt equation;

$$1 + \gamma_l \cos\theta = 2[(\gamma_s^d \gamma_l^d)^{1/2} + (\gamma_s^p \gamma_l^p)^{1/2}] \quad (1)$$

$$\gamma^t = \gamma_s^d + \gamma_s^p \quad (2)$$

Where γ_l is the surface tension of liquid.

γ^p_s and γ^d_s are the polar and dispersion terms of solid surface energy, respectively.

γ^p_l and γ^d_l are the polar and dispersion terms of liquid surface tension, respectively.

From (1) and (2), if the θ decreases, the term of cos θ will increase. Therefore, the total surface energy will increase [71]. It is indicated that the contact angle of all samples after UV irradiation decrease resulting in hydrophilicity because the surface energy of the films increase as shown in Fig. 4-46. In addition, after UV irradiation the polar component of surface energy increased while the dispersive component decreased. It is indicated that the UV irradiation could increase surface energy resulting in enhancing hydrophilicity.

Furthermore, the total energies of all samples have two contributions such as polar and dispersive as shown in Fig. 4-46. The various research groups showed that polar surface energy is important factor to improve the protein adsorption and cellular adhesion [13,72]. However, some papers showed that the correlation between polar

surface energy and protein adsorption was not found. Other factors such as surface charges and/or chemical composition may influence on protein adsorption [72].

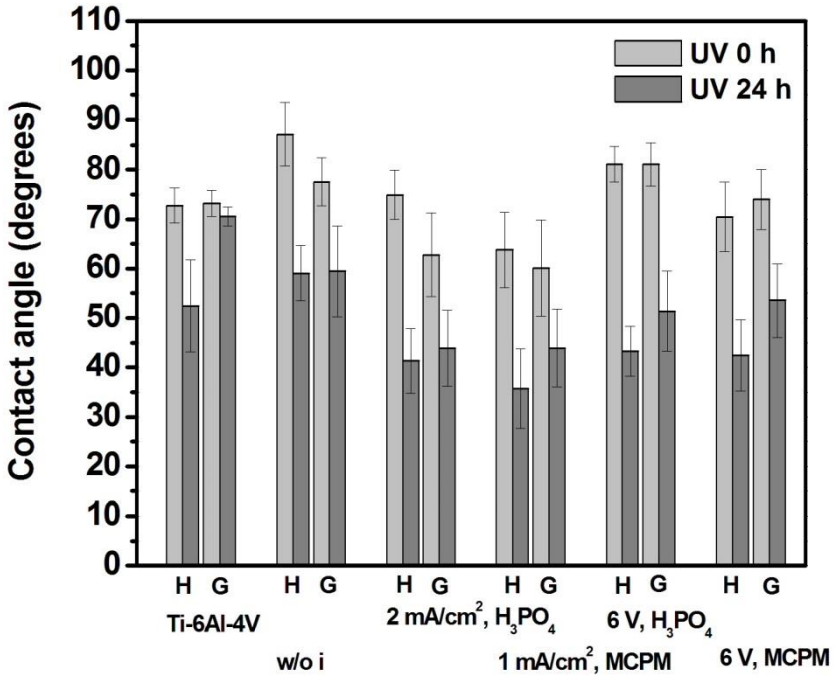

Fig. 4-45 Contact angle of H_2O and Glycerol of the untreated Ti-6Al-4V, the films formed without current and the anodized films formed at 2 mA/cm^2 in 1M H_3PO_4, 1 mA/cm^2 in 1M MCPM and 6 V in either 1M H_3PO_4 or in 1M MCPM before and after UV irradiation; H = H_2O, G = Glycerol

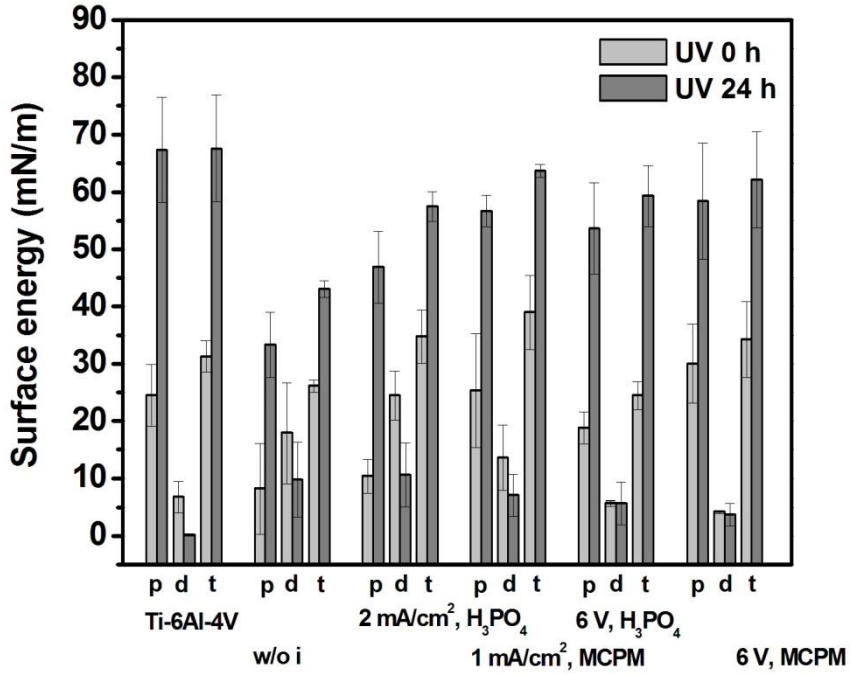

Fig. 4-46 Surface energies of the untreated Ti-6Al-4V, the films formed without current and the anodized films formed at 2 mA/cm^2 in 1M H_3PO_4, 1 mA/cm^2 in 1M MCPM and 6 V in either 1M H_3PO_4 or in 1M MCPM before and after UV irradiation before and after UV irradiation; p = polar, d = dispersive, t = total surface energy

4.3.7. Discussion

According to the photocatalytic property of TiO_2, it shows a good UV-induced hydrophilicity due to the chemisorption of water molecules from the air at both Ti^{3+} surface sites and oxygen vacancies generated by UV irradiation [21,22,73]. The result from XPS spectra show that the anodized films after UV irradiation show the increase in Ti $2p_{3/2}$ at lower binding energy due to the conversion of Ti^{4+} to Ti^{3+} and in O 1s at higher binding energy due to the adsorption of hydroxyl group [16,22,39,40]. In addition, the surface energy could enhance after UV irradiation [45]. However, the surface morphology did not change after UV irradiation [22].

However, in this study, the anodized films formed at low current density or low voltage showed a weak or no defect formation on TiO_2 surfaces because the XPS spectra were found only the increase in intensity of Ti 2p and O 1s peak and the decrease in those of C 1s peak. The position of binding energy did not change. Therefore, the anodized films formed at low current density and low voltage may be not TiO_2. It may be hydroxylated TiO_x so it show the behavior after UV irradiation differ from TiO_2. Therefore, these anodized films could enhance hydrophilicity to the films. It may be due to the heat from UV and increasing of surface energy after UV irradiation resulting in hydrophilicity.

Sirghi et al. reported that there are three main causes that may explain the UV-induced hydrophilicity of the amorphous TiO_2 films [73]. Firstly, the smooth surface may contained a low defects or low surface area which might cause a low photocatalytic activity. Secondly, the films could adsorb only partially UV irradiation. Lastly, the charge separation caused by the energy band distortion at the films interface the formation of charge carries in the bulk and their transportation to the surface when they interact with the adsorbate molecules [73].

Moreover, the anodized films were kept in the dark for a week. The results show that the hydrophilicity decreases. It is indicated that the hydrophilicity of the anodized films after store in the dark can convert to hydrophobicity.

In addition, the anodized films formed at low current density show low contact angle as well as the anodized films formed at high current density; the contact angle

of the anodized films formed at high current density (galvanostatic method) of 5, 20 and 80 mA/cm^2 in 1M H_3PO_4 or 1M MCPM decreased to 48.3^o ± 8.1^o, 41.5^o ± 5.7^o, 45.3^o ± 7.7^o, 24.3^o ± 6.1^o, 17.2^o ± 3.2^o and 21.7^o ± 6.6^o, respectively. In addition, the contact angle of the anodized films formed at high current voltage (potentiostatic method) of 5, 10, 50, 100 and 150 V in 1M H_3PO_4 or 1M MCPM decreased to 48.8^o ± 5.44^o, 48.53^o ± 1.77^o, 46.4^o ± 8.82^o, 59.73^o ± 4.77^o and 37.87^o ± 3.16^o, 50.87^o ± 6.62^o, 52.87^o ± 4.83^o, 51.6^o ± 3.62^o, 50.47^o ± 4.97^o and 26.2^o ± 4.8^o, respectively. Therefore, it is good alternative for the anodized films preparation with low current density or low voltage in order to save energy, save cost and safety to prepare the films.

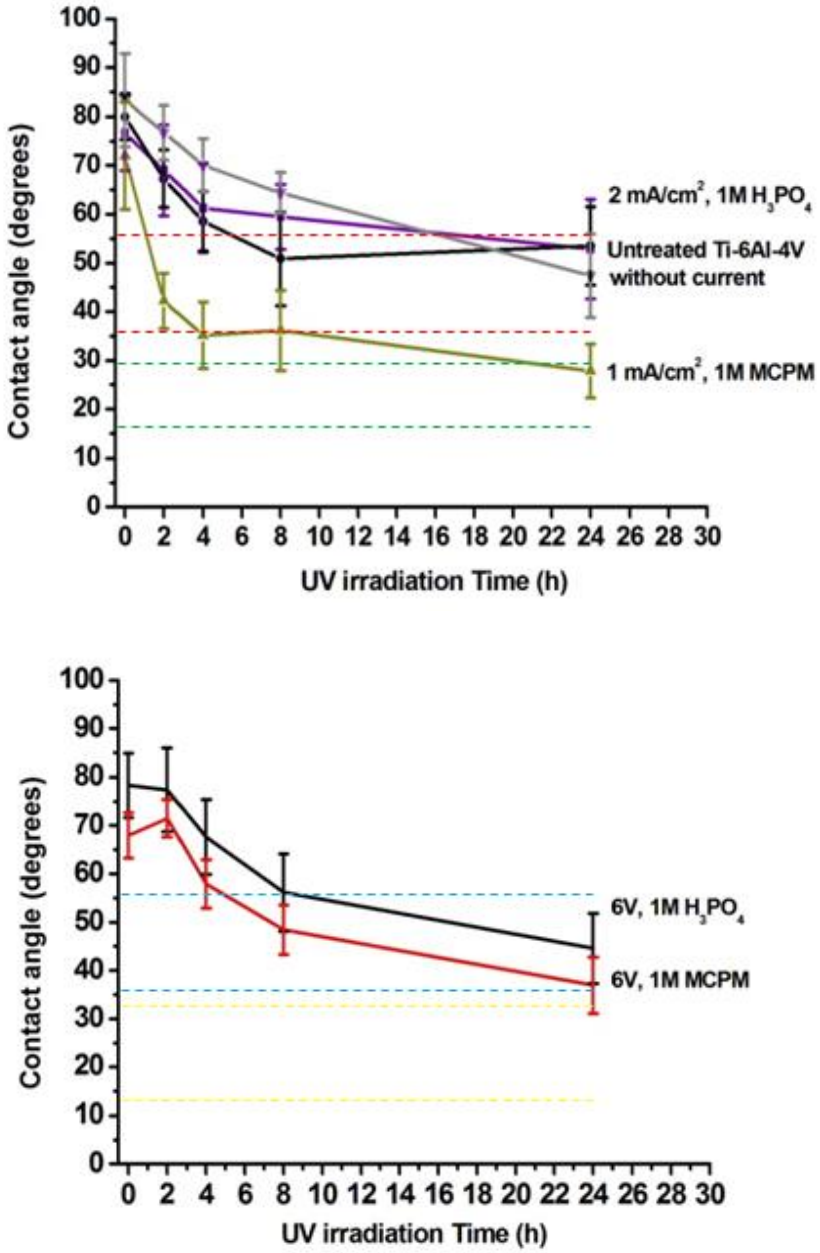

Fig. 4-47 Comparison of contact angle between the anodized films formed at low and high current density or voltage

4.4. Effect of ethanol treatment on hydrophilicity of the anodized films

In this part, the ethanol treatment was used in order to improve the hydrophilicity to the anodized films. The result from previous part, it is indicated that the electrolyte that come from H_2O as solvent can form the OH group on the surface of the films. However, this OH group was not stable under UV irradiation. Therefore, the ethanol treatment was considered to solve this problem. The ethanol was used as an electrolyte because it is used in medical application due to antibacterial property. Moreover, there is the difference in bonding between OH group and H (from H_2O as solvent) and Alkyl group (from ethanol). Therefore, this work aims to study the effect of electrolyte from H_2O and ethanol as solvent on hydrophilicity to the anodized films.

Fig. 4-48 shows the surface morphologies of the anodized films formed at 2 mA/cm^2 in 1M H_3PO_4 (Ano 1), the anodized films formed at 2 mA/cm^2 in 1M H_3PO_4 + 6%, 18% and 30% v/v Ethanol (Ano mix), the Ano 1 treated at 2 mA/cm^2 in 1M H_3PO_4 + 6%, 18% and 30% v/v (Ano 2). The surface morphology of Ano 1 sample is similar to that of the Ano mix sample. While the Ano 2 presents more surface roughness than Ano 1 and Ano mix. Therefore, the Ano 2 may enhance surface roughness.

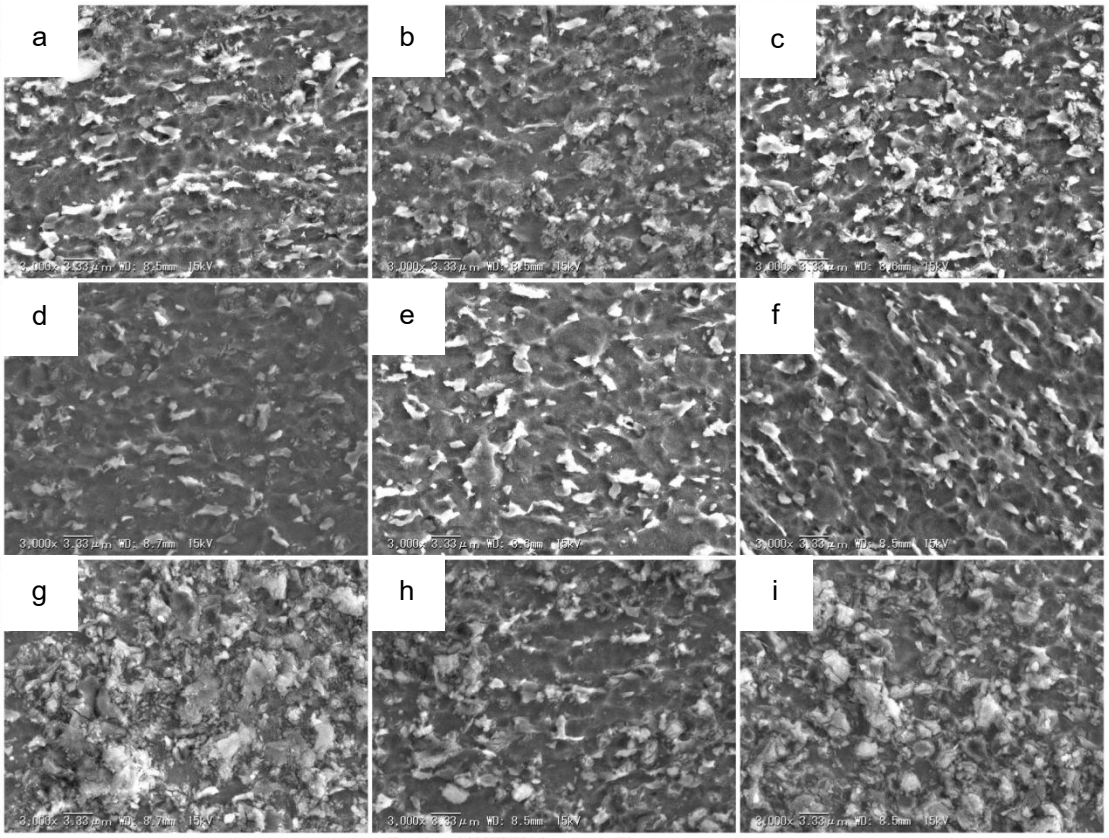

Fig. 4-48 Surface morphologies of the samples treated by different process, (a-c) Ano 1; (d-f) Ano mix; (g-i) Ano 2 with 6%, 18% and 30% v/v ethanol respectively

Fig. 4-49 shows the ATR-FTIR spectra of Ano 1, Ano 2 and Ano mix with different ethanol concentration. There are broad band at 3500-3000 cm^{-1}. This vibration band should result from the presence of hydroxyl groups such as Ti-OH or Ti-H_2O on TiO_2 films.[74].

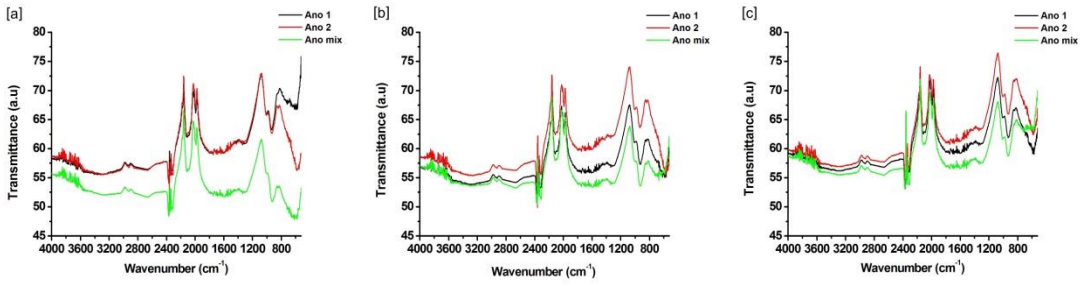

Fig. 4-49 FTIR spectra of the Ano 1, Ano mix and Ano 2 with ethanol concentrations of (a) 6%, (b) 18% and (c) 30% v/v

According to the ATR-FTIR results of Ano 1, Ano 2 and Ano mix, the bonding mode of hydroxyl groups on the surface in different ethanol concentration have been

known to be similar. The influence of ethanol concentration on the amount of films adsorption may arise from the change of electronic interactions between the ethanol and the surface groups of the films. For further insight, the XPS analyses of the anodized films treated by ethanol were performed.

Information on the chemical species of the anodized films was obtained from XPS spectra as shown in Fig. 4-50 and Fig. 4-51. Fig. 4-50 shows the Ti 2p XPS results of the anodized films formed at 2 mA/cm^2 in 1M H_3PO_4 (Ano 1), the anodized films formed at 2 mA/cm^2 in 1M H_3PO_4 + 6%, 18% and 30% v/v Ethanol (Ano mix), the Ano 1 treated at 2 mA/cm^2 in 1M H_3PO_4 + 6%, 18% and 30% v/v (Ano 2). The Ti 2p spectra of Ano 2 show TiO_2 asymmetric broadening and shift to higher binding energy. It is indicated that Ano 2 composed of TiO_2 more than Ano 1 and Ano mix.

Fig. 4-51 shows the O 1s XPS spectra of the anodized films formed at 2 mA/cm^2 in 1M H_3PO_4 (Ano 1), the anodized films formed at 2 mA/cm^2 in 1M H_3PO_4 + 6%, 18% and 30% v/v Ethanol (Ano mix), the Ano 1 treated at 2 mA/cm^2 in 1M H_3PO_4 + 6%, 18% and 30% v/v (Ano 2). The O 1s spectra of Ano 2 show asymmetric broadening, which has been known to come from Ti-OH and/or Ti-H_2O groups on TiO_2 surface at higher binding energy. According to Xia ‘s work, the O1s peak can be deconvoluted into three Gaussian peaks corresponding with the oxygen in the TiO_2 bulk, the oxygen of Ti-OH and the oxygen of Ti-H_2O from low to high binding energies [75]. It is indicated that the anodized films treated by ethanol could enhance hydroxyl groups to the anodized films.

By comparing the deconvoluted components of the XPS of the anodized films treated with different ethanol concentration as shown in Fig. 4-52. The result shows that the hydroxyl groups increase with the ethanol concentration. These results suggest that the ethanol treatment could enhance the hydroxyl group on TiO_2 films and lead to more Ti-OH and Ti-H_2O in more ethanol concentration [74].

The contact angle of the anodized films formed at 2 mA/cm^2 in 1M H_3PO_4 (Ano 1), the anodized films formed at 2 mA/cm^2 in 1M H_3PO_4 + 30% v/v Ethanol (Ano mix), the Ano 1 treated at 2 mA/cm^2 in 1M H_3PO_4 + 30% v/v ethanol (Ano 2) are shown in Fig. 4-53. The Ano 2 had a lower contact angle (30.24 ± 5^o) than the Ano 1 (70.06 ± 8.96^o) and Ano mix (56.61 ± 4.04^o). The Ano 2 is significant different ($p<0.05$)

in water contact angle compared with Ano 1 and Ano mix. It is indicated that the anodized films after ethanol treatment could enhance hydrophilicity to the anodized films.

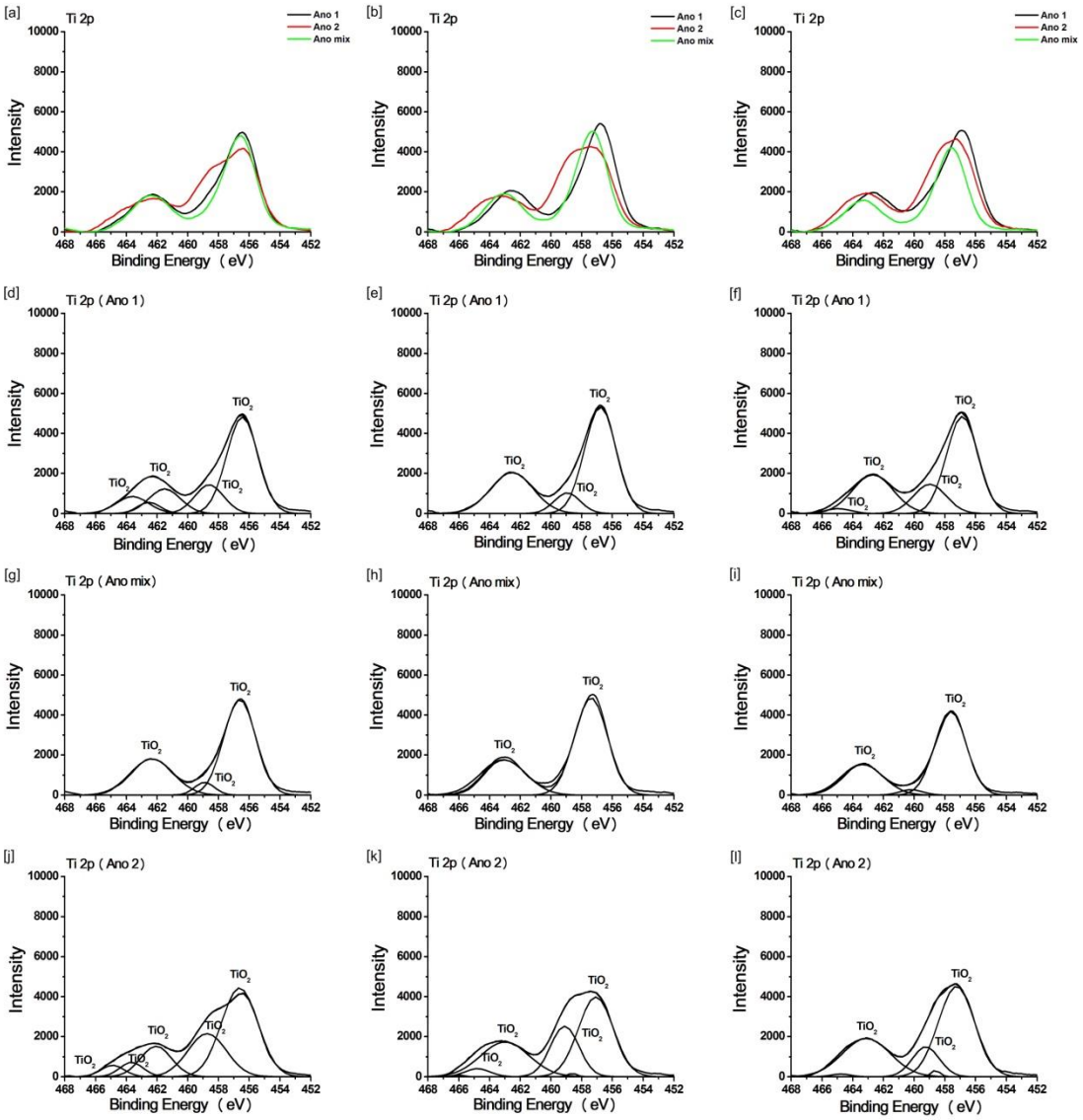

Fig. 4-50 Ti 2p XPS results of the anodized films formed at 2 mA/cm^2 in 1M H_3PO_4 (Ano 1), the anodized films formed at 2 mA/cm^2 in 1M H_3PO_4 + 6%, 18% and 30% v/v Ethanol (Ano mix), the Ano 1 treated at 2 mA/cm^2 in 1M H_3PO_4 + 6%, 18% and 30% v/v (Ano 2)

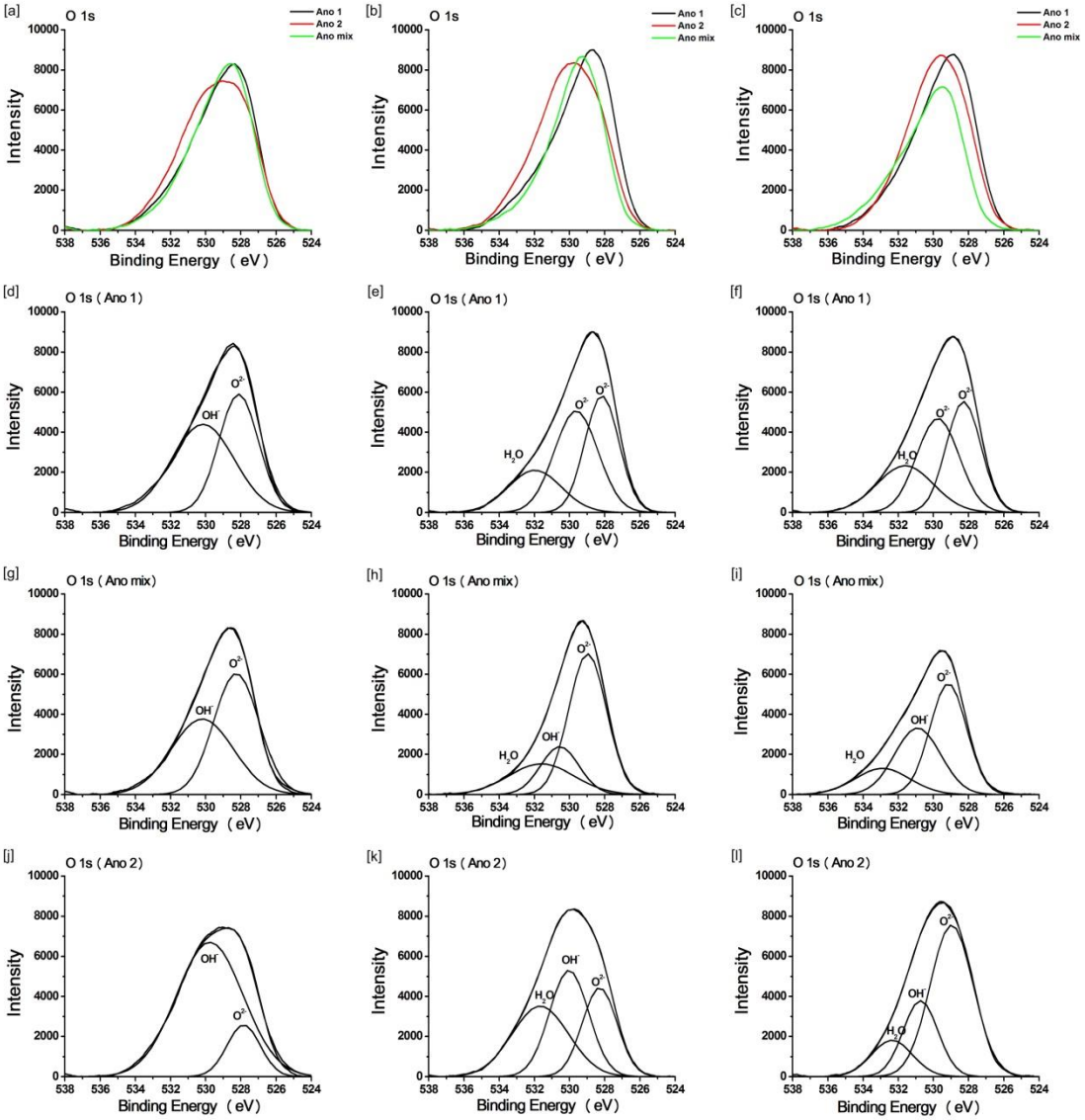

Fig. 4-51 O 1s XPS results of the anodized films formed at 2 mA/cm^2 in 1M H_3PO_4 (Ano 1), the anodized films formed at 2 mA/cm^2 in 1M H_3PO_4 + 6%, 18% and 30% v/v Ethanol (Ano mix), the Ano 1 treated at 2 mA/cm^2 in 1M H_3PO_4 + 6%, 18% and 30% v/v (Ano 2)

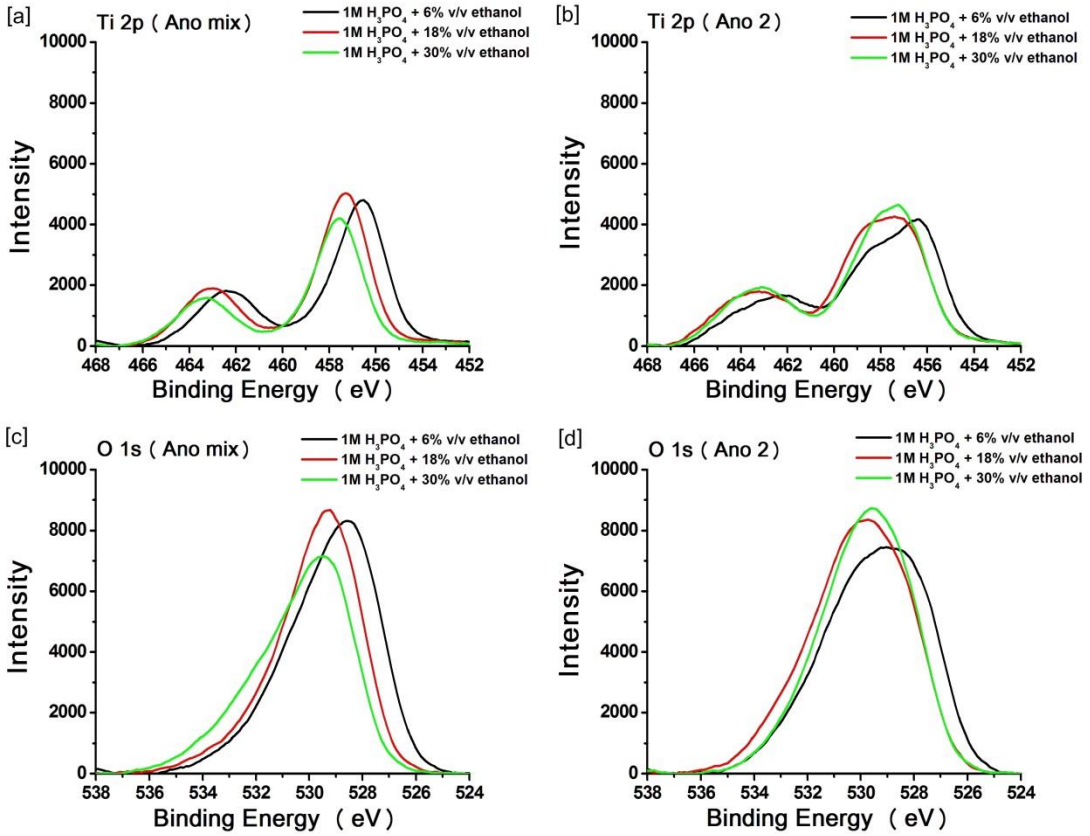

Fig. 4-52 Ti 2p and O 1s XPS results of the Ano mix and Ano 2 in various ethanol concentrations of 6%, 18% and 30% v/v

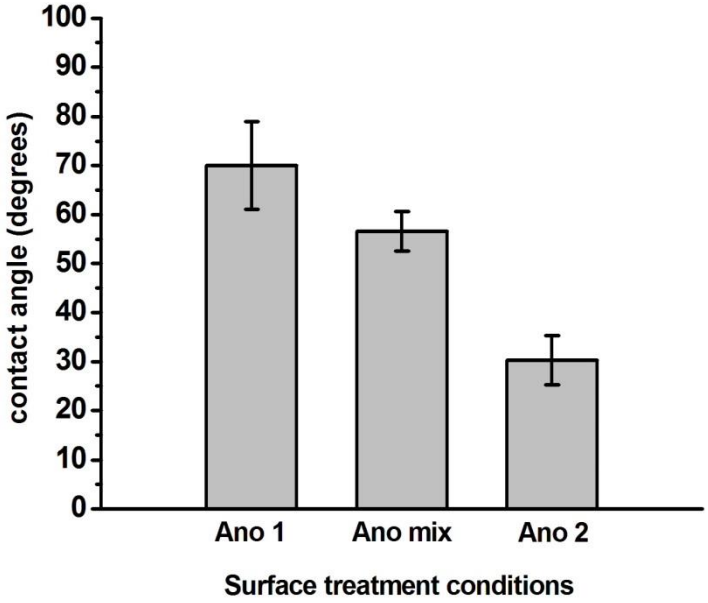

Fig. 4-53 Contact angle of Ano 1, Ano mix and Ano 2 with 30% v/v Ethanol

4.4.1. Discussion

It is interesting that the anodized films after ethanol treatment could increase the opportunity to form hydroxyl groups and surface roughness which both parameters resulting in improving of the hydrophilicity to the films.

Many works have been done to enhance hydrophilicity to the films by UV irradiation. The photo-induced hydrophilicity was explained by the formation of oxygen vacancies or removal hydrocarbon. Moreover, Meng et al. [76] studied about thermo-induced hydrophilicity. Its mechanism was explain by the cleansing effect, the crystal phase transition, the effect of Ti^{3+} defect sites and oxygen vacancy sites and the change of surface roughness. In this work, TiO_2 films were prepared by two step preparation; the first step the anodized films were prepared by galvanostatic method in 1M H_3PO_4. In order to improve the hydrophilicitity to the films, the anodized films treated in 1M H_3PO_4 (Ano 1) were further treated by galvanostatic method in a mixing of 1M H_3PO_4 and different ethanol concentration (Ano 2). The surface roughness formed on all samples, Ano 1, Ano mix and Ano 2. The surface roughness and Ti-OH groups identified by XPS were improved on Ano 2 surface, which led to the improving hydrophilicity on the anodized films surface after ethanol treatment. It is indicated that the anodized films after ethanol treatment can increase the opportunity to enhance hydrophilicity due to the surface roughness and the formation of hydroxyl groups on the films surface. The combination of the anodizing process in H_3PO_4 and further treated by ethanol treatment show beneficial effects on hydrophilicity. The result shows that the hydrophilicity could enhance by this method. It is one choice to improve hydrophilicity to the anodized films formed at low current density or low voltage.

CHAPTER 5
CONCLUSIONS AND RECOMMENDATIONS

5.1. Conclusions

5.1.1. Effect of anodizing conditions on hydrophilicity of the films

The hydrophilicity of the anodized films has been developed via galvanostatic method at various current densities ranging 5-80 mA/cm^2 in both 1M H_3PO_4 or 1M MCPM electrolyte and potentiostatic method at voltage of 5-150 V in 1M MCPM. The highest hydrophilicity observed by the lower of water contact angle appeared on the anodized film surface formed at 20 mA/cm^2 in both 1M H_3PO_4 and 1M MCPM electrolyte and at 150 V in 1M MCPM. Even though the range of current densities and voltages were not in the expected ranges. The low current densities and voltages range according to our desire were 0.25-2 mA/cm^2 and 2-10 V. respectively. It is postulated that these low current densities and voltages were not sufficient enough to create the roughness and proper hydroxyl groups on the surface of anodized films. For this reason, the medium current densities at 20 mA/cm^2 or medium voltage at 150 V should be considered to apply in anodization process to form anodized film on Ti-6Al-4V. The microstructure of the anodized films depended on applied current density and voltage. Either high current density or high voltage can promote the formation of titanium dioxide (TiO_2) with porous surfaces. Contrarily, without applied current density, it cannot offer enough energy to form completely TiO_2. The hydroxide and adsorbed water are formed on the surface of the anodized films and result in the increasing of hydrophilicity of the films. It can be concluded that the hydrophilicity of the anodized films formed at 20 mA/cm^2 and 150 V in 1 M MCPM was increased because the formation of porous surface and O1s spectra indicated that hydroxide and adsorbed water (O 1s) was also induced in anodized films. It is worth nothing that good hydrophilicity of anodic oxide film on Ti-6Al-4V is synergistic properties of surface morphologies and chemical species on the films.

5.1.2. Effect of UV irradiation on hydrophilicity of the films

The anodized films formed at low current density or low voltage could enhance hydrophilicity after UV irradiation. The XPS spectra showed the increasing in intensity of Ti 2p and O 1s peak and the decreasing in those of C 1s peak. However, the position of binding energy did not change. Therefore, the anodized films formed at low current density and low voltage are not TiO_2. It might be hydroxylated TiO_x thus, the behavior of the film formed at low current densities and voltages after UV irradiation completely differed from TiO_2 film which could be induced at high current densities and voltages. Therefore, these anodized films could enhance hydrophilicity to the films. It may be due to the heat from UV and increasing of surface energy after UV irradiation resulting in hydrophilicity.

The anodized films formed at low current density or low voltage after UV irradiation show low contact angle as well as the anodized films formed at high current density or high voltage. Therefore, it is one of an alternative for preparation of anodized films on Ti6Al-4V using applied low current densities or voltages. It can save energy, save cost and safety process in comparison with the anodization technique with applied high current densities or voltages.

5.1.3. Effect of ethanol treatment on hydrophilicity of the films

In order to improve the hydrophilicity to the films, the anodized films treated in 1M H_3PO_4 (Ano 1) were further treated by galvanostatic method in a mixing of 1M H_3PO_4 and different ethanol concentration (Ano 2). The surface roughness formed on all samples, Ano 1, Ano mix and Ano 2. The surface roughness and Ti-OH groups identified by XPS were improved on Ano 2 surface, which led to the improving hydrophilicity on the anodized films surface after ethanol treatment. It is indicated that the anodized films after ethanol treatment can enhance hydrophilicity due to the surface roughness and the formation of hydroxyl groups on the films surface. The combination of the anodizing process in H_3PO_4 and further treated by ethanol treatment show beneficial effects on hydrophilicity.

5.2. Recommendations

The UV irradiation could enhance hydrophilicity to the anodized films formed at low current density and low voltage and the hydrophilicity behavior tend to decrease after storage in the dark. Therefore, the stability of hydrophilicity behavior and properties of the films after storage in the dark should be further studied.

The anodized films treated in 1M H_3PO_4 (Ano 1) were further treated by galvanostatic method in a mixing of 1M H_3PO_4 and different ethanol concentration (Ano 2). This method can increase the opportunity to enhance hydrophilicity due to the surface roughness and the formation of hydroxyl groups on the films surface. Therefore, the mixing of MCPM or alkaline solution with different ethanol concentrations as co-electrolyte should be further studied.

REFERENCES

[1] Cvijović-Alagić, I., Cvijović, Z., Mitrović, S., Panić, V. and Rakin, M. Wear and corrosion behaviour of Ti–13Nb–13Zr and Ti–6Al–4V alloys in simulated physiological solution. Corrosion Science 53(2) (2011): 796-808.

[2] Szesz, E. M., et al. Electrochemical and morphological analyses on the titanium surface modified by shot blasting and anodic oxidation processes. Thin Solid Films 528 (2013): 163-166.

[3] Huang, Y., Luo, Q., Li, X., Zhang, F. and Zhao, S. Fabrication and in vitro evaluation of the collagen/hyaluronic acid PEM coating crosslinked with functionalized RGD peptide on titanium. Acta Biomaterialia 8(2) (2012): 866-877.

[4] Aloia Games, L., et al. Chemical and mechanical properties of anodized cp-titanium in NH_4 H_2PO_4/NH_4F media for biomedical applications. Surface and Coatings Technology 206(23) (2012): 4791-4798.

[5] Pohrelyuk, I. M., Fedirko, V. M., Tkachuk, O. V. and Proskurnyak, R. V. Corrosion resistance of Ti–6Al–4V alloy with nitride coatings in Ringer's solution. Corrosion Science 66 (2013): 392-398.

[6] Popa, M. V., et al. Corrosion susceptibility of implant materials Ti–5Al–4V and Ti–6Al–4Fe in artificial extra-cellular fluids. Electrochimica Acta 49(13) (2004): 2113-2121.

[7] Wilks, R. G., et al. Characterization of oxide layers formed on electrochemically treated Ti by using soft X-ray absorption measurements. Journal of Electron Spectroscopy and Related Phenomena 169(1) (2009): 46-50.

[8] Chug, A., Shukla, S., Mahesh, L. and Jadwani, S. Osseointegration—Molecular events at the bone–implant interface: A review. Journal of Oral and Maxillofacial Surgery, Medicine, and Pathology 25(1) (2013): 1-4.

[9] Khan, S. N., Ramachandran, M., Senthil Kumar, S., Krishnan, V. and Sundaram, R. Osseointegration and more–A review of literature. Indian Journal of Dentistry 3(2) (2012): 72-76.

[10] Seo, H. S., Kim, B. H. and Ko, Y. M. Fabrication of anodized titanium with immobilization of hyaluronic acid to improve biological performance. Progress in Organic Coatings 69(1) (2010): 38-44.

[11] Gittens, R. A., et al. The roles of titanium surface micro/nanotopography and wettability on the differential response of human osteoblast lineage cells. Acta Biomaterialia 9(4) (2013): 6268-6277.

[12] Song, H.-J., Park, S.-H., Jeong, S.-H. and Park, Y.-J. Surface characteristics and bioactivity of oxide films formed by anodic spark oxidation on titanium in different electrolytes. Journal of Materials Processing Technology 209(2) (2009): 864-870.

[13] Shabalovskaya, S. A., Siegismund, D., Heurich, E. and Rettenmayr, M. Evaluation of wettability and surface energy of native Nitinol surfaces in relation to hemocompatibility. Materials Science and Engineering: C 33(1) (2013): 127-132.

[14] Kim, J.-U., Jeong, Y.-H. and Choe, H.-C. Morphology of hydroxyapatite coated nanotube surface of Ti–35Nb–xHf alloys for implant materials. Thin Solid Films 520(2) (2011): 793-799.

[15] Eliaz, N., et al. The effect of surface treatment on the surface texture and contact angle of electrochemically deposited hydroxyapatite coating and on its interaction with bone-forming cells. Acta Biomaterialia 5(8) (2009): 3178-3191.

[16] Masahashi, N., Semboshi, S., Ohtsu, N. and Oku, M. Microstructure and superhydrophilicity of anodic TiO_2 films on pure titanium. Thin Solid Films 516(21) (2008): 7488-7496.

[17] Narayanan, R. and Seshadri, S. K. Phosphoric acid anodization of Ti–6Al–4V – Structural and corrosion aspects. Corrosion Science 49(2) (2007): 542-558.

[18] Zhang, C-Y., et al. Bioinspired Crystallization of Continuous Calcium Phosphate Films on a Langmuir Monolayer of Zein Protein: Their Mechanical Performance, Hydrophilicity, and Biocompatibility. Crystal growth & design 13(2013): 3505-3513.

[19] Ibrahim, M. A. M., Pongkao, D. and Yoshimura, M. The electrochemical behavior and characterization of the anodic oxide film formed on titanium in NaOH solutions. Journal Solid State Electrochem 6 (2002): 341-350.

[20] Oshida, Y. Bioscience and Bioengineering of Titanium Materials. Oxford: Elsevier BV, 2007.

[21] Fujishima, A., Hashimoto, K. and Watanabe, T. TiO_2 Photocatalysis Fundamentals and Application. Tokyo: Bkc, Inc., 1999.

[22] Han, Y., Chen, D., Sun, J., Zhang, Y. and Xu, K. UV-enhanced bioactivity and cell response of micro-arc oxidized titania coatings. Acta Biomaterialia 4(5) (2008): 1518-1529.

[23] Yates Jr, J. T. Photochemistry on TiO_2: Mechanisms behind the surface chemistry. Surface Science 603(10–12) (2009): 1605-1612.

[24] Aita, H., et al. The effect of ultraviolet functionalization of titanium on integration with bone. Biomaterials 30(6) (2009): 1015-1025.

[25] Brunette, D. M., Tengvall, P., Textor, M. and Thomsen, P. Titanium in Medicine. Germany: Springer-Verlag Berlin Heidelberg, 2001.

[26] Huang, R. and Han, Y. The effect of SMAT-induced grain refinement and dislocations on the corrosion behavior of Ti–25Nb–3Mo–3Zr–2Sn alloy. Materials Science and Engineering: C 33(4) (2013): 2353-2359.

[27] Nouri, A. and Wen, C. (2015). 1 - Introduction to surface coating and modification for metallic biomaterials. Surface Coating and Modification of Metallic Biomaterials. C. Wen, Woodhead Publishing: 3-60.

[28] "Surface Energy." from http://www.rochestermagnet.com/Adhesive-Tapes/Tape-Reference-Guide.aspx.

[29] Dalmau, A., Guiñón Pina, V., Devesa, F., Amigó, V. and Igual Muñoz, A. Influence of fabrication process on electrochemical and surface properties of Ti–6Al–4V alloy for medical applications. Electrochimica Acta 95 (2013): 102-111.

[30] Atapour, M., Pilchak, A. L., Shamanian, M. and Fathi, M. H. Corrosion behavior of Ti–8Al–1Mo–1V alloy compared to Ti–6Al–4V. Materials & Design 32(3) (2011): 1692-1696.

[31] Jiang, B. L. and Wang, Y. M. (2010). 5 - Plasma electrolytic oxidation treatment of aluminium and titanium alloys. Surface Engineering of Light Alloys. H. Dong, Woodhead Publishing: 110-154.

[32] Jakubowicz, J. Formation of porous TiO_x biomaterials in H_3PO_4 electrolytes. Electrochemistry Communications 10(5) (2008): 735-739.

[33] Zhu, X., Kim, K.-H. and Jeong, Y. Anodic oxide films containing Ca and P of titanium biomaterial. Biomaterials 22(16) (2001): 2199-2206.

[34] de Souza, G. B., et al. Tribo-mechanical characterization of rough, porous and bioactive Ti anodic layers. Journal of the Mechanical Behavior of Biomedical Materials 4(5) (2011): 796-806.

[35] Masahashi, N., Mizukoshi, Y., Semboshi, S., Ohmura, K. and Hanada, S. Photo-induced properties of anodic oxide films on Ti6Al4V. Thin Solid Films 520(15) (2012): 4956-4964.

[36] Lewandowska, M., et al. Nanoscale characterization of anodic oxide films on Ti-6Al-4V alloy. Thin Solid Films 515(16) (2007): 6460-6464.

[37] Quintero, D., Galvis, O., Calderón, J. A., Castaño, J. G. and Echeverría, F. Effect of electrochemical parameters on the formation of anodic films on commercially pure titanium by plasma electrolytic oxidation. Surface and Coatings Technology 258 (2014): 1223-1231.

[38] Quintero, D., Galvis, O., Calderón, J. A., Castaño, J. G. and Echeverría, F. Effect of electrochemical parameters on the formation of anodic films on commercially pure titanium by plasma electrolytic oxidation. Surface and Coatings Technology.

[39] Guillemot, F., Porté, M. C., Labrugère, C. and Baquey, C. Ti^{4+} to Ti^{3+} Conversion of TiO_2 Uppermost Layer by Low-Temperature Vacuum Annealing: Interest for Titanium Biomedical Applications. Journal of Colloid and Interface Science 255(1) (2002): 75-78.

[40] Zhao, X.-T., et al. Hydrophilicity of TiO_2 thin films obtained by RF magnetron sputtering deposition. Current Applied Physics 6(5) (2006): 931-933.

[41] K. Hashimoto, H. Irie and Fujishima, A. TiO_2 Photocatalysis: A Historical Overview and Future Prospects. Japanese Journal of Applied Physics 44(2005): 8269-8285.

[42] Zou, L., et al. Excellent resistive switching property and physical mechanism of amorphous TiO_2 thin films fabricated by a low-temperature photochemical solution deposition method. Applied Surface Science 311(2014): 697-702.

[43] Zhu, Z., et al. FTIR study of the photocatalytic degradation of gaseous benzene over UV-irradiated TiO_2 nanoballs synthesized by hydrothermal treatment in alkaline solution. Materials Research Bulletin 45(12) (2010): 1889-1893.

[44] Kaliwoh, N., Zhang, J.-Y. and Boyd, I. W. Photo-induced preparation of $(Ta_2O_5)_{1-x}(TiO_2)_x$ dielectric thin films using sol–gel processing with xenon excimer lamps. Applied Surface Science 168(1–4) (2000): 13-16.

[45] Jaleh, B. and Shahbazi, N. Surface properties of UV irradiated PC–TiO_2 nanocomposite film. Applied Surface Science 313(2014): 251-258.

[46] Liu, J., Ye, J., Xu, C., Jiang, S. P. and Tong, Y. Kinetics of ethanol electrooxidation at Pd electrodeposited on Ti. Electrochemistry Communications 9(9) (2007): 2334-2339.

[47] H. Y, E. Surface Chemistry of Solid and Liquid Interfaces. John Wiley & Sons, 2006.

[48] "Nobel Biocare™ IMPLANTS." from http://genieoss.com/manufacturer/nbimplant.html.

[49] Kang, B.-S., Sul, Y.-T., Oh, S.-J., Lee, H.-J. and Albrektsson, T. XPS, AES and SEM analysis of recent dental implants. Acta Biomaterialia 5(6) (2009): 2222-2229.

[50] Sul, Y. T., et al. Characteristics of the surface oxides on turned and electrochemically oxidized pure titanium implants up to dielectric breakdown: the oxide thickness, micropore configurations, surface roughness, crystal structure and chemical composition. Biomaterials 23(2) (January 2002): 491-501.

[51] Simka, W., et al. Modification of a Ti–Mo alloy surface via plasma electrolytic oxidation in a solution containing calcium and phosphorus. Electrochimica Acta 96(2013): 180-190.

[52] Zeng, G., Li, K.-K., Yang, H.-G. and Zhang, Y.-H. Micro-Raman mapping on an anatase TiO_2 single crystal with a large percentage of reactive (001) facets. Vibrational Spectroscopy 68(2013): 279-284.

[53] Frank, O., et al. Raman spectra of titanium dioxide (anatase, rutile) with identified oxygen isotopes (16, 17, 18). Phys. Chem. Chem. Phys. 14(2012): 14567–14572.

[54] Siebert, F., and Hildebrandt, P. Theory of Infrared Absorption and Raman Spectroscopy. KGaA, Weinheim: WILEY-VCH Verlag GmbH & Co., 2008.

[55] Atkins, P., and Paula, J. D. Physical Chemical. United States: W. H. Freeman and Company, 2010.

[56] Yan, J., et al. (2013). "Understanding the effects of surface/bulk defects on the photocatalytic activity of TiO_2 : Anatase versus Rutile." Physical Chemistry Chemical Physics, from http://www.rsc.org/suppdata/cp/c3/c3cp50927c/c3cp50927c.pdf.

[57] (2011). "How to Explain Potentiodynamic Polarization Curve & its Relation to Passivation of Behaviour of Metals." from http://srizam-expro.blogspot.com/2011/03/how-to-explain-potentiodynamic.html.

[58] Karambakhsh, A., Afshar, A. and Malekinejad, P. Corrosion resistance and color properties of anodized Ti-6Al-4V. Journal of Materials Engineering and Performance 21(1) (2012): 121-127.

[59] Bayati, M. R., Molaei, R. and Golestani-Fard, F. Enhancing photoinduced hydrophilicity of micro arc oxidized TiO_2 nanostructured porous layers by V-doping. Colloids and Surfaces A: Physicochemical and Engineering Aspects 373(1–3) (2011): 51-60.

[60] Bayati, M. R., et al. Investigation on hydrophilicity of micro-arc oxidized TiO_2 nano/micro-porous layers. Electrochimica Acta 55(20) (2010): 5786-5792.

[61] Michaelis, A. and Schweinsberg, M. An anisotropy microellipsometry (AME) study of anodic film formation on Ti and Zr single grains. Thin Solid Films 313–314 (1998): 756-763.

[62] Davepon, B., Schultze, J. W., König, U. and Rosenkranz, C. Crystallographic orientation of single grains of polycrystalline titanium and their influence on electrochemical processes. Surface and Coatings Technology 169–170(2003): 85-90.

[63] Schreiber, A., Rosenkranz, C. and Lohrengel, M. M. Grain-dependent anodic dissolution of iron. Electrochimica Acta 52(27) (2007): 7738-7745.

[64] Wanhill, R. and Barter, S. Fatigue of Beta Processed and Beta Heat-treated Titanium Alloys. SpringerBriefs in Applied Sciences and Technology (2012): 5-10.

[65] Smith, W. and Hasshemi, J. Foundations of Materials Science and Engineering 4th edition. Mc Graw Hill, 2008.

[66] "Phase Diagrams a Review." Retrieved 25 April, 2015, from https://feaweb.aub.edu.lb/research/cfd/documents/02%20Phase%20Diagrams.pdf.

[67] Center, t. N. R. "Solidification." Retrieved 25 April, 2015, from https://www.nde-ed.org/EducationResources/CommunityCollege/Materials/Structure/solidification.htm.

[68] Tarr, M. "Metals basics." Retrieved 25 April, 2015, from http://www.ami.ac.uk/courses/topics/0131_mb/.

[69] Du, J., et al. Effect of hydroxyl groups on hydrophilic and photocatalytic activities of rare earth doped titanium dioxide thin films. Journal of Rare Earths 33(2) (2015): 148-153.

[70] Han, Y., Yan, Y. Y. and and Lu, C. G. Ultraviolet-enhanced bioactivity of ZrO_2 films prepared by micro-arc oxidation. Thin Solid Films 517(5) (2009): 1577-1581.

[71] Eskandari, A., Sangpour, P. and Vaezi, M. R. Hydrophilic Cu_2O nanostructured thin films prepared by facile spin coating method: Investigation of surface energy and roughness. Materials Chemistry and Physics 147(3) (2014): 1204-1209.

[72] Michiardi, A., Aparicio, C., Ratner, B. D., Planell, J. A. and Gil, J. The influence of surface energy on competitive protein adsorption on oxidized NiTi surfaces. Biomaterials 28(4) (2007): 586-594.

[73] Sirghi, L. and Hatanaka, Y. Hydrophilicity of amorphous TiO_2 ultra-thin films. Surface Science 530(3) (2003): L323-L327.

[74] Kuo, Y.-Y., Li, T.-H., Yao, J.-N., Lin, C.-Y. and Chien, C.-H. Hydrothermal crystallization and modification of surface hydroxyl groups of anodized TiO_2 nanotube-arrays for more efficient photoenergy conversion. Electrochimica Acta 78(2012): 236-243.

[75] Xia, Z. B., et al. Crystallization of the anodic oxide on titanium in sulphuric acids solution at a very low potential. Electrochemistry Communications 9(4) (2007): 850-856.

[76] Meng, F., Xiao, L. and Sun, Z. Thermo-induced hydrophilicity of nano-TiO_2 thin films prepared by RF magnetron sputtering. J. Alloy. Compd. 485(1–2) (2009): 848-852.

APPENDIXS

APPENDIX A

Contact angle and the statistical analysis of the anodized films formed by Galvanostatic method

Oneway

Descriptives

angle

	N	Mean	Std. Deviation	Std. Error	95% Confidence Interval for Mean		Minimum	Maximum
					Lower Bound	Upper Bound		
untreated Ti-6Al-4V	3	84.6667	.41633	.24037	83.6324	85.7009	84.20	85.00
H3PO4 0 mA	3	75.9333	2.64071	1.52461	69.3735	82.4932	73.60	78.80
H3PO4 0.25	3	72.4000	1.90788	1.10151	67.6606	77.1394	70.20	73.60
H3PO4 1	3	79.1333	1.85831	1.07290	74.5170	83.7496	77.00	80.40
H3PO4 2	3	69.8667	2.64071	1.52461	63.3068	76.4265	67.00	72.20
H3PO4 5	3	48.3333	7.93557	4.58161	28.6203	68.0464	40.00	55.80
H3PO4 20	3	41.4667	4.72582	2.72845	29.7271	53.2062	37.80	46.80
H3PO4 80	3	45.2667	6.40104	3.69564	29.3656	61.1677	40.80	52.60
MCPM 0	3	81.2667	1.62891	.94045	77.2202	85.3131	79.40	82.40
MCPM 0.25	3	70.8000	2.49800	1.44222	64.5946	77.0054	68.00	72.80
MCPM 1	3	66.8667	.83267	.48074	64.7982	68.9351	66.20	67.80
MCPM 2	3	73.0000	3.46987	2.00333	64.3804	81.6196	69.00	75.20
MCPM 5	3	24.2667	4.79305	2.76727	12.3601	36.1733	21.40	29.80
MCPM 20	3	17.2000	1.90788	1.10151	12.4606	21.9394	16.00	19.40
MCPM 80	3	21.6667	5.44549	3.14395	8.1393	35.1940	17.40	27.80
Total	45	58.1422	22.82027	3.40185	51.2863	64.9982	16.00	85.00

Post Hoc Tests

Multiple Comparisons

Dependent Variable: angle

Bonferroni

(I) anodize	(J) anodize	Mean Difference (I-J)	Std. Error	Sig.	95% Confidence Interval	
					Lower Bound	Upper Bound
untreated Ti-6Al-4V	H3PO4 0 mA	8.73333	3.16499	1.000	-3.6718	21.1385
	H3PO4 0.25	12.26667	3.16499	.056	-.1385	24.6718
	H3PO4 1	5.53333	3.16499	1.000	-6.8718	17.9385
	H3PO4 2	14.80000*	3.16499	.006	2.3949	27.2051
	H3PO4 5	36.33333*	3.16499	.000	23.9282	48.7385
	H3PO4 20	43.20000*	3.16499	.000	30.7949	55.6051
	H3PO4 80	39.40000*	3.16499	.000	26.9949	51.8051
	MCPM 0	3.40000	3.16499	1.000	-9.0051	15.8051
	MCPM 0.25	13.86667*	3.16499	.014	1.4615	26.2718
	MCPM 1	17.80000*	3.16499	.000	5.3949	30.2051
	MCPM 2	11.66667	3.16499	.094	-.7385	24.0718
	MCPM 5	60.40000*	3.16499	.000	47.9949	72.8051
	MCPM 20	67.46667*	3.16499	.000	55.0615	79.8718
	MCPM 80	63.00000*	3.16499	.000	50.5949	75.4051
H3PO4 0 mA	untreated Ti-6Al-4V	-8.73333	3.16499	1.000	-21.1385	3.6718

	MCPM 80	63.00000*	3.16499	.000	50.5949	75.4051
H3PO4 0 mA	untreated Ti-6Al-4V	-8.73333	3.16499	1.000	-21.1385	3.6718
	H3PO4 0.25	3.53333	3.16499	1.000	-8.8718	15.9385
	H3PO4 1	-3.20000	3.16499	1.000	-15.6051	9.2051
	H3PO4 2	6.06667	3.16499	1.000	-6.3385	18.4718
	H3PO4 5	27.60000*	3.16499	.000	15.1949	40.0051
	H3PO4 20	34.46667*	3.16499	.000	22.0615	46.8718
	H3PO4 80	30.66667*	3.16499	.000	18.2615	43.0718
	MCPM 0	-5.33333	3.16499	1.000	-17.7385	7.0718
	MCPM 0.25	5.13333	3.16499	1.000	-7.2718	17.5385
	MCPM 1	9.06667	3.16499	.793	-3.3385	21.4718
	MCPM 2	2.93333	3.16499	1.000	-9.4718	15.3385
	MCPM 5	51.66667*	3.16499	.000	39.2615	64.0718
	MCPM 20	58.73333*	3.16499	.000	46.3282	71.1385
	MCPM 80	54.26667*	3.16499	.000	41.8615	66.6718
H3PO4 0.25	untreated Ti-6Al-4V	-12.26667	3.16499	.056	-24.6718	.1385
	H3PO4 0 mA	-3.53333	3.16499	1.000	-15.9385	8.8718
	H3PO4 1	-6.73333	3.16499	1.000	-19.1385	5.6718
	H3PO4 2	2.53333	3.16499	1.000	-9.8718	14.9385
	H3PO4 5	24.06667*	3.16499	.000	11.6615	36.4718
	H3PO4 20	30.93333*	3.16499	.000	18.5282	43.3385
	H3PO4 80	27.13333*	3.16499	.000	14.7282	39.5385
	MCPM 0	-8.86667	3.16499	.926	-21.2718	3.5385
	MCPM 0.25	1.60000	3.16499	1.000	-10.8051	14.0051
	MCPM 1	5.53333	3.16499	1.000	-6.8718	17.9385
	MCPM 2	-.60000	3.16499	1.000	-13.0051	11.8051
	MCPM 5	48.13333*	3.16499	.000	35.7282	60.5385
	MCPM 20	55.20000*	3.16499	.000	42.7949	67.6051
	MCPM 80	50.73333*	3.16499	.000	38.3282	63.1385
H3PO4 1	untreated Ti-6Al-4V	-5.53333	3.16499	1.000	-17.9385	6.8718

	MCPM 80	50.73333*	3.16499	.000	38.3282	63.1385
H3PO4 1	untreated Ti-6Al-4V	-5.53333	3.16499	1.000	-17.9385	6.8718
	H3PO4 0 mA	3.20000	3.16499	1.000	-9.2051	15.6051
	H3PO4 0.25	6.73333	3.16499	1.000	-5.6718	19.1385
	H3PO4 2	9.26667	3.16499	.678	-3.1385	21.6718
	H3PO4 5	30.80000*	3.16499	.000	18.3949	43.2051
	H3PO4 20	37.66667*	3.16499	.000	25.2615	50.0718
	H3PO4 80	33.86667*	3.16499	.000	21.4615	46.2718
	MCPM 0	-2.13333	3.16499	1.000	-14.5385	10.2718
	MCPM 0.25	8.33333	3.16499	1.000	-4.0718	20.7385
	MCPM 1	12.26667	3.16499	.056	-.1385	24.6718
	MCPM 2	6.13333	3.16499	1.000	-6.2718	18.5385
	MCPM 5	54.86667*	3.16499	.000	42.4615	67.2718
	MCPM 20	61.93333*	3.16499	.000	49.5282	74.3385
	MCPM 80	57.46667*	3.16499	.000	45.0615	69.8718
H3PO4 2	untreated Ti-6Al-4V	-14.80000*	3.16499	.006	-27.2051	-2.3949
	H3PO4 0 mA	-6.06667	3.16499	1.000	-18.4718	6.3385
	H3PO4 0.25	-2.53333	3.16499	1.000	-14.9385	9.8718
	H3PO4 1	-9.26667	3.16499	.678	-21.6718	3.1385
	H3PO4 5	21.53333*	3.16499	.000	9.1282	33.9385
	H3PO4 20	28.40000*	3.16499	.000	15.9949	40.8051
	H3PO4 80	24.60000*	3.16499	.000	12.1949	37.0051
	MCPM 0	-11.40000	3.16499	.118	-23.8051	1.0051
	MCPM 0.25	-.93333	3.16499	1.000	-13.3385	11.4718
	MCPM 1	3.00000	3.16499	1.000	-9.4051	15.4051
	MCPM 2	-3.13333	3.16499	1.000	-15.5385	9.2718
	MCPM 5	45.60000*	3.16499	.000	33.1949	58.0051
	MCPM 20	52.66667*	3.16499	.000	40.2615	65.0718
	MCPM 80	48.20000*	3.16499	.000	35.7949	60.6051
H3PO4 5	untreated Ti-6Al-4V	-36.33333*	3.16499	.000	-48.7385	-23.9282

	MCPM 80	48.20000*	3.16499	.000	35.7949	60.6051
H3PO4 5	untreated Ti-6Al-4V	-36.33333*	3.16499	.000	-48.7385	-23.9282
	H3PO4 0 mA	-27.60000*	3.16499	.000	-40.0051	-15.1949
	H3PO4 0.25	-24.06667*	3.16499	.000	-36.4718	-11.6615
	H3PO4 1	-30.80000*	3.16499	.000	-43.2051	-18.3949
	H3PO4 2	-21.53333*	3.16499	.000	-33.9385	-9.1282
	H3PO4 20	6.86667	3.16499	1.000	-5.5385	19.2718
	H3PO4 80	3.06667	3.16499	1.000	-9.3385	15.4718
	MCPM 0	-32.93333*	3.16499	.000	-45.3385	-20.5282
	MCPM 0.25	-22.46667*	3.16499	.000	-34.8718	-10.0615
	MCPM 1	-18.53333*	3.16499	.000	-30.9385	-6.1282
	MCPM 2	-24.66667*	3.16499	.000	-37.0718	-12.2615
	MCPM 5	24.06667*	3.16499	.000	11.6615	36.4718
	MCPM 20	31.13333*	3.16499	.000	18.7282	43.5385
	MCPM 80	26.66667*	3.16499	.000	14.2615	39.0718
H3PO4 20	untreated Ti-6Al-4V	-43.20000*	3.16499	.000	-55.6051	-30.7949
	H3PO4 0 mA	-34.46667*	3.16499	.000	-46.8718	-22.0615
	H3PO4 0.25	-30.93333*	3.16499	.000	-43.3385	-18.5282
	H3PO4 1	-37.66667*	3.16499	.000	-50.0718	-25.2615
	H3PO4 2	-28.40000*	3.16499	.000	-40.8051	-15.9949
	H3PO4 5	-6.86667	3.16499	1.000	-19.2718	5.5385
	H3PO4 80	-3.80000	3.16499	1.000	-16.2051	8.6051
	MCPM 0	-39.80000*	3.16499	.000	-52.2051	-27.3949
	MCPM 0.25	-29.33333*	3.16499	.000	-41.7385	-16.9282
	MCPM 1	-25.40000*	3.16499	.000	-37.8051	-12.9949
	MCPM 2	-31.53333*	3.16499	.000	-43.9385	-19.1282
	MCPM 5	17.20000*	3.16499	.001	4.7949	29.6051
	MCPM 20	24.26667*	3.16499	.000	11.8615	36.6718
	MCPM 80	19.80000*	3.16499	.000	7.3949	32.2051
H3PO4 80	untreated Ti-6Al-4V	-39.40000*	3.16499	.000	-51.8051	-26.9949

	MCPM 80	19.80000*	3.16499	.000	7.3949	32.2051
H3PO4 80	untreated Ti-6Al-4V	-39.40000*	3.16499	.000	-51.8051	-26.9949
	H3PO4 0 mA	-30.66667*	3.16499	.000	-43.0718	-18.2615
	H3PO4 0.25	-27.13333*	3.16499	.000	-39.5385	-14.7282
	H3PO4 1	-33.86667*	3.16499	.000	-46.2718	-21.4615
	H3PO4 2	-24.60000*	3.16499	.000	-37.0051	-12.1949
	H3PO4 5	-3.06667	3.16499	1.000	-15.4718	9.3385
	H3PO4 20	3.80000	3.16499	1.000	-8.6051	16.2051
	MCPM 0	-36.00000*	3.16499	.000	-48.4051	-23.5949
	MCPM 0.25	-25.53333*	3.16499	.000	-37.9385	-13.1282
	MCPM 1	-21.60000*	3.16499	.000	-34.0051	-9.1949
	MCPM 2	-27.73333*	3.16499	.000	-40.1385	-15.3282
	MCPM 5	21.00000*	3.16499	.000	8.5949	33.4051
	MCPM 20	28.06667*	3.16499	.000	15.6615	40.4718
	MCPM 80	23.60000*	3.16499	.000	11.1949	36.0051
MCPM 0	untreated Ti-6Al-4V	-3.40000	3.16499	1.000	-15.8051	9.0051
	H3PO4 0 mA	5.33333	3.16499	1.000	-7.0718	17.7385
	H3PO4 0.25	8.86667	3.16499	.926	-3.5385	21.2718
	H3PO4 1	2.13333	3.16499	1.000	-10.2718	14.5385
	H3PO4 2	11.40000	3.16499	.118	-1.0051	23.8051
	H3PO4 5	32.93333*	3.16499	.000	20.5282	45.3385
	H3PO4 20	39.80000*	3.16499	.000	27.3949	52.2051
	H3PO4 80	36.00000*	3.16499	.000	23.5949	48.4051
	MCPM 0.25	10.46667	3.16499	.258	-1.9385	22.8718
	MCPM 1	14.40000*	3.16499	.009	1.9949	26.8051
	MCPM 2	8.26667	3.16499	1.000	-4.1385	20.6718
	MCPM 5	57.00000*	3.16499	.000	44.5949	69.4051
	MCPM 20	64.06667*	3.16499	.000	51.6615	76.4718
	MCPM 80	59.60000*	3.16499	.000	47.1949	72.0051
MCPM 0.25	untreated Ti-6Al-4V	-13.86667*	3.16499	.014	-26.2718	-1.4615

	MCPM 80	59.60000*	3.16499	.000	47.1949	72.0051
MCPM 0.25	untreated Ti-6Al-4V	-13.86667*	3.16499	.014	-26.2718	-1.4615
	H3PO4 0 mA	-5.13333	3.16499	1.000	-17.5385	7.2718
	H3PO4 0.25	-1.60000	3.16499	1.000	-14.0051	10.8051
	H3PO4 1	-8.33333	3.16499	1.000	-20.7385	4.0718
	H3PO4 2	.93333	3.16499	1.000	-11.4718	13.3385
	H3PO4 5	22.46667*	3.16499	.000	10.0615	34.8718
	H3PO4 20	29.33333*	3.16499	.000	16.9282	41.7385
	H3PO4 80	25.53333*	3.16499	.000	13.1282	37.9385
	MCPM 0	-10.46667	3.16499	.258	-22.8718	1.9385
	MCPM 1	3.93333	3.16499	1.000	-8.4718	16.3385
	MCPM 2	-2.20000	3.16499	1.000	-14.6051	10.2051
	MCPM 5	46.53333*	3.16499	.000	34.1282	58.9385
	MCPM 20	53.60000*	3.16499	.000	41.1949	66.0051
	MCPM 80	49.13333*	3.16499	.000	36.7282	61.5385
MCPM 1	untreated Ti-6Al-4V	-17.80000*	3.16499	.000	-30.2051	-5.3949
	H3PO4 0 mA	-9.06667	3.16499	.793	-21.4718	3.3385
	H3PO4 0.25	-5.53333	3.16499	1.000	-17.9385	6.8718
	H3PO4 1	-12.26667	3.16499	.056	-24.6718	.1385
	H3PO4 2	-3.00000	3.16499	1.000	-15.4051	9.4051
	H3PO4 5	18.53333*	3.16499	.000	6.1282	30.9385
	H3PO4 20	25.40000*	3.16499	.000	12.9949	37.8051
	H3PO4 80	21.60000*	3.16499	.000	9.1949	34.0051
	MCPM 0	-14.40000*	3.16499	.009	-26.8051	-1.9949
	MCPM 0.25	-3.93333	3.16499	1.000	-16.3385	8.4718
	MCPM 2	-6.13333	3.16499	1.000	-18.5385	6.2718
	MCPM 5	42.60000*	3.16499	.000	30.1949	55.0051
	MCPM 20	49.66667*	3.16499	.000	37.2615	62.0718
	MCPM 80	45.20000*	3.16499	.000	32.7949	57.6051
MCPM 2	untreated Ti-6Al-4V	-11.66667	3.16499	.094	-24.0718	.7385

	MCPM 80	45.20000*	3.16499	.000	32.7949	57.6051
MCPM 2	untreated Ti-6Al-4V	-11.66667	3.16499	.094	-24.0718	.7385
	H3PO4 0 mA	-2.93333	3.16499	1.000	-15.3385	9.4718
	H3PO4 0.25	.60000	3.16499	1.000	-11.8051	13.0051
	H3PO4 1	-6.13333	3.16499	1.000	-18.5385	6.2718
	H3PO4 2	3.13333	3.16499	1.000	-9.2718	15.5385
	H3PO4 5	24.66667*	3.16499	.000	12.2615	37.0718
	H3PO4 20	31.53333*	3.16499	.000	19.1282	43.9385
	H3PO4 80	27.73333*	3.16499	.000	15.3282	40.1385
	MCPM 0	-8.26667	3.16499	1.000	-20.6718	4.1385
	MCPM 0.25	2.20000	3.16499	1.000	-10.2051	14.6051
	MCPM 1	6.13333	3.16499	1.000	-6.2718	18.5385
	MCPM 5	48.73333*	3.16499	.000	36.3282	61.1385
	MCPM 20	55.80000*	3.16499	.000	43.3949	68.2051
	MCPM 80	51.33333*	3.16499	.000	38.9282	63.7385
MCPM 5	untreated Ti-6Al-4V	-60.40000*	3.16499	.000	-72.8051	-47.9949
	H3PO4 0 mA	-51.66667*	3.16499	.000	-64.0718	-39.2615
	H3PO4 0.25	-48.13333*	3.16499	.000	-60.5385	-35.7282
	H3PO4 1	-54.86667*	3.16499	.000	-67.2718	-42.4615
	H3PO4 2	-45.60000*	3.16499	.000	-58.0051	-33.1949
	H3PO4 5	-24.06667*	3.16499	.000	-36.4718	-11.6615
	H3PO4 20	-17.20000*	3.16499	.001	-29.6051	-4.7949
	H3PO4 80	-21.00000*	3.16499	.000	-33.4051	-8.5949
	MCPM 0	-57.00000*	3.16499	.000	-69.4051	-44.5949
	MCPM 0.25	-46.53333*	3.16499	.000	-58.9385	-34.1282
	MCPM 1	-42.60000*	3.16499	.000	-55.0051	-30.1949
	MCPM 2	-48.73333*	3.16499	.000	-61.1385	-36.3282
	MCPM 20	7.06667	3.16499	1.000	-5.3385	19.4718
	MCPM 80	2.60000	3.16499	1.000	-9.8051	15.0051
MCPM 20	untreated Ti-6Al-4V	-67.46667*	3.16499	.000	-79.8718	-55.0615

	MCPM 80	2.60000	3.16499	1.000	-9.8051	15.0051
MCPM 20	untreated Ti-6Al-4V	-67.46667*	3.16499	.000	-79.8718	-55.0615
	H3PO4 0 mA	-58.73333*	3.16499	.000	-71.1385	-46.3282
	H3PO4 0.25	-55.20000*	3.16499	.000	-67.6051	-42.7949
	H3PO4 1	-61.93333*	3.16499	.000	-74.3385	-49.5282
	H3PO4 2	-52.66667*	3.16499	.000	-65.0718	-40.2615
	H3PO4 5	-31.13333*	3.16499	.000	-43.5385	-18.7282
	H3PO4 20	-24.26667*	3.16499	.000	-36.6718	-11.8615
	H3PO4 80	-28.06667*	3.16499	.000	-40.4718	-15.6615
	MCPM 0	-64.06667*	3.16499	.000	-76.4718	-51.6615
	MCPM 0.25	-53.60000*	3.16499	.000	-66.0051	-41.1949
	MCPM 1	-49.66667*	3.16499	.000	-62.0718	-37.2615
	MCPM 2	-55.80000*	3.16499	.000	-68.2051	-43.3949
	MCPM 5	-7.06667	3.16499	1.000	-19.4718	5.3385
	MCPM 80	-4.46667	3.16499	1.000	-16.8718	7.9385
MCPM 80	untreated Ti-6Al-4V	-63.00000*	3.16499	.000	-75.4051	-50.5949
	H3PO4 0 mA	-54.26667*	3.16499	.000	-66.6718	-41.8615
	H3PO4 0.25	-50.73333*	3.16499	.000	-63.1385	-38.3282
	H3PO4 1	-57.46667*	3.16499	.000	-69.8718	-45.0615
	H3PO4 2	-48.20000*	3.16499	.000	-60.6051	-35.7949
	H3PO4 5	-26.66667*	3.16499	.000	-39.0718	-14.2615
	H3PO4 20	-19.80000*	3.16499	.000	-32.2051	-7.3949
	H3PO4 80	-23.60000*	3.16499	.000	-36.0051	-11.1949
	MCPM 0	-59.60000*	3.16499	.000	-72.0051	-47.1949
	MCPM 0.25	-49.13333*	3.16499	.000	-61.5385	-36.7282
	MCPM 1	-45.20000*	3.16499	.000	-57.6051	-32.7949
	MCPM 2	-51.33333*	3.16499	.000	-63.7385	-38.9282
	MCPM 5	-2.60000	3.16499	1.000	-15.0051	9.8051
	MCPM 20	4.46667	3.16499	1.000	-7.9385	16.8718

*. The mean difference is significant at the .05 level.

APPENDIX B

Contact angle and the statistical analysis of the anodized films formed by Potentiostatic method

Oneway

Descriptives

angle

	N	Mean	Std. Deviation	Std. Error	95% Confidence Interval for Mean		Minimum	Maximum
					Lower Bound	Upper Bound		
untreated Ti-6Al-4V	3	84.6667	.41633	.24037	83.6324	85.7009	84.20	85.00
H3PO4 0 V	3	75.9333	2.64071	1.52461	69.3735	82.4932	73.60	78.80
H3PO4 2	3	52.6667	7.57188	4.37163	33.8571	71.4763	44.00	58.00
H3PO4 4	3	48.6667	8.08290	4.66667	28.5876	68.7457	44.00	58.00
H3PO4 6	3	50.0000	2.00000	1.15470	45.0317	54.9683	48.00	52.00
H3PO4 8	3	55.3333	3.05505	1.76383	47.7442	62.9225	52.00	58.00
H3PO4 5	3	48.8000	4.84974	2.80000	36.7526	60.8474	43.60	53.20
H3PO4 10	3	48.5333	.92376	.53333	46.2386	50.8281	48.00	49.60
H3PO4 50	3	46.4000	9.45727	5.46016	22.9068	69.8932	39.60	57.20
H3PO4 100	3	59.7333	5.37153	3.10125	46.3897	73.0770	53.60	63.60
H3PO4 150	3	37.8667	1.89033	1.09138	33.1708	42.5625	36.40	40.00
MCPM 0	3	81.2667	1.62891	.94045	77.2202	85.3131	79.40	82.40
MCPM 2	3	60.0000	6.00000	3.46410	45.0952	74.9048	54.00	66.00
MCPM 4	3	60.6667	1.15470	.66667	57.7982	63.5351	60.00	62.00
MCPM 6	3	48.6667	4.16333	2.40370	38.3244	59.0090	44.00	52.00
MCPM 8	3	52.0000	6.92820	4.00000	34.7894	69.2106	44.00	56.00
MCPM 5	3	50.6000	2.50599	1.44684	44.3748	56.8252	48.00	53.00
MCPM 10	3	52.8667	3.94631	2.27840	43.0635	62.6698	50.20	57.40
MCPM 50	3	51.6000	1.70880	.98658	47.3551	55.8449	50.00	53.40
MCPM 100	3	50.4667	3.69504	2.13333	41.2877	59.6457	46.20	52.60
MCPM 150	3	26.2000	2.77849	1.60416	19.2979	33.1021	24.40	29.40
Total	63	54.4254	13.60932	1.71461	50.9979	57.8529	24.40	85.00

Post Hoc Tests

Multiple Comparisons

Dependent Variable: angle
Bonferroni

(I) anodize	(J) anodize	Mean Difference (I-J)	Std. Error	Sig.	95% Confidence Interval	
					Lower Bound	Upper Bound
untreated Ti-6Al-4V	H3PO4 0 V	8.73333	3.74104	1.000	-6.2982	23.7649
	H3PO4 2	32.00000*	3.74104	.000	16.9685	47.0315
	H3PO4 4	36.00000*	3.74104	.000	20.9685	51.0315
	H3PO4 6	34.66667*	3.74104	.000	19.6351	49.6982
	H3PO4 8	29.33333*	3.74104	.000	14.3018	44.3649
	H3PO4 5	35.86667*	3.74104	.000	20.8351	50.8982
	H3PO4 10	36.13333*	3.74104	.000	21.1018	51.1649
	H3PO4 50	38.26667*	3.74104	.000	23.2351	53.2982
	H3PO4 100	24.93333*	3.74104	.000	9.9018	39.9649
	H3PO4 150	46.80000*	3.74104	.000	31.7685	61.8315
	MCPM 0	3.40000	3.74104	1.000	-11.6315	18.4315
	MCPM 2	24.66667*	3.74104	.000	9.6351	39.6982
	MCPM 4	24.00000*	3.74104	.000	8.9685	39.0315
	MCPM 6	36.00000*	3.74104	.000	20.9685	51.0315
	MCPM 8	32.66667*	3.74104	.000	17.6351	47.6982
	MCPM 5	34.06667*	3.74104	.000	19.0351	49.0982
	MCPM 10	31.80000*	3.74104	.000	16.7685	46.8315
	MCPM 50	33.06667*	3.74104	.000	18.0351	48.0982
	MCPM 100	34.20000*	3.74104	.000	19.1685	49.2315
	MCPM 150	58.46667*	3.74104	.000	43.4351	73.4982
H3PO4 0 V	untreated Ti-6Al-4V	-8.73333	3.74104	1.000	-23.7649	6.2982
	MCPM 150	58.46667*	3.74104	.000	43.4351	73.4982
H3PO4 0 V	untreated Ti-6Al-4V	-8.73333	3.74104	1.000	-23.7649	6.2982
	H3PO4 2	23.26667*	3.74104	.000	8.2351	38.2982
	H3PO4 4	27.26667*	3.74104	.000	12.2351	42.2982
	H3PO4 6	25.93333*	3.74104	.000	10.9018	40.9649
	H3PO4 8	20.60000*	3.74104	.000	5.5685	35.6315
	H3PO4 5	27.13333*	3.74104	.000	12.1018	42.1649
	H3PO4 10	27.40000*	3.74104	.000	12.3685	42.4315
	H3PO4 50	29.53333*	3.74104	.000	14.5018	44.5649
	H3PO4 100	16.20000*	3.74104	.019	1.1685	31.2315
	H3PO4 150	38.06667*	3.74104	.000	23.0351	53.0982
	MCPM 0	-5.33333	3.74104	1.000	-20.3649	9.6982
	MCPM 2	15.93333*	3.74104	.024	.9018	30.9649
	MCPM 4	15.26667*	3.74104	.041	.2351	30.2982
	MCPM 6	27.26667*	3.74104	.000	12.2351	42.2982
	MCPM 8	23.93333*	3.74104	.000	8.9018	38.9649
	MCPM 5	25.33333*	3.74104	.000	10.3018	40.3649
	MCPM 10	23.06667*	3.74104	.000	8.0351	38.0982
	MCPM 50	24.33333*	3.74104	.000	9.3018	39.3649
	MCPM 100	25.46667*	3.74104	.000	10.4351	40.4982
	MCPM 150	49.73333*	3.74104	.000	34.7018	64.7649
H3PO4 2	untreated Ti-6Al-4V	-32.00000*	3.74104	.000	-47.0315	-16.9685

	MCPM 150	49.73333*	3.74104	.000	34.7018	64.7649
H3PO4 2	untreated Ti-6Al-4V	-32.00000*	3.74104	.000	-47.0315	-16.9685
	H3PO4 0 V	-23.26667*	3.74104	.000	-38.2982	-8.2351
	H3PO4 4	4.00000	3.74104	1.000	-11.0315	19.0315
	H3PO4 6	2.66667	3.74104	1.000	-12.3649	17.6982
	H3PO4 8	-2.66667	3.74104	1.000	-17.6982	12.3649
	H3PO4 5	3.86667	3.74104	1.000	-11.1649	18.8982
	H3PO4 10	4.13333	3.74104	1.000	-10.8982	19.1649
	H3PO4 50	6.26667	3.74104	1.000	-8.7649	21.2982
	H3PO4 100	-7.06667	3.74104	1.000	-22.0982	7.9649
	H3PO4 150	14.80000	3.74104	.060	-.2315	29.8315
	MCPM 0	-28.60000*	3.74104	.000	-43.6315	-13.5685
	MCPM 2	-7.33333	3.74104	1.000	-22.3649	7.6982
	MCPM 4	-8.00000	3.74104	1.000	-23.0315	7.0315
	MCPM 6	4.00000	3.74104	1.000	-11.0315	19.0315
	MCPM 8	.66667	3.74104	1.000	-14.3649	15.6982
	MCPM 5	2.06667	3.74104	1.000	-12.9649	17.0982
	MCPM 10	-.20000	3.74104	1.000	-15.2315	14.8315
	MCPM 50	1.06667	3.74104	1.000	-13.9649	16.0982
	MCPM 100	2.20000	3.74104	1.000	-12.8315	17.2315
	MCPM 150	26.46667*	3.74104	.000	11.4351	41.4982
H3PO4 4	untreated Ti-6Al-4V	-36.00000*	3.74104	.000	-51.0315	-20.9685

	MCPM 150	26.46667*	3.74104	.000	11.4351	41.4982
H3PO4 4	untreated Ti-6Al-4V	-36.00000*	3.74104	.000	-51.0315	-20.9685
	H3PO4 0 V	-27.26667*	3.74104	.000	-42.2982	-12.2351
	H3PO4 2	-4.00000	3.74104	1.000	-19.0315	11.0315
	H3PO4 6	-1.33333	3.74104	1.000	-16.3649	13.6982
	H3PO4 8	-6.66667	3.74104	1.000	-21.6982	8.3649
	H3PO4 5	-.13333	3.74104	1.000	-15.1649	14.8982
	H3PO4 10	.13333	3.74104	1.000	-14.8982	15.1649
	H3PO4 50	2.26667	3.74104	1.000	-12.7649	17.2982
	H3PO4 100	-11.06667	3.74104	1.000	-26.0982	3.9649
	H3PO4 150	10.80000	3.74104	1.000	-4.2315	25.8315
	MCPM 0	-32.60000*	3.74104	.000	-47.6315	-17.5685
	MCPM 2	-11.33333	3.74104	.878	-26.3649	3.6982
	MCPM 4	-12.00000	3.74104	.538	-27.0315	3.0315
	MCPM 6	.00000	3.74104	1.000	-15.0315	15.0315
	MCPM 8	-3.33333	3.74104	1.000	-18.3649	11.6982
	MCPM 5	-1.93333	3.74104	1.000	-16.9649	13.0982
	MCPM 10	-4.20000	3.74104	1.000	-19.2315	10.8315
	MCPM 50	-2.93333	3.74104	1.000	-17.9649	12.0982
	MCPM 100	-1.80000	3.74104	1.000	-16.8315	13.2315
	MCPM 150	22.46667*	3.74104	.000	7.4351	37.4982
H3PO4 6	untreated Ti-6Al-4V	-34.66667*	3.74104	.000	-49.6982	-19.6351

	MCPM 150	22.46667*	3.74104	.000	7.4351	37.4982
H3PO4 6	untreated Ti-6Al-4V	-34.66667*	3.74104	.000	-49.6982	-19.6351
	H3PO4 0 V	-25.93333*	3.74104	.000	-40.9649	-10.9018
	H3PO4 2	-2.66667	3.74104	1.000	-17.6982	12.3649
	H3PO4 4	1.33333	3.74104	1.000	-13.6982	16.3649
	H3PO4 8	-5.33333	3.74104	1.000	-20.3649	9.6982
	H3PO4 5	1.20000	3.74104	1.000	-13.8315	16.2315
	H3PO4 10	1.46667	3.74104	1.000	-13.5649	16.4982
	H3PO4 50	3.60000	3.74104	1.000	-11.4315	18.6315
	H3PO4 100	-9.73333	3.74104	1.000	-24.7649	5.2982
	H3PO4 150	12.13333	3.74104	.487	-2.8982	27.1649
	MCPM 0	-31.26667*	3.74104	.000	-46.2982	-16.2351
	MCPM 2	-10.00000	3.74104	1.000	-25.0315	5.0315
	MCPM 4	-10.66667	3.74104	1.000	-25.6982	4.3649
	MCPM 6	1.33333	3.74104	1.000	-13.6982	16.3649
	MCPM 8	-2.00000	3.74104	1.000	-17.0315	13.0315
	MCPM 5	-.60000	3.74104	1.000	-15.6315	14.4315
	MCPM 10	-2.86667	3.74104	1.000	-17.8982	12.1649
	MCPM 50	-1.60000	3.74104	1.000	-16.6315	13.4315
	MCPM 100	-.46667	3.74104	1.000	-15.4982	14.5649
	MCPM 150	23.80000*	3.74104	.000	8.7685	38.8315
H3PO4 8	untreated Ti-6Al-4V	-29.33333*	3.74104	.000	-44.3649	-14.3018

	MCPM 150	23.80000*	3.74104	.000	8.7685	38.8315
H3PO4 8	untreated Ti-6Al-4V	-29.33333*	3.74104	.000	-44.3649	-14.3018
	H3PO4 0 V	-20.60000*	3.74104	.000	-35.6315	-5.5685
	H3PO4 2	2.66667	3.74104	1.000	-12.3649	17.6982
	H3PO4 4	6.66667	3.74104	1.000	-8.3649	21.6982
	H3PO4 6	5.33333	3.74104	1.000	-9.6982	20.3649
	H3PO4 5	6.53333	3.74104	1.000	-8.4982	21.5649
	H3PO4 10	6.80000	3.74104	1.000	-8.2315	21.8315
	H3PO4 50	8.93333	3.74104	1.000	-6.0982	23.9649
	H3PO4 100	-4.40000	3.74104	1.000	-19.4315	10.6315
	H3PO4 150	17.46667*	3.74104	.007	2.4351	32.4982
	MCPM 0	-25.93333*	3.74104	.000	-40.9649	-10.9018
	MCPM 2	-4.66667	3.74104	1.000	-19.6982	10.3649
	MCPM 4	-5.33333	3.74104	1.000	-20.3649	9.6982
	MCPM 6	6.66667	3.74104	1.000	-8.3649	21.6982
	MCPM 8	3.33333	3.74104	1.000	-11.6982	18.3649
	MCPM 5	4.73333	3.74104	1.000	-10.2982	19.7649
	MCPM 10	2.46667	3.74104	1.000	-12.5649	17.4982
	MCPM 50	3.73333	3.74104	1.000	-11.2982	18.7649
	MCPM 100	4.86667	3.74104	1.000	-10.1649	19.8982
	MCPM 150	29.13333*	3.74104	.000	14.1018	44.1649
H3PO4 5	untreated Ti-6Al-4V	-35.86667*	3.74104	.000	-50.8982	-20.8351

	MCPM 150	29.13333*	3.74104	.000	14.1018	44.1649
H3PO4 5	untreated Ti-6Al-4V	-35.86667*	3.74104	.000	-50.8982	-20.8351
	H3PO4 0 V	-27.13333*	3.74104	.000	-42.1649	-12.1018
	H3PO4 2	-3.86667	3.74104	1.000	-18.8982	11.1649
	H3PO4 4	.13333	3.74104	1.000	-14.8982	15.1649
	H3PO4 6	-1.20000	3.74104	1.000	-16.2315	13.8315
	H3PO4 8	-6.53333	3.74104	1.000	-21.5649	8.4982
	H3PO4 10	.26667	3.74104	1.000	-14.7649	15.2982
	H3PO4 50	2.40000	3.74104	1.000	-12.6315	17.4315
	H3PO4 100	-10.93333	3.74104	1.000	-25.9649	4.0982
	H3PO4 150	10.93333	3.74104	1.000	-4.0982	25.9649
	MCPM 0	-32.46667*	3.74104	.000	-47.4982	-17.4351
	MCPM 2	-11.20000	3.74104	.966	-26.2315	3.8315
	MCPM 4	-11.86667	3.74104	.594	-26.8982	3.1649
	MCPM 6	.13333	3.74104	1.000	-14.8982	15.1649
	MCPM 8	-3.20000	3.74104	1.000	-18.2315	11.8315
	MCPM 5	-1.80000	3.74104	1.000	-16.8315	13.2315
	MCPM 10	-4.06667	3.74104	1.000	-19.0982	10.9649
	MCPM 50	-2.80000	3.74104	1.000	-17.8315	12.2315
	MCPM 100	-1.66667	3.74104	1.000	-16.6982	13.3649
	MCPM 150	22.60000*	3.74104	.000	7.5685	37.6315
H3PO4 10	untreated Ti-6Al-4V	-36.13333*	3.74104	.000	-51.1649	-21.1018

	MCPM 150	22.60000*	3.74104	.000	7.5685	37.6315
H3PO4 10	untreated Ti-6Al-4V	-36.13333*	3.74104	.000	-51.1649	-21.1018
	H3PO4 0 V	-27.40000*	3.74104	.000	-42.4315	-12.3685
	H3PO4 2	-4.13333	3.74104	1.000	-19.1649	10.8982
	H3PO4 4	-.13333	3.74104	1.000	-15.1649	14.8982
	H3PO4 6	-1.46667	3.74104	1.000	-16.4982	13.5649
	H3PO4 8	-6.80000	3.74104	1.000	-21.8315	8.2315
	H3PO4 5	-.26667	3.74104	1.000	-15.2982	14.7649
	H3PO4 50	2.13333	3.74104	1.000	-12.8982	17.1649
	H3PO4 100	-11.20000	3.74104	.966	-26.2315	3.8315
	H3PO4 150	10.66667	3.74104	1.000	-4.3649	25.6982
	MCPM 0	-32.73333*	3.74104	.000	-47.7649	-17.7018
	MCPM 2	-11.46667	3.74104	.797	-26.4982	3.5649
	MCPM 4	-12.13333	3.74104	.487	-27.1649	2.8982
	MCPM 6	-.13333	3.74104	1.000	-15.1649	14.8982
	MCPM 8	-3.46667	3.74104	1.000	-18.4982	11.5649
	MCPM 5	-2.06667	3.74104	1.000	-17.0982	12.9649
	MCPM 10	-4.33333	3.74104	1.000	-19.3649	10.6982
	MCPM 50	-3.06667	3.74104	1.000	-18.0982	11.9649
	MCPM 100	-1.93333	3.74104	1.000	-16.9649	13.0982
	MCPM 150	22.33333*	3.74104	.000	7.3018	37.3649
H3PO4 50	untreated Ti-6Al-4V	-38.26667*	3.74104	.000	-53.2982	-23.2351

	MCPM 150	22.33333*	3.74104	.000	7.3018	37.3649
H3PO4 50	untreated Ti-6Al-4V	-38.26667*	3.74104	.000	-53.2982	-23.2351
	H3PO4 0 V	-29.53333*	3.74104	.000	-44.5649	-14.5018
	H3PO4 2	-6.26667	3.74104	1.000	-21.2982	8.7649
	H3PO4 4	-2.26667	3.74104	1.000	-17.2982	12.7649
	H3PO4 6	-3.60000	3.74104	1.000	-18.6315	11.4315
	H3PO4 8	-8.93333	3.74104	1.000	-23.9649	6.0982
	H3PO4 5	-2.40000	3.74104	1.000	-17.4315	12.6315
	H3PO4 10	-2.13333	3.74104	1.000	-17.1649	12.8982
	H3PO4 100	-13.33333	3.74104	.194	-28.3649	1.6982
	H3PO4 150	8.53333	3.74104	1.000	-6.4982	23.5649
	MCPM 0	-34.86667*	3.74104	.000	-49.8982	-19.8351
	MCPM 2	-13.60000	3.74104	.158	-28.6315	1.4315
	MCPM 4	-14.26667	3.74104	.093	-29.2982	.7649
	MCPM 6	-2.26667	3.74104	1.000	-17.2982	12.7649
	MCPM 8	-5.60000	3.74104	1.000	-20.6315	9.4315
	MCPM 5	-4.20000	3.74104	1.000	-19.2315	10.8315
	MCPM 10	-6.46667	3.74104	1.000	-21.4982	8.5649
	MCPM 50	-5.20000	3.74104	1.000	-20.2315	9.8315
	MCPM 100	-4.06667	3.74104	1.000	-19.0982	10.9649
	MCPM 150	20.20000*	3.74104	.001	5.1685	35.2315
H3PO4 100	untreated Ti-6Al-4V	-24.93333*	3.74104	.000	-39.9649	-9.9018

	MCPM 150	20.20000*	3.74104	.001	5.1685	35.2315
H3PO4 100	untreated Ti-6Al-4V	-24.93333*	3.74104	.000	-39.9649	-9.9018
	H3PO4 0 V	-16.20000*	3.74104	.019	-31.2315	-1.1685
	H3PO4 2	7.06667	3.74104	1.000	-7.9649	22.0982
	H3PO4 4	11.06667	3.74104	1.000	-3.9649	26.0982
	H3PO4 6	9.73333	3.74104	1.000	-5.2982	24.7649
	H3PO4 8	4.40000	3.74104	1.000	-10.6315	19.4315
	H3PO4 5	10.93333	3.74104	1.000	-4.0982	25.9649
	H3PO4 10	11.20000	3.74104	.966	-3.8315	26.2315
	H3PO4 50	13.33333	3.74104	.194	-1.6982	28.3649
	H3PO4 150	21.86667*	3.74104	.000	6.8351	36.8982
	MCPM 0	-21.53333*	3.74104	.000	-36.5649	-6.5018
	MCPM 2	-.26667	3.74104	1.000	-15.2982	14.7649
	MCPM 4	-.93333	3.74104	1.000	-15.9649	14.0982
	MCPM 6	11.06667	3.74104	1.000	-3.9649	26.0982
	MCPM 8	7.73333	3.74104	1.000	-7.2982	22.7649
	MCPM 5	9.13333	3.74104	1.000	-5.8982	24.1649
	MCPM 10	6.86667	3.74104	1.000	-8.1649	21.8982
	MCPM 50	8.13333	3.74104	1.000	-6.8982	23.1649
	MCPM 100	9.26667	3.74104	1.000	-5.7649	24.2982
	MCPM 150	33.53333*	3.74104	.000	18.5018	48.5649
H3PO4 150	untreated Ti-6Al-4V	-46.80000*	3.74104	.000	-61.8315	-31.7685

	MCPM 150	33.53333*	3.74104	.000	18.5018	48.5649
H3PO4 150	untreated Ti-6Al-4V	-46.80000*	3.74104	.000	-61.8315	-31.7685
	H3PO4 0 V	-38.06667*	3.74104	.000	-53.0982	-23.0351
	H3PO4 2	-14.80000	3.74104	.060	-29.8315	.2315
	H3PO4 4	-10.80000	3.74104	1.000	-25.8315	4.2315
	H3PO4 6	-12.13333	3.74104	.487	-27.1649	2.8982
	H3PO4 8	-17.46667*	3.74104	.007	-32.4982	-2.4351
	H3PO4 5	-10.93333	3.74104	1.000	-25.9649	4.0982
	H3PO4 10	-10.66667	3.74104	1.000	-25.6982	4.3649
	H3PO4 50	-8.53333	3.74104	1.000	-23.5649	6.4982
	H3PO4 100	-21.86667*	3.74104	.000	-36.8982	-6.8351
	MCPM 0	-43.40000*	3.74104	.000	-58.4315	-28.3685
	MCPM 2	-22.13333*	3.74104	.000	-37.1649	-7.1018
	MCPM 4	-22.80000*	3.74104	.000	-37.8315	-7.7685
	MCPM 6	-10.80000	3.74104	1.000	-25.8315	4.2315
	MCPM 8	-14.13333	3.74104	.103	-29.1649	.8982
	MCPM 5	-12.73333	3.74104	.309	-27.7649	2.2982
	MCPM 10	-15.00000	3.74104	.051	-30.0315	.0315
	MCPM 50	-13.73333	3.74104	.142	-28.7649	1.2982
	MCPM 100	-12.60000	3.74104	.342	-27.6315	2.4315
	MCPM 150	11.66667	3.74104	.688	-3.3649	26.6982
MCPM 0	untreated Ti-6Al-4V	-3.40000	3.74104	1.000	-18.4315	11.6315

	MCPM 150	11.66667	3.74104	.688	-3.3649	26.6982
MCPM 0	untreated Ti-6Al-4V	-3.40000	3.74104	1.000	-18.4315	11.6315
	H3PO4 0 V	5.33333	3.74104	1.000	-9.6982	20.3649
	H3PO4 2	28.60000*	3.74104	.000	13.5685	43.6315
	H3PO4 4	32.60000*	3.74104	.000	17.5685	47.6315
	H3PO4 6	31.26667*	3.74104	.000	16.2351	46.2982
	H3PO4 8	25.93333*	3.74104	.000	10.9018	40.9649
	H3PO4 5	32.46667*	3.74104	.000	17.4351	47.4982
	H3PO4 10	32.73333*	3.74104	.000	17.7018	47.7649
	H3PO4 50	34.86667*	3.74104	.000	19.8351	49.8982
	H3PO4 100	21.53333*	3.74104	.000	6.5018	36.5649
	H3PO4 150	43.40000*	3.74104	.000	28.3685	58.4315
	MCPM 2	21.26667*	3.74104	.000	6.2351	36.2982
	MCPM 4	20.60000*	3.74104	.000	5.5685	35.6315
	MCPM 6	32.60000*	3.74104	.000	17.5685	47.6315
	MCPM 8	29.26667*	3.74104	.000	14.2351	44.2982
	MCPM 5	30.66667*	3.74104	.000	15.6351	45.6982
	MCPM 10	28.40000*	3.74104	.000	13.3685	43.4315
	MCPM 50	29.66667*	3.74104	.000	14.6351	44.6982
	MCPM 100	30.80000*	3.74104	.000	15.7685	45.8315
	MCPM 150	55.06667*	3.74104	.000	40.0351	70.0982
MCPM 2	untreated Ti-6Al-4V	-24.66667*	3.74104	.000	-39.6982	-9.6351

	MCPM 150	55.06667*	3.74104	.000	40.0351	70.0982
MCPM 2	untreated Ti-6Al-4V	-24.66667*	3.74104	.000	-39.6982	-9.6351
	H3PO4 0 V	-15.93333*	3.74104	.024	-30.9649	-.9018
	H3PO4 2	7.33333	3.74104	1.000	-7.6982	22.3649
	H3PO4 4	11.33333	3.74104	.878	-3.6982	26.3649
	H3PO4 6	10.00000	3.74104	1.000	-5.0315	25.0315
	H3PO4 8	4.66667	3.74104	1.000	-10.3649	19.6982
	H3PO4 5	11.20000	3.74104	.966	-3.8315	26.2315
	H3PO4 10	11.46667	3.74104	.797	-3.5649	26.4982
	H3PO4 50	13.60000	3.74104	.158	-1.4315	28.6315
	H3PO4 100	.26667	3.74104	1.000	-14.7649	15.2982
	H3PO4 150	22.13333*	3.74104	.000	7.1018	37.1649
	MCPM 0	-21.26667*	3.74104	.000	-36.2982	-6.2351
	MCPM 4	-.66667	3.74104	1.000	-15.6982	14.3649
	MCPM 6	11.33333	3.74104	.878	-3.6982	26.3649
	MCPM 8	8.00000	3.74104	1.000	-7.0315	23.0315
	MCPM 5	9.40000	3.74104	1.000	-5.6315	24.4315
	MCPM 10	7.13333	3.74104	1.000	-7.8982	22.1649
	MCPM 50	8.40000	3.74104	1.000	-6.6315	23.4315
	MCPM 100	9.53333	3.74104	1.000	-5.4982	24.5649
	MCPM 150	33.80000*	3.74104	.000	18.7685	48.8315
MCPM 4	untreated Ti-6Al-4V	-24.00000*	3.74104	.000	-39.0315	-8.9685

	MCPM 150	33.80000*	3.74104	.000	18.7685	48.8315
MCPM 4	untreated Ti-6Al-4V	-24.00000*	3.74104	.000	-39.0315	-8.9685
	H3PO4 0 V	-15.26667*	3.74104	.041	-30.2982	-.2351
	H3PO4 2	8.00000	3.74104	1.000	-7.0315	23.0315
	H3PO4 4	12.00000	3.74104	.538	-3.0315	27.0315
	H3PO4 6	10.66667	3.74104	1.000	-4.3649	25.6982
	H3PO4 8	5.33333	3.74104	1.000	-9.6982	20.3649
	H3PO4 5	11.86667	3.74104	.594	-3.1649	26.8982
	H3PO4 10	12.13333	3.74104	.487	-2.8982	27.1649
	H3PO4 50	14.26667	3.74104	.093	-.7649	29.2982
	H3PO4 100	.93333	3.74104	1.000	-14.0982	15.9649
	H3PO4 150	22.80000*	3.74104	.000	7.7685	37.8315
	MCPM 0	-20.60000*	3.74104	.000	-35.6315	-5.5685
	MCPM 2	.66667	3.74104	1.000	-14.3649	15.6982
	MCPM 6	12.00000	3.74104	.538	-3.0315	27.0315
	MCPM 8	8.66667	3.74104	1.000	-6.3649	23.6982
	MCPM 5	10.06667	3.74104	1.000	-4.9649	25.0982
	MCPM 10	7.80000	3.74104	1.000	-7.2315	22.8315
	MCPM 50	9.06667	3.74104	1.000	-5.9649	24.0982
	MCPM 100	10.20000	3.74104	1.000	-4.8315	25.2315
	MCPM 150	34.46667*	3.74104	.000	19.4351	49.4982
MCPM 6	untreated Ti-6Al-4V	-36.00000*	3.74104	.000	-51.0315	-20.9685

	MCPM 150	34.46667*	3.74104	.000	19.4351	49.4982
MCPM 6	untreated Ti-6Al-4V	-36.00000*	3.74104	.000	-51.0315	-20.9685
	H3PO4 0 V	-27.26667*	3.74104	.000	-42.2982	-12.2351
	H3PO4 2	-4.00000	3.74104	1.000	-19.0315	11.0315
	H3PO4 4	.00000	3.74104	1.000	-15.0315	15.0315
	H3PO4 6	-1.33333	3.74104	1.000	-16.3649	13.6982
	H3PO4 8	-6.66667	3.74104	1.000	-21.6982	8.3649
	H3PO4 5	-.13333	3.74104	1.000	-15.1649	14.8982
	H3PO4 10	.13333	3.74104	1.000	-14.8982	15.1649
	H3PO4 50	2.26667	3.74104	1.000	-12.7649	17.2982
	H3PO4 100	-11.06667	3.74104	1.000	-26.0982	3.9649
	H3PO4 150	10.80000	3.74104	1.000	-4.2315	25.8315
	MCPM 0	-32.60000*	3.74104	.000	-47.6315	-17.5685
	MCPM 2	-11.33333	3.74104	.878	-26.3649	3.6982
	MCPM 4	-12.00000	3.74104	.538	-27.0315	3.0315
	MCPM 8	-3.33333	3.74104	1.000	-18.3649	11.6982
	MCPM 5	-1.93333	3.74104	1.000	-16.9649	13.0982
	MCPM 10	-4.20000	3.74104	1.000	-19.2315	10.8315
	MCPM 50	-2.93333	3.74104	1.000	-17.9649	12.0982
	MCPM 100	-1.80000	3.74104	1.000	-16.8315	13.2315
	MCPM 150	22.46667*	3.74104	.000	7.4351	37.4982
MCPM 8	untreated Ti-6Al-4V	-32.66667*	3.74104	.000	-47.6982	-17.6351

	MCPM 150	22.46667*	3.74104	.000	7.4351	37.4982
MCPM 8	untreated Ti-6Al-4V	-32.66667*	3.74104	.000	-47.6982	-17.6351
	H3PO4 0 V	-23.93333*	3.74104	.000	-38.9649	-8.9018
	H3PO4 2	-.66667	3.74104	1.000	-15.6982	14.3649
	H3PO4 4	3.33333	3.74104	1.000	-11.6982	18.3649
	H3PO4 6	2.00000	3.74104	1.000	-13.0315	17.0315
	H3PO4 8	-3.33333	3.74104	1.000	-18.3649	11.6982
	H3PO4 5	3.20000	3.74104	1.000	-11.8315	18.2315
	H3PO4 10	3.46667	3.74104	1.000	-11.5649	18.4982
	H3PO4 50	5.60000	3.74104	1.000	-9.4315	20.6315
	H3PO4 100	-7.73333	3.74104	1.000	-22.7649	7.2982
	H3PO4 150	14.13333	3.74104	.103	-.8982	29.1649
	MCPM 0	-29.26667*	3.74104	.000	-44.2982	-14.2351
	MCPM 2	-8.00000	3.74104	1.000	-23.0315	7.0315
	MCPM 4	-8.66667	3.74104	1.000	-23.6982	6.3649
	MCPM 6	3.33333	3.74104	1.000	-11.6982	18.3649
	MCPM 5	1.40000	3.74104	1.000	-13.6315	16.4315
	MCPM 10	-.86667	3.74104	1.000	-15.8982	14.1649
	MCPM 50	.40000	3.74104	1.000	-14.6315	15.4315
	MCPM 100	1.53333	3.74104	1.000	-13.4982	16.5649
	MCPM 150	25.80000*	3.74104	.000	10.7685	40.8315
MCPM 5	untreated Ti-6Al-4V	-34.06667*	3.74104	.000	-49.0982	-19.0351

	MCPM 150	25.80000*	3.74104	.000	10.7685	40.8315
MCPM 5	untreated Ti-6Al-4V	-34.06667*	3.74104	.000	-49.0982	-19.0351
	H3PO4 0 V	-25.33333*	3.74104	.000	-40.3649	-10.3018
	H3PO4 2	-2.06667	3.74104	1.000	-17.0982	12.9649
	H3PO4 4	1.93333	3.74104	1.000	-13.0982	16.9649
	H3PO4 6	.60000	3.74104	1.000	-14.4315	15.6315
	H3PO4 8	-4.73333	3.74104	1.000	-19.7649	10.2982
	H3PO4 5	1.80000	3.74104	1.000	-13.2315	16.8315
	H3PO4 10	2.06667	3.74104	1.000	-12.9649	17.0982
	H3PO4 50	4.20000	3.74104	1.000	-10.8315	19.2315
	H3PO4 100	-9.13333	3.74104	1.000	-24.1649	5.8982
	H3PO4 150	12.73333	3.74104	.309	-2.2982	27.7649
	MCPM 0	-30.66667*	3.74104	.000	-45.6982	-15.6351
	MCPM 2	-9.40000	3.74104	1.000	-24.4315	5.6315
	MCPM 4	-10.06667	3.74104	1.000	-25.0982	4.9649
	MCPM 6	1.93333	3.74104	1.000	-13.0982	16.9649
	MCPM 8	-1.40000	3.74104	1.000	-16.4315	13.6315
	MCPM 10	-2.26667	3.74104	1.000	-17.2982	12.7649
	MCPM 50	-1.00000	3.74104	1.000	-16.0315	14.0315
	MCPM 100	.13333	3.74104	1.000	-14.8982	15.1649
	MCPM 150	24.40000*	3.74104	.000	9.3685	39.4315
MCPM 10	untreated Ti-6Al-4V	-31.80000*	3.74104	.000	-46.8315	-16.7685

	MCPM 150	24.40000*	3.74104	.000	9.3685	39.4315
MCPM 10	untreated Ti-6Al-4V	-31.80000*	3.74104	.000	-46.8315	-16.7685
	H3PO4 0 V	-23.06667*	3.74104	.000	-38.0982	-8.0351
	H3PO4 2	.20000	3.74104	1.000	-14.8315	15.2315
	H3PO4 4	4.20000	3.74104	1.000	-10.8315	19.2315
	H3PO4 6	2.86667	3.74104	1.000	-12.1649	17.8982
	H3PO4 8	-2.46667	3.74104	1.000	-17.4982	12.5649
	H3PO4 5	4.06667	3.74104	1.000	-10.9649	19.0982
	H3PO4 10	4.33333	3.74104	1.000	-10.6982	19.3649
	H3PO4 50	6.46667	3.74104	1.000	-8.5649	21.4982
	H3PO4 100	-6.86667	3.74104	1.000	-21.8982	8.1649
	H3PO4 150	15.00000	3.74104	.051	-.0315	30.0315
	MCPM 0	-28.40000*	3.74104	.000	-43.4315	-13.3685
	MCPM 2	-7.13333	3.74104	1.000	-22.1649	7.8982
	MCPM 4	-7.80000	3.74104	1.000	-22.8315	7.2315
	MCPM 6	4.20000	3.74104	1.000	-10.8315	19.2315
	MCPM 8	.86667	3.74104	1.000	-14.1649	15.8982
	MCPM 5	2.26667	3.74104	1.000	-12.7649	17.2982
	MCPM 50	1.26667	3.74104	1.000	-13.7649	16.2982
	MCPM 100	2.40000	3.74104	1.000	-12.6315	17.4315
	MCPM 150	26.66667*	3.74104	.000	11.6351	41.6982
MCPM 50	untreated Ti-6Al-4V	-33.06667*	3.74104	.000	-48.0982	-18.0351

	MCPM 150	26.66667*	3.74104	.000	11.6351	41.6982
MCPM 50	untreated Ti-6Al-4V	-33.06667*	3.74104	.000	-48.0982	-18.0351
	H3PO4 0 V	-24.33333*	3.74104	.000	-39.3649	-9.3018
	H3PO4 2	-1.06667	3.74104	1.000	-16.0982	13.9649
	H3PO4 4	2.93333	3.74104	1.000	-12.0982	17.9649
	H3PO4 6	1.60000	3.74104	1.000	-13.4315	16.6315
	H3PO4 8	-3.73333	3.74104	1.000	-18.7649	11.2982
	H3PO4 5	2.80000	3.74104	1.000	-12.2315	17.8315
	H3PO4 10	3.06667	3.74104	1.000	-11.9649	18.0982
	H3PO4 50	5.20000	3.74104	1.000	-9.8315	20.2315
	H3PO4 100	-8.13333	3.74104	1.000	-23.1649	6.8982
	H3PO4 150	13.73333	3.74104	.142	-1.2982	28.7649
	MCPM 0	-29.66667*	3.74104	.000	-44.6982	-14.6351
	MCPM 2	-8.40000	3.74104	1.000	-23.4315	6.6315
	MCPM 4	-9.06667	3.74104	1.000	-24.0982	5.9649
	MCPM 6	2.93333	3.74104	1.000	-12.0982	17.9649
	MCPM 8	-.40000	3.74104	1.000	-15.4315	14.6315
	MCPM 5	1.00000	3.74104	1.000	-14.0315	16.0315
	MCPM 10	-1.26667	3.74104	1.000	-16.2982	13.7649
	MCPM 100	1.13333	3.74104	1.000	-13.8982	16.1649
	MCPM 150	25.40000*	3.74104	.000	10.3685	40.4315
MCPM 100	untreated Ti-6Al-4V	-34.20000*	3.74104	.000	-49.2315	-19.1685

	MCPM 150	25.40000*	3.74104	.000	10.3685	40.4315
MCPM 100	untreated Ti-6Al-4V	-34.20000*	3.74104	.000	-49.2315	-19.1685
	H3PO4 0 V	-25.46667*	3.74104	.000	-40.4982	-10.4351
	H3PO4 2	-2.20000	3.74104	1.000	-17.2315	12.8315
	H3PO4 4	1.80000	3.74104	1.000	-13.2315	16.8315
	H3PO4 6	.46667	3.74104	1.000	-14.5649	15.4982
	H3PO4 8	-4.86667	3.74104	1.000	-19.8982	10.1649
	H3PO4 5	1.66667	3.74104	1.000	-13.3649	16.6982
	H3PO4 10	1.93333	3.74104	1.000	-13.0982	16.9649
	H3PO4 50	4.06667	3.74104	1.000	-10.9649	19.0982
	H3PO4 100	-9.26667	3.74104	1.000	-24.2982	5.7649
	H3PO4 150	12.60000	3.74104	.342	-2.4315	27.6315
	MCPM 0	-30.80000*	3.74104	.000	-45.8315	-15.7685
	MCPM 2	-9.53333	3.74104	1.000	-24.5649	5.4982
	MCPM 4	-10.20000	3.74104	1.000	-25.2315	4.8315
	MCPM 6	1.80000	3.74104	1.000	-13.2315	16.8315
	MCPM 8	-1.53333	3.74104	1.000	-16.5649	13.4982
	MCPM 5	-.13333	3.74104	1.000	-15.1649	14.8982
	MCPM 10	-2.40000	3.74104	1.000	-17.4315	12.6315
	MCPM 50	-1.13333	3.74104	1.000	-16.1649	13.8982
	MCPM 150	24.26667*	3.74104	.000	9.2351	39.2982
MCPM 150	untreated Ti-6Al-4V	-58.46667*	3.74104	.000	-73.4982	-43.4351

	MCPM 150	24.26667*	3.74104	.000	9.2351	39.2982
MCPM 150	untreated Ti-6Al-4V	-58.46667*	3.74104	.000	-73.4982	-43.4351
	H3PO4 0 V	-49.73333*	3.74104	.000	-64.7649	-34.7018
	H3PO4 2	-26.46667*	3.74104	.000	-41.4982	-11.4351
	H3PO4 4	-22.46667*	3.74104	.000	-37.4982	-7.4351
	H3PO4 6	-23.80000*	3.74104	.000	-38.8315	-8.7685
	H3PO4 8	-29.13333*	3.74104	.000	-44.1649	-14.1018
	H3PO4 5	-22.60000*	3.74104	.000	-37.6315	-7.5685
	H3PO4 10	-22.33333*	3.74104	.000	-37.3649	-7.3018
	H3PO4 50	-20.20000*	3.74104	.001	-35.2315	-5.1685
	H3PO4 100	-33.53333*	3.74104	.000	-48.5649	-18.5018
	H3PO4 150	-11.66667	3.74104	.688	-26.6982	3.3649
	MCPM 0	-55.06667*	3.74104	.000	-70.0982	-40.0351
	MCPM 2	-33.80000*	3.74104	.000	-48.8315	-18.7685
	MCPM 4	-34.46667*	3.74104	.000	-49.4982	-19.4351
	MCPM 6	-22.46667*	3.74104	.000	-37.4982	-7.4351
	MCPM 8	-25.80000*	3.74104	.000	-40.8315	-10.7685
	MCPM 5	-24.40000*	3.74104	.000	-39.4315	-9.3685
	MCPM 10	-26.66667*	3.74104	.000	-41.6982	-11.6351
	MCPM 50	-25.40000*	3.74104	.000	-40.4315	-10.3685
	MCPM 100	-24.26667*	3.74104	.000	-39.2982	-9.2351

*. The mean difference is significant at the .05 level.

APPENDIX C

Contact angle and the statistical analysis of the anodized films before UV irradiation

Oneway

Descriptives

angle

	N	Mean	Std. Deviation	Std. Error	95% Confidence Interval for Mean		Minimum	Maximum
					Lower Bound	Upper Bound		
untreated Ti-6Al-4V	3	79.9200	5.53953	3.19825	66.1590	93.6810	73.92	84.84
woi	3	82.7533	2.55533	1.47532	76.4055	89.1011	80.52	85.54
H3PO4 2	3	75.8467	1.24857	.72086	72.7450	78.9483	74.42	76.74
MCPM 1	3	71.9600	10.63344	6.13922	45.5451	98.3749	59.76	79.26
H3PO4 6	3	76.9000	6.31506	3.64600	61.2125	92.5875	72.30	84.10
MCPM 6	3	67.0267	3.45869	1.99688	58.4348	75.6185	63.34	70.20
Total	18	75.7344	7.20317	1.69780	72.1524	79.3165	59.76	85.54

Post Hoc Tests

Multiple Comparisons

Dependent Variable: angle

Bonferroni

(I) anodize	(J) anodize	Mean Difference (I-J)	Std. Error	Sig.	95% Confidence Interval	
					Lower Bound	Upper Bound
untreated Ti-6Al-4V	woi	-2.83333	4.75731	1.000	-20.1922	14.5255
	H3PO4 2	4.07333	4.75731	1.000	-13.2855	21.4322
	MCPM 1	7.96000	4.75731	1.000	-9.3989	25.3189
	H3PO4 6	3.02000	4.75731	1.000	-14.3389	20.3789
	MCPM 6	12.89333	4.75731	.284	-4.4655	30.2522
woi	untreated Ti-6Al-4V	2.83333	4.75731	1.000	-14.5255	20.1922
	H3PO4 2	6.90667	4.75731	1.000	-10.4522	24.2655
	MCPM 1	10.79333	4.75731	.638	-6.5655	28.1522
	H3PO4 6	5.85333	4.75731	1.000	-11.5055	23.2122
	MCPM 6	15.72667	4.75731	.094	-1.6322	33.0855
H3PO4 2	untreated Ti-6Al-4V	-4.07333	4.75731	1.000	-21.4322	13.2855
	woi	-6.90667	4.75731	1.000	-24.2655	10.4522
	MCPM 1	3.88667	4.75731	1.000	-13.4722	21.2455
	H3PO4 6	-1.05333	4.75731	1.000	-18.4122	16.3055
	MCPM 6	8.82000	4.75731	1.000	-8.5389	26.1789
MCPM 1	untreated Ti-6Al-4V	-7.96000	4.75731	1.000	-25.3189	9.3989
	woi	-10.79333	4.75731	.638	-28.1522	6.5655
	H3PO4 2	-3.88667	4.75731	1.000	-21.2455	13.4722
	H3PO4 6	-4.94000	4.75731	1.000	-22.2989	12.4189
	MCPM 6	4.93333	4.75731	1.000	-12.4255	22.2922
H3PO4 6	untreated Ti-6Al-4V	-3.02000	4.75731	1.000	-20.3789	14.3389

	MCPM 6	4.93333	4.75731	1.000	-12.4255	22.2922
H3PO4 6	untreated Ti-6Al-4V	-3.02000	4.75731	1.000	-20.3789	14.3389
	woi	-5.85333	4.75731	1.000	-23.2122	11.5055
	H3PO4 2	1.05333	4.75731	1.000	-16.3055	18.4122
	MCPM 1	4.94000	4.75731	1.000	-12.4189	22.2989
	MCPM 6	9.87333	4.75731	.902	-7.4855	27.2322
MCPM 6	untreated Ti-6Al-4V	-12.89333	4.75731	.284	-30.2522	4.4655
	woi	-15.72667	4.75731	.094	-33.0855	1.6322
	H3PO4 2	-8.82000	4.75731	1.000	-26.1789	8.5389
	MCPM 1	-4.93333	4.75731	1.000	-22.2922	12.4255
	H3PO4 6	-9.87333	4.75731	.902	-27.2322	7.4855

APPENDIX D

Contact angle and the statistical analysis of the anodized films after UV irradiation for 24 h

Post Hoc Tests

Multiple Comparisons

Dependent Variable: angle
Bonferroni

(I) anodize	(J) anodize	Mean Difference (I-J)	Std. Error	Sig.	95% Confidence Interval	
					Lower Bound	Upper Bound
b UV untreated Ti-6Al-4V	a UV untreated Ti-6Al-4V	26.44000*	4.63239	.000	8.5775	44.3025
	b UV woi	-2.83333	4.63239	1.000	-20.6958	15.0291
	a UV woi	32.53333*	4.63239	.000	14.6709	50.3958
	b UV H3PO4 2	6.78000	4.63239	1.000	-11.0825	24.6425
	a UV H3PO4 2	27.05333*	4.63239	.000	9.1909	44.9158
	b UV MCPM 1	12.43333	4.63239	.856	-5.4291	30.2958
	a UV MCPM 1	52.06000*	4.63239	.000	34.1975	69.9225
	b UV H3PO4 6	5.93333	4.63239	1.000	-11.9291	23.7958
	a UV H3PO4 6	35.32667*	4.63239	.000	17.4642	53.1891
	b UV MCPM 6	12.89333	4.63239	.681	-4.9691	30.7558
	a UV MCPM 6	43.00667*	4.63239	.000	25.1442	60.8691
b UV woi	b UV untreated Ti-6Al-4V	2.83333	4.63239	1.000	-15.0291	20.6958
	a UV untreated Ti-6Al-4V	29.27333*	4.63239	.000	11.4109	47.1358
	a UV woi	35.36667*	4.63239	.000	17.5042	53.2291
	b UV H3PO4 2	9.61333	4.63239	1.000	-8.2491	27.4758
	a UV H3PO4 2	29.88667*	4.63239	.000	12.0242	47.7491
	b UV MCPM 1	15.26667	4.63239	.201	-2.5958	33.1291
	a UV MCPM 1	54.89333*	4.63239	.000	37.0309	72.7558
	b UV H3PO4 6	8.76667	4.63239	1.000	-9.0958	26.6291
	a UV H3PO4 6	38.16000*	4.63239	.000	20.2975	56.0225
	b UV MCPM 6	15.72667	4.63239	.158	-2.1358	33.5891
	a UV MCPM 6	45.84000*	4.63239	.000	27.9775	63.7025
b UV H3PO4 2	b UV untreated Ti-6Al-4V	-6.78000	4.63239	1.000	-24.6425	11.0825
	a UV untreated Ti-6Al-4V	19.66000*	4.63239	.019	1.7975	37.5225
	b UV woi	-9.61333	4.63239	1.000	-27.4758	8.2491
	a UV woi	25.75333*	4.63239	.001	7.8909	43.6158
	a UV H3PO4 2	20.27333*	4.63239	.013	2.4109	38.1358
	b UV MCPM 1	5.65333	4.63239	1.000	-12.2091	23.5158
	a UV MCPM 1	45.28000*	4.63239	.000	27.4175	63.1425
	b UV H3PO4 6	-.84667	4.63239	1.000	-18.7091	17.0158
	a UV H3PO4 6	28.54667*	4.63239	.000	10.6842	46.4091
	b UV MCPM 6	6.11333	4.63239	1.000	-11.7491	23.9758
	a UV MCPM 6	36.22667*	4.63239	.000	18.3642	54.0891

b UV MCPM 1	b UV untreated Ti-6Al-4V	-12.43333	4.63239	.856	-30.2958	5.4291
	a UV untreated Ti-6Al-4V	14.00667	4.63239	.387	-3.8558	31.8691
	b UV woi	-15.26667	4.63239	.201	-33.1291	2.5958
	a UV woi	20.10000*	4.63239	.015	2.2375	37.9625
	b UV H3PO4 2	-5.65333	4.63239	1.000	-23.5158	12.2091
	a UV H3PO4 2	14.62000	4.63239	.282	-3.2425	32.4825
	a UV MCPM 1	39.62667*	4.63239	.000	21.7642	57.4891
	b UV H3PO4 6	-6.50000	4.63239	1.000	-24.3625	11.3625
	a UV H3PO4 6	22.89333*	4.63239	.003	5.0309	40.7558
	b UV MCPM 6	.46000	4.63239	1.000	-17.4025	18.3225
	a UV MCPM 6	30.57333*	4.63239	.000	12.7109	48.4358

b UV H3PO4 6	b UV untreated Ti-6Al-4V	-5.93333	4.63239	1.000	-23.7958	11.9291
	a UV untreated Ti-6Al-4V	20.50667*	4.63239	.012	2.6442	38.3691
	b UV woi	-8.76667	4.63239	1.000	-26.6291	9.0958
	a UV woi	26.60000*	4.63239	.000	8.7375	44.4625
	b UV H3PO4 2	.84667	4.63239	1.000	-17.0158	18.7091
	a UV H3PO4 2	21.12000*	4.63239	.008	3.2575	38.9825
	b UV MCPM 1	6.50000	4.63239	1.000	-11.3625	24.3625
	a UV MCPM 1	46.12667*	4.63239	.000	28.2642	63.9891
	a UV H3PO4 6	29.39333*	4.63239	.000	11.5309	47.2558
	b UV MCPM 6	6.96000	4.63239	1.000	-10.9025	24.8225
	a UV MCPM 6	37.07333*	4.63239	.000	19.2109	54.9358

b UV MCPM 6	b UV untreated Ti-6Al-4V	-12.89333	4.63239	.681	-30.7558	4.9691
	a UV untreated Ti-6Al-4V	13.54667	4.63239	.490	-4.3158	31.4091
	b UV woi	-15.72667	4.63239	.158	-33.5891	2.1358
	a UV woi	19.64000*	4.63239	.019	1.7775	37.5025
	b UV H3PO4 2	-6.11333	4.63239	1.000	-23.9758	11.7491
	a UV H3PO4 2	14.16000	4.63239	.358	-3.7025	32.0225
	b UV MCPM 1	-.46000	4.63239	1.000	-18.3225	17.4025
	a UV MCPM 1	39.16667*	4.63239	.000	21.3042	57.0291
	b UV H3PO4 6	-6.96000	4.63239	1.000	-24.8225	10.9025
	a UV H3PO4 6	22.43333*	4.63239	.004	4.5709	40.2958
	a UV MCPM 6	30.11333*	4.63239	.000	12.2509	47.9758

APPENDIX E

Statistical analysis of the anodized films formed by Ethanol treatment

Post Hoc Tests

Multiple Comparisons

Dependent Variable: angle

Bonferroni

(I) anodize	(J) anodize	Mean Difference (I-J)	Std. Error	Sig.	95% Confidence Interval	
					Lower Bound	Upper Bound
Ano 1	Ano mix	13.44667	4.99041	.108	-2.9591	29.8524
	Ano 2	39.82000*	4.99041	.001	23.4142	56.2258
Ano mix	Ano 1	-13.44667	4.99041	.108	-29.8524	2.9591
	Ano 2	26.37333*	4.99041	.006	9.9676	42.7791
Ano 2	Ano 1	-39.82000*	4.99041	.001	-56.2258	-23.4142
	Ano mix	-26.37333*	4.99041	.006	-42.7791	-9.9676

*. The mean difference is significant at the .05 level.

APPENDIX F

2θ, intensity and hkl of TiO_2 from JCPDS 00-021-1272

Pattern : 00-021-1272 **Radiation =** 1.540598 **Quality :** High

TiO_2

Titanium Oxide
Anatase, syn

Lattice : Body-centered tetragonal
S.G. : I41/amd (141)

a = 3.78520
c = 9.51390

Z = 4

Mol. weight = 79.90
Volume [CD] = 136.31
Dx = 3.893
I/Icor = 3.30

Color: Colorless
Sample source or locality: Sample obtained from National Lead Co., South Amboy, New Jersey, USA.
General comments: Anatase and another polymorph, brookite (orthorhombic), are converted to rutile (tetragonal) by heating above 700 C.
General comments: Pattern reviewed by Holzer, J., McCarthy, G., North Dakota State Univ., Fargo, North Dakota, USA, *ICDD Grant-in-Aid* (1990). Agrees well with experimental and calculated patterns.
Additional pattern: Validated by calculated pattern.
Temperature of data collection: Pattern taken at 25 C.
Additional pattern: See ICSD 9852 (PDF 71-1166).
Data collection flag: Ambient.

Natl. Bur. Stand. (U.S.) Monogr. 25, volume 7, page 82 (1969)

Radiation :

SS/FOM : F30= 74(0.0116,35)

Filter : Not specified
d-sp : Not given

2th	i	h	k	l
25.281	100	1	0	1
36.947	10	1	0	3
37.801	20	0	0	4
38.576	10	1	1	2
48.050	35	2	0	0
53.891	20	1	0	5
55.062	20	2	1	1
62.121	4	2	1	3
62.690	14	2	0	4
68.762	6	1	1	6
70.311	6	2	2	0
74.031	2	1	0	7
75.032	10	2	1	5
76.020	4	3	0	1
80.727	2	0	0	8
82.139	2	3	0	3
82.662	6	2	2	4
83.149	4	3	1	2
93.220	2	2	1	7
94.181	4	3	0	5
95.143	4	3	2	1
98.318	2	1	0	9
99.804	2	2	0	8
101.221	2	3	2	3
107.448	4	3	1	6
108.963	4	4	0	0
112.840	2	3	0	7
113.861	2	3	2	5
114.909	2	4	1	1
118.439	4	2	1	9
120.104	2	2	2	8
121.725	2	4	1	3
122.336	2	4	0	4
131.035	2	4	2	0
135.998	2	3	2	7
137.391	4	4	1	5
143.887	2	3	0	9
150.039	4	4	2	4
152.633	2	0	0	12

VITA

Miss Phanawan Whangdee was born in Ubonratchathani on March 5th, 1985. In 2008, she finished her Bachelor's Degree in Physics from faculty of Science, Khon Kaen University. Then, she studied for Master's Degree in ceramic technology, department of materials science, Chulalongkorn University and graduated in 2010. After that, she continued her education in Materials science at the same department.

Publications

P. Whangdee, S. Chukasorn, V. Srimaneepong, T. Watanabe and D. P. Kashima. Vol. 664 (2013). Effects of Surface Roughness and Chemical Species on Hydrophilicity of Anodized Film on Ti-6Al-4V Formed at a Low Current Density. Advanced Materials Research, 774-779.

P. Whangdee, S. Sriprasertsuk, V. Srimaneepong and D. P. Kashima. Vol. 608 (2014) Surface Characteristics and Hydrophilicity of the as-Anodized Films Formed at High Current Density on Ti-6Al-4V in Different Electrolytes. Key Engineering Materials, 274-279.

S. Sriprasertsuk, P. Whangdee, S. Jinawath, P. Thanyakitpaisal and D. P. Kashima. Vol. 608 (2014) Anodic Oxide Film Formed on Ti-6Al-4V at a Low Current Density in Monocalciumphosphate Monohydrate (MCPM) Electrolyte and its Biocompatibility. Key Engineering Materials, 212-217.

Academic Conference Presentation

-Conference: The 6th International Symposium in Science and Technology at Kansai University 2011, Osaka, Japan (August 24-26, 2011).

-Conference: International Conference on Traditional and Advanced Ceramics, Bangkok (August 22-25, 2012).

-1st Joint Seminar and Workshop on the Advancement in Energy-and Bio-related Materials and Technology at School of Mechanical and Aerospace Engineering, Nanyang Technological University, Singapore (March 3-10, 2013).

-Conference: The Mathematics and Physical Science Graduate Congress at the University of Malaya in Kuala Lumpur, Malaysia (January 8-10, 2014).

-Conference: The 17th International Conference on Medical and Biomedical Engineering (ICMBE 2015) at Toronto, Canada (June 15-16, 2015).